CDF/PHYS/TOP/GROUP/6845
Version 1.5
May 2004

Updated Measurement of the Top Quark Mass in the Lepton+Jets Channel

Erik Brubaker, Adam Gibson *(UC Berkeley / LBNL)*
Jahred Adelman, Young-Kee Kim,
Mel Shochet, Un-Ki Yang *(The University of Chicago)*
Jean-Francois Arguin, Pekka Sinervo *(The University of Toronto)*
for the Top Mass Group

Abstract

This document presents a measurement of the top quark mass in the lepton + jets decay channel with b tags. The data sample was collected with the CDF run II detector between March 2002 and September 2003, and corresponds to an integrated luminosity of approximately 162 pb^{-1}. Thirty-seven candidate $t\bar{t}$ events are found with at least one b jet tagged by SecVtx. A likelihood fit to the distribution of reconstructed masses in the data sample gives a top mass of 174.9 $^{+7.1}_{-7.7}$ (stat.) $\pm$ 6.5 (syst.) GeV/c^2.

1 Introduction

We report a preliminary measurement of the top quark mass in the lepton + jets decay channel using the SecVtx b tagger. We apply the method used to measure the top quark mass in run I [1], with minor modifications. The top quark mass was measured for summer conferences with about 108 pb^{-1} of data [2]; the current result is an update using the full currently available dataset, about 162 pb^{-1} after good silicon runs are required. The analysis is based on the `4.11.1` version of CDF software, though various patches have been applied.

The note is structured as follows. Section 2 discusses the corrections applied to the jets, leptons, and missing transverse energy ($\not\!\!E_T$) for the event selection, and defines the sample of events which are used in the measurement of the top quark mass. Section 3 describes the corrections applied to the physics objects in the event, as well as the algorithm used to reconstruct the top quark mass on an event-by-event basis using the corrected four-vectors of those objects. To measure the top mass, we compare the reconstructed mass distribution from data to our Monte Carlo expectations using an unbinned likelihood fit, described in section 4. Section 5 gives the result of that fit on the data. The systematic uncertainties associated with this top quark mass measurement are presented in section 6. Finally, section 7 discusses additional checks and presents the distributions of various kinematic variables. Throughout the note, footnotes are used to indicate probable or possible improvements for the next iteration of the analysis.

2 Event Selection

The starting point for our event selection is the official set of acceptance cuts from the lepton + jets group, details of which can be found in CDF note 6574 [3]. In particular, we consider only $t\bar{t}$ candidate events in the lepton + jets channel. We require exactly one tight lepton in the event, as determined by `TopEventModule`. Conversions are vetoed for electron events, and cosmics are vetoed for muon events. Events are vetoed if they contain, in addition to the primary lepton, an isolated phoenix electron in the plug. We require $\not\!\!E_T > 20$ GeV, where $\not\!\!E_T$ is adjusted for level 4 corrections to the jets in the event. We find jets using the `JETCLU` algorithm with a cone of $R = 0.4$, and count jets using cuts on detector η and E_T, after level 4 jet corrections have been applied.[1]

In addition to this standard selection, we apply some cuts specific to the top mass analysis. Since we attempt to reconstruct the top and anti-top decay chains, there must be at least four jets in the event (two b jets and two jets from the hadronic W decay). Additional jets are permitted. The pre-tagged mass analysis seeks to maintain a roughly 1:1 signal-to-background ratio by requiring four jets with $E_T > 15$ GeV and $|\eta| < 2.0$ [4]. Events that satisfy this jet requirement will be referred to as "4-jet events." Due to the higher purity of tagged events, on the other hand, this mass analysis with b tags requires just three such jets and relaxes the cut on the fourth jet to $E_T > 8$ GeV; events in which 8 GeV $< E_T^{j4} <$ 15 GeV will be called "3.5-jet events." The E_T cut of 8 GeV on the fourth jet was initially chosen to match the run I analysis, but note that, in contrast to the run I analysis, the η cut is *not* relaxed for the fourth jet. The acceptance increase from a looser fourth-jet η cut was not considered worth the additional complication of using jets from the poorly understood far-forward region.

Figure 1 (top left) illustrates the effect that various cuts on the fourth jet E_T have on the acceptance of signal and background events. As the E_T^{j4} cut increases from 8 GeV to 15 GeV, the number of $t\bar{t}$ events decreases by 24% while the number of $Wb\bar{b}$ background events decreases by 56%. The mean and RMS values of the reconstructed mass distributions for the background sample increase with the E_T^{j4} cut, while those for the signal samples remain quite stable, as expected (see Figure 1, bottom).

The cut on the fourth jet E_T was chosen to increase the $t\bar{t}$ acceptance without diluting too much the signal over background. However, this cut has not been optimized for its effect on the top mass sensitivity.[2]

Positive tags from the SecVtx secondary vertex tagger are used to identify at least one b jet in each event.[3] Parameters and recommendations from the high-p_T b-tagging group are used [5].[4] In particular, only jets with $E_T > 15$ GeV are considered by the tagger. No soft

[1] Future versions of this analysis will track improvements in the standard selections. For example, a cut on $\Delta\phi$ between the leading jet and the $\not\!\!E_T$ has been shown to substantially reduce the QCD background with only a small effect on signal acceptance.

[2] This optimization should, of course, be performed.

[3] In run I, events with exactly one tag and events with two tags were treated separately in order to take advantage of better mass measurements and lower background content in the double-tag sample. That separation has not yet been implemented in this analysis, but is being investigated.

[4] Improved understanding of the contribution of tags due to interactions with detector material to the positive tagging rate, as well as of the contribution of heavy-flavor jets to the negative tag rate, has prompted several fixes and improvements to the SecVtx b-tagging algorithm. The updated algorithm will be used in

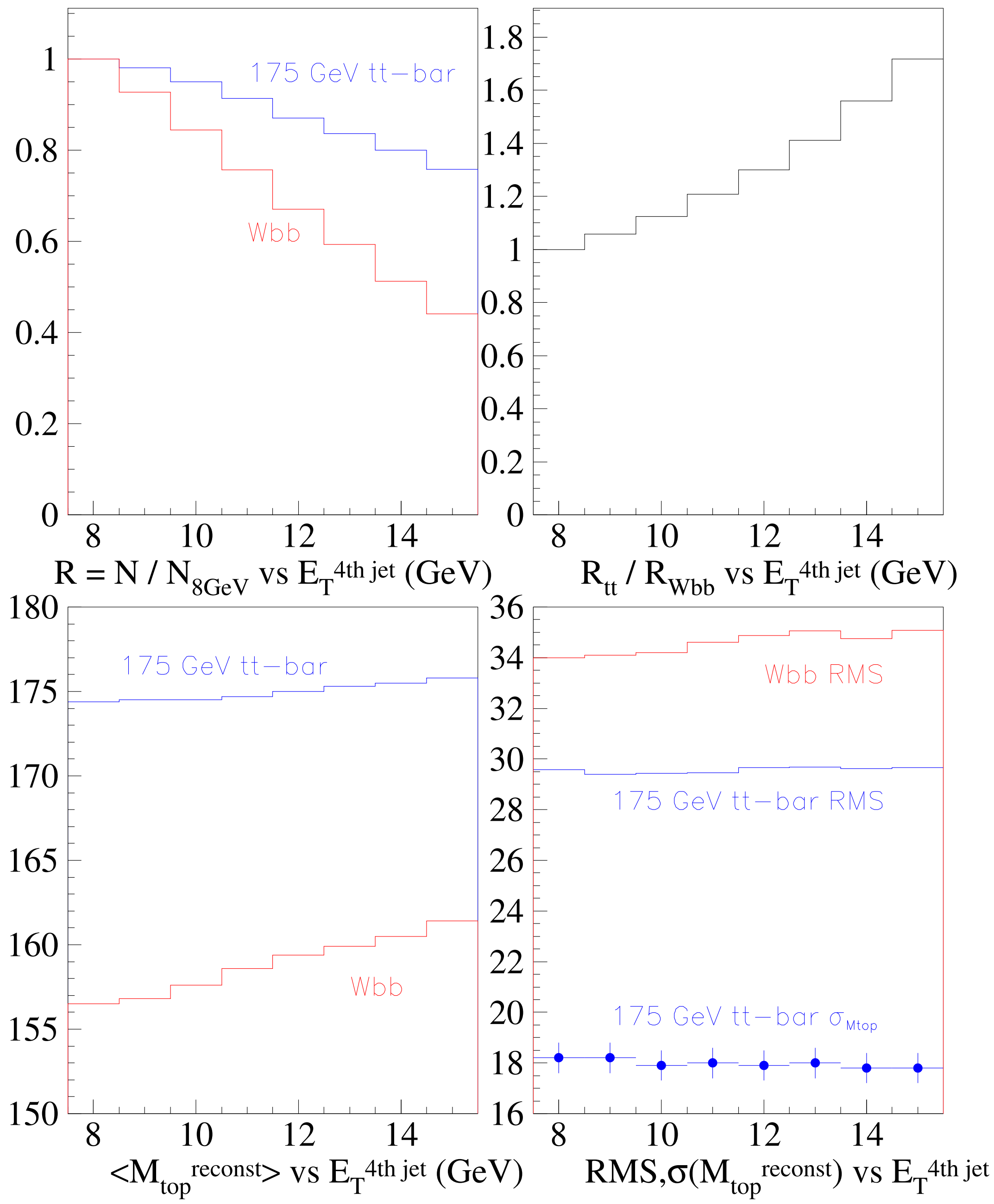

Figure 1: Top left: the acceptance as a function of the E_T^{j4} cut with respect to that of the $E_T^{j4} > 8$ GeV cut: the $t\bar{t}$ sample with $\mathrm{M_{top}} = 175$ GeV/c^2 ($R_{t\bar{t}}$) in blue and the $Wb\bar{b}$ background sample ($R_{Wb\bar{b}}$) in red. Top right: $R_{t\bar{t}}/R_{Wb\bar{b}}$ as a function of E_T^{j4}. Bottom: the average (left) and RMS (right) of the reconstructed top mass distribution between 80 GeV/c^2 and 380 GeV/c^2. The width (σ) of the Gaussian fit between 140 GeV/c^2 and 210 GeV/c^2 is also shown in bottom-right for $t\bar{t}$ (points).

lepton tagging is used.[5]

The Monte Carlo datasets used, along with a brief description of each, are given in Table 1. The primary $t\bar{t}$ signal datasets are generated with HERWIG. Other datasets, including background samples and samples used to estimate systematics, were generated with HERWIG, Pythia, and ALPGEN. All samples, unless noted otherwise, use the defaults for 4.9.1 MC processing, including realistic silicon coverage and offset beamline.

The data used in this analysis originated from the `v4.11.1 REMAKE` set of samples described in CDF note 6548 [8]. Events are required to come from runs between 141544 and 167716 that are marked as good including silicon, according to the good run list v4.0 [9].[6] The CMX muon dataset is limited to runs after 150145, corresponding to $\sim$ 153 pb^{-1}. In the data, we require the `ELECTRON_CENTRAL_18` trigger for electrons, the `MUON_CMUP18` trigger for CMUP muons, and the `MUON_CMX18` trigger for CMX muons. (No trigger simulation is run on Monte Carlo events, and no trigger requirement is imposed.)

Using the selection described above, a total of 27 4-jet events and 10 3.5-jet events are found with at least one b tag, and 4 4-jet event and 1 3.5-jet event have two b tags (see Table 2). The selected events are listed in Table 3 (events that pass an additional cut in the mass reconstruction, $\chi^2_{\rm min} < 9$) and Table 4 (events that fail the $\chi^2_{\rm min} < 9$ cut). For each event the tables give the run and event numbers, lepton type, lepton E_T, raw $\not\!\!E_T$, the four leading jets' raw p_T, the reconstructed top mass, and the $\chi^2_{\rm min}$ of the mass reconstruction. A description of the top mass reconstruction, including a definition of $\chi^2_{\rm min}$, is given in section 3. Section 7 features various checks on our understanding of our data sample.

3 Top Mass Reconstruction

For each event that has been selected according to section 2, we extract a single quantity through a series of corrections to the raw detector measurements and a multi-parameter fit in MINUIT. This quantity is intended to have a strong dependence on the top quark pole mass, so that we can use its distribution in the data to determine the top mass through a likelihood fit to the distributions we extract from various Monte Carlo samples (see section 4).

Specifically, we do our best to reconstruct the invariant mass of the top quark in each event, assuming the event is $t\bar{t}$ signal with top quark decays and kinematics according to standard model predictions. Every event is treated identically, whether signal or background, data or Monte Carlo (except as noted below). Some events "fail" the mass reconstruction and are discarded. This amounts to one more event selection requirement, and will be described below in detail.

Note that, although this quantity is referred to as the reconstructed top mass, it is *not* used as an independent measurement of the top mass in each event. It is simply an experimental quantity that will be used to discriminate among the range of possible true values of the standard model top quark mass.

the future.

[5]It is under consideration to use muon soft lepton tags ([6, 7]) in the next iteration of this analysis.

[6]One hopes that some runs or portions of runs currently excluded due to minor problems can be recovered.

Table 1: The Monte Carlo datasets used in this analysis are listed, along with a brief description of each. The three groups separate datasets used for signal templates, background templates, and systematic studies. The dataset ID is a unique identifier in the CDF data catalog. A more comprehensive list of top group Monte Carlo samples is at http://www-cdf.fnal.gov/internal/physics/top/mc/mc_samples_491.shtml.

Dataset ID	**Description**
Samples used for signal templates	
ttopgk, ttophk, ttopik, ttopjk, ttopkk, ttoplk, ttopmk, ttop5l, ttopnk, ttopok, ttoppk, ttopqk, ttopli, ttoprk, ttopsk, ttoptk, ttopuk, ttop6l, ttopvk, ttop7l, ttopwk, ttop8l, ttopxk, ttopyk, ttopzk, ttop1l, ttop2l, ttop3l, ttop4l	Signal $t\bar{t}$ mass samples with $\mathrm{M_{top}} = 130 - 230$ GeV/c^2 in $2.5 - 5$ GeV/c^2 steps. HEPG-level lepton filter is applied.
Samples used for background templates	
atop04, atop0a	W+4 parton samples, with $W \to e\nu$ and $W \to \mu\nu$, respectively
atop32, atop48	$Wb\bar{b}$ samples, with $W \to e\nu$ and $W \to \mu\nu$, respectively
ttop0s, ttop1s	Single top samples, s-channel and t-channel, respectively
Samples used for systematic studies	
ttopli, ttopei	Large inclusive $t\bar{t}$ samples with $\mathrm{M_{top}} = 175$ GeV/c^2, generated using HERWIG and Pythia tune A, respectively
ttop0e	$t\bar{t}$ sample generated using Pythia tune A with no QCD or QED initial state radiation
ttop3e, ttop4e	$t\bar{t}$ samples using MRST72 (central α_s) and MRST75 (lower α_s) PDF sets, respectively
ttop5e	$t\bar{t}$ sample generated using Pythia tune B
"Unofficial" samples	$t\bar{t}$ samples for PDF uncertainties: see http://www-cdf.fnal.gov/internal/physics/top/RunIIWjets/summer03_herwig_pdfs.txt

Table 2: The number of events found in each jet bin with 1 or 2 b-tagged jets. The numbers in parentheses indicate the number of events used in the top mass measurement, that is, with $\chi^2_{\mathrm{min}} < 9$ in mass reconstruction (see section 3 for χ^2_{min} description).

	3.5-jet events	4-jet events	$\geq$ 3.5-jet events
Events with == 1 tag	9 (8)	23 (18)	32 (26)
Events with == 2 tags	1 (1)	4 (1)	5 (2)
Events with $\geq$ 1 tag	10 (9)	27 (19)	37 (28)

Table 3: The run and event numbers of the 28 top candidate events used in the top mass measurement, and their lepton, jet, and $\not\!\!E_T$ values without jet corrections and track curvature corrections. These events *passed* the $\chi^2_{\rm min} < 9$ cut in the mass reconstruction (see section 3 for $\chi^2_{\rm min}$ description). The events marked by "†" have two b-tagged jets among the four leading jets.

$\chi^2_{\rm min} < 9$ (events used in mass extraction)								
Run	Event	Njt	Type	E_T^{lep} GeV	$\not\!\!E_T$ GeV	p_T, four leading jets GeV	χ^2	$M_{\rm top}$ GeV/c^2
141597	1353293	3.5	CMUP	51.2	30.9	50.3, 39.4, 36.4, 12.0	3.4	135.2
144674	1782954	3.5	CEM	98.7	31.6	45.4, 39.5, 36.0, 10.5	4.9	132.6
145036	245760	4	CMUP	28.2	67.4	95.9, 64.1, 19.1, 17.4	5.3	175.9
148153	6088	3.5	CEM	54.9	48.2	67.0, 46.7, 18.0, 8.8	0.3	144.3
149387	2551061	3.5	CEM	66.8	29.7	34.0, 22.2, 17.7, 7.9	4.2	122.0
152266	3554	4	CMUP	30.6	40.2	54.9, 40.3, 17.4, 16.7	0.6	153.6
153693	799494	4	CMUP	54.4	37.1	94.8, 65.7, 52.9, 36.8	0.4	176.8
153694	1694029	4	CEM	31.8	31.5	118.8, 59.9, 36.5, 23.3	5.0	154.0
153738	2083102	4	CEM	23.0	67.2	100.1, 48.6, 52.5, 23.0	2.6	216.8
154175	1630925	4	CEM	30.4	115.1	111.5, 29.4, 17.0, 15.4	0.8	131.6
†155145	132579	3.5	CEM	52.9	31.7	65.7, 59.8, 27.2, 14.2	0.3	169.9
155345	3194866	3.5	CEM	26.4	61.9	41.6, 40.2, 13.6, 7.8	3.8	122.9
160153	1270879	4	CEM	93.2	52.1	87.6, 50.2, 24.0, 16.3	0.2	170.2
160437	280173	4	CMUP	43.1	29.9	56.5, 51.3, 49.2, 17.2	0.1	178.6
161379	494836	4	CEM	155.4	29.7	94.0, 37.8, 30.1, 15.2	1.3	152.8
161633	1571961	4	CEM	48.6	36.8	75.3, 46.2, 24.3, 13.1	2.6	134.5
161788	361577	4	CMUP	37.1	62.9	123.7, 87.5, 60.4, 53.1	0.7	177.1
162423	261933	4	CEM	73.3	30.5	36.9, 27.9, 26.0, 15.1	0.9	129.6
162519	931923	3.5	CMX	72.6	33.8	36.9, 24.2, 16.6, 11.9	3.3	131.1
162631	7109631	4	CMX	84.5	22.3	70.7, 34.4, 18.4, 12.0	4.5	169.8
162986	1538897	4	CEM	52.2	51.7	102.2, 59.1, 38.3, 25.4	1.5	264.6
163012	2249546	4	CMUP	80.2	34.5	93.4, 57.2, 29.4, 24.3	6.4	192.3
164274	2932602	3.5	CMUP	77.6	24.2	30.0, 29.7, 19.6, 8.4	1.3	148.6
164819	2297394	4	CEM	31.5	46.8	33.1, 35.4, 15.9, 15.4	0.7	159.2
165314	1155563	3.5	CMUP	28.8	12.6	44.4, 20.8, 18.6, 8.3	1.0	126.4
166007	498553	4	CEM	44.7	52.7	65.2, 54.9, 43.1, 13.9	2.9	190.5
†166567	11615607	4	CMUP	39.7	50.1	69.0, 75.4, 36.0, 31.0	5.6	247.0
166614	804529	4	CEM	111.2	29.4	97.3, 51.1, 42.1, 20.1	0.6	184.6

Table 4: The run and event number of the nine top candidate events that *failed* the $\chi^2_{\min} < 9$ cut in the mass reconstruction, and their lepton, jet, and $\not{E}_T$ values without jet corrections and track curvature corrections. (See section 3 for $\chi^2_{\min}$ description.) The events marked by "†" have two b-tagged jets among the four leading jets.

$\chi^2_{\min} > 9$								
Run	Event	Njt	Type	E_T^{lep} GeV	$\not{E}_T$ GeV	p_T, four leading jets GeV	χ^2	$\mathrm{M_{top}}$ GeV/c^2
155320	480816	4	CEM	99.4	28.1	51.0, 31.3, 19.3, 16.4	41.6	146.2
†156116	6116596	4	CEM	25.3	28.2	69.8, 51.2, 29.4, 27.9	367	231.7
160591	894406	4	CMUP	114.8	110.5	148.8, 67.5, 55.6, 14.4	9.6	232.2
161013	111162	4	CEM	78.6	71.9	96.6, 90.0, 21.3, 20.8	9.6	172.6
161678	5912849	4	CEM	27.6	54.7	97.4, 75.4, 38.9, 28.0	10.3	200.0
165313	1770456	3.5	CMUP	112.0	22.9	85.8, 18.7, 12.9, 12.7	20.9	137.8
166805	2534588	4	CMUP	59.1	56.8	123.9, 27.3, 27.1, 17.6	13.6	172.1
†167139	1191211	4	CMX	31.2	63.5	56.6, 38.7, 37.3, 21.5	13.6	175.0
†167551	7969376	4	CEM	77.2	54.9	75.8, 38.5, 24.9, 23.1	174	278.0

3.1 Correcting measured quantities

We will provide as input to the MINUIT fit the four-vectors of the various physics objects identified in the event. We first apply all known corrections to the measured quantities, and establish an uncertainty on the quantities that will be permitted to vary in the fit. These corrections are performed by `TopEventModule` and `TopMassFitModule`.

3.1.1 Lepton Corrections

For both electrons and muons, we use the corrected four-vector from `TopEventModule` (via the `TopSummary` object). In the case of electrons, this includes standard corrections for tower map response. The electron energy is the two-tower calorimeter energy, while the angles are taken from the beam-constrained COT-only track. The electron mass is set to zero in the four-vector, and the angles are taken as perfectly measured quantities. The transverse momentum ($p_T^e = p \sin\theta$) of the electron is given an uncertainty of

$$\frac{\sigma_{p_T^e}}{p_T^e} = \sqrt{\left(\frac{0.135}{\sqrt{p_T^e[\mathrm{GeV}/c]}}\right)^2 + (0.02)^2}. \tag{3.1}$$

Since the angles are fixed, this amounts to an uncertainty on the magnitude of the full electron momentum vector, not just the transverse component.

For muons, the corrected four-vector uses the three-vector of the beam-constrained COT-only track, also with a mass of zero. We apply in addition the muon curvature corrections due to chamber misalignment:

$$\frac{1}{p_T^{\mu}[\mathrm{GeV}/c]} = \frac{1}{p_T^{\mu}[\mathrm{GeV}/c]} - 0.00037 - 0.00110 \sin(\phi + 0.28) \tag{3.2}$$

(data only; no such correction is applied to Monte Carlo muons). Again the angle and mass are given no uncertainty; the transverse momentum is given an uncertainty of

$$\sigma_{1/p_T^\mu[\mathrm{GeV}/c]} = 0.0011 \quad \rightarrow \quad \frac{\sigma_{p_T^\mu}}{p_T^\mu} = 0.0011 \cdot p_T^\mu[\mathrm{GeV}/c], \tag{3.3}$$

which is equivalent to an uncertainty on $|p|$, as for electrons. The electron and muon transverse momentum uncertainties are from run I.

3.1.2 Generic Jet Corrections

Jets are first corrected with the generic jet corrections provided by the Jet Corrections Group. These are encoded in the package `JetUser`; we use the version tagged by "`jetCorr00`." For the purposes of mass fitting (as opposed to event selection), we apply level 5 corrections, which are intended to return, on average, the in-cone hadronic energy for a jet in a dijet event with flat p_T spectrum. Generic jet corrections simply scale a jet four-vector by a factor, so angles are unaffected, while E and p (and mass!) change. The various sources of uncertainty in the CDF jet energy scale and simulation are quantified in the systematic uncertainties on these jet corrections (see section 6.1).

3.1.3 Top-Specific Jet Corrections

As mentioned above, the generic jet corrections are extracted from dijet events assuming a flat p_T^{jet} spectrum. Jet corrections derived specifically for the $t\bar{t}$ process are needed to account for the different fragmentation of light quark jets from W-boson decay (W jets) and b jets, as well as the non-flat p_T spectrum of jets from $t\bar{t}$ decay. In addition, the top-specific corrections account for the energy falling outside the jet cone. W jets and b jets are corrected with separate functions, but no separate correction is attempted for b jets with semi-leptonic decays.[7]

The $t\bar{t}$-specific corrections also provide uncertainties on the jet energies (i.e. the measurement resolution, not systematic uncertainties). As for the lepton four-vectors, the angles of jets are assumed to be perfectly measured;[8] only the $\sigma_{p_T^{jet}}$ is parameterized.

At least two such sets of $t\bar{t}$-specific corrections are available in run II. (See [11] for the run I derivation of similar corrections.) We use the JF corrections, which are described in CDF note 6404 [12]; the study that prompted this choice is documented in CDF note 6794 [13]. The JF corrections are functions of p_T^{jet} and η^{jet}. They are extracted from a large sample of HERWIG $t\bar{t}$ events in which the four leading jets in E_T are matched with the four HEPG partons from $t\bar{t}$ decay. As a crosscheck, the correction functions and their effect on the reconstructed invariant mass of the hadronic top quark have been shown to be consistent with those extracted from a large Pythia sample. Since the last version of CDF 6404, updated JF corrections have been derived that use the most probable value of the jet response curve, rather than the median, to extract the correction. Additionally, the JF corrections are now defined on jets corrected to level 5, rather than to level 7. These changes,

[7]Such a correction is being explored for SLT muons, and has been shown in principle to improve the resolution of the mass measurement. Details of the implementation are being worked out.

[8]See CDF note 6927 [10] for some exploration of this assumption.

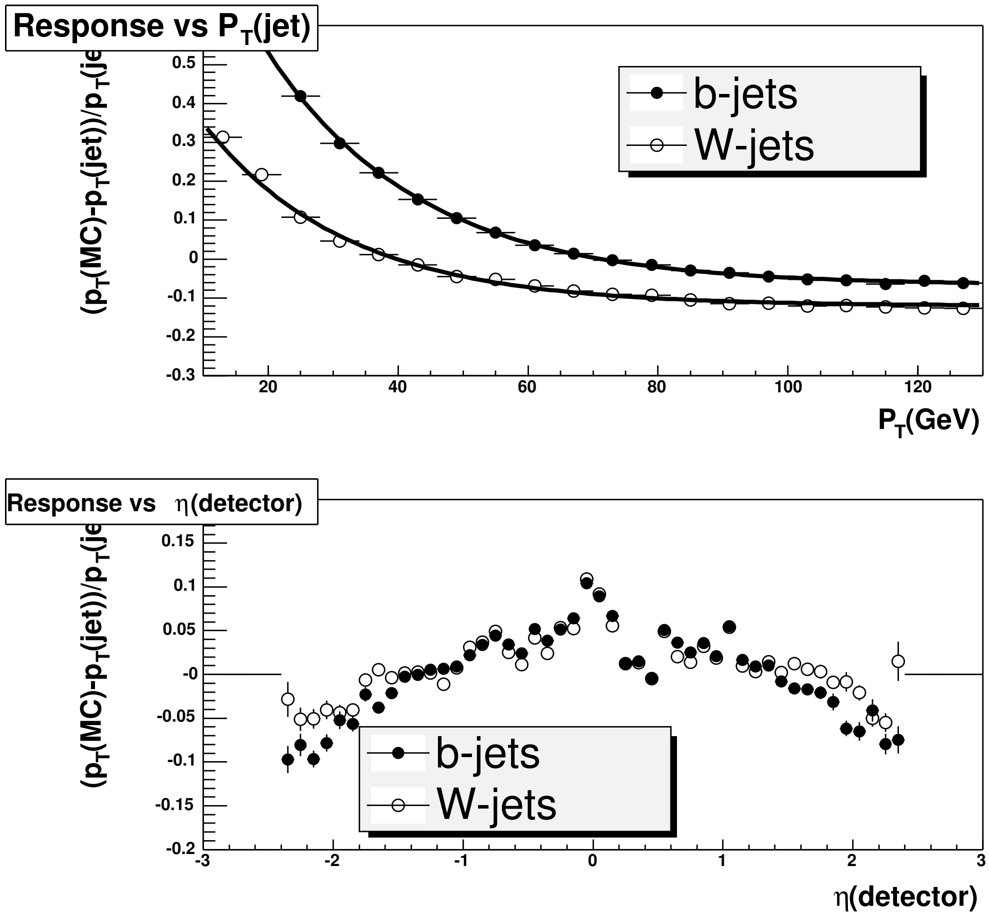

Figure 2: Upper plot: jet response, $(p_T^{parton} - p_T^{jet})/p_T^{jet}$, as a function of p_T^{jet} for b-jets and W-jets after only generic corrections are applied. Lower plot: jet response as a function of η^{jet} after applying $t\bar{t}$-specific corrections that depend only on p_T^{jet}.

along with an optimization of the χ^2 cut described below, have been shown to significantly improve the power of the method.

Figure 2 illustrates the need for the $t\bar{t}$-specific corrections. (It uses the original JF corrections, described in CDF 6404.) The upper plot shows significant differences between parton momentum and jet momentum with $p_T^{jet} < 40$ GeV$/c$ after generic corrections. The $t\bar{t}$-specific corrections remove the dependence of the jet response as a function of p_T^{jet} separately for b-jets and W-jets. In addition, the p_T spectrum of jets from $t\bar{t}$ decay is strongly η-dependent. Therefore we expect η dependence in the jet response after any $t\bar{t}$-specific corrections that depend only on p_T^{jet}. This is illustrated in the lower plot of Figure 2. The JF corrections are therefore extracted as a function of both p_T^{jet} and η^{jet} in order to remove this effect.

One way to check the effectiveness of the $t\bar{t}$-specific corrections is to look at the reconstructed invariant mass of the jets matched to the W-boson daughters as a function of the p_T^W and average η of daughter jets. As shown in Figure 3, no significant dependences are observed after applying the $t\bar{t}$-specific corrections (again using the original JF corrections). The

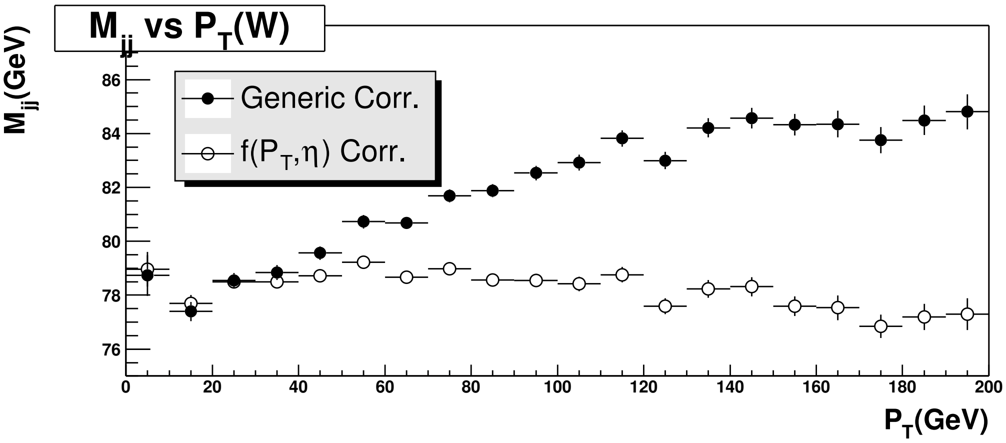

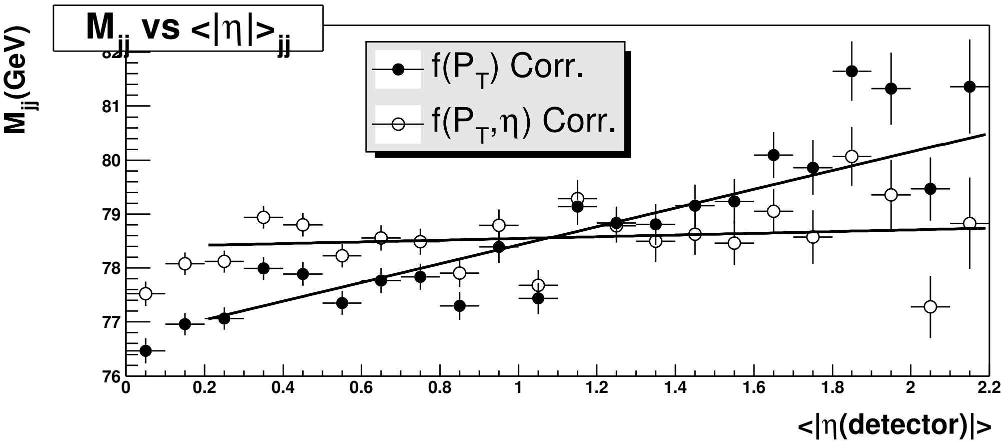

Figure 3: Upper plot: invariant mass of jets from W daughters as a function of p_T^W after applying generic corrections (full circles) and p_T- and η-dependent corrections (open circles). Lower plot: invariant mass of jets from W daughters as a function of the average η of W jets after applying only p_T-dependent corrections (full circles) and p_T- and η-dependent corrections (open circles). In both plots, MC events with a good jet-parton match are used.

overall W mass distribution has mean and Gaussian mean of 78.6 GeV/c^2 and 79.5 GeV/c^2, respectively. We can also look at the effect on the reconstructed invariant mass of the three jets from the hadronic top. The JF corrections have been shown to improve the RMS of the hadronic invariant mass distribution by $\approx 10\%$.

The JF corrections produce another scale factor by which the full jet four-vector is multiplied. Thus again the angles do not change. Note that, since the JF corrections depend on the flavor of the jet, they must be applied after a hypothesis has been selected for the assignment of the measured jets to partons from the $t\bar{t}$ decay chain.

As a final step, the jet momentum is held fixed while the jet energy is adjusted so that the jet has a mass according to its flavor hypothesis. A mass of 0.5 GeV is used for W jets, and a mass of 5.0 GeV is used for b jets.

3.1.4 Additional jets, unclustered energy, and missing energy

"Additional jets" in an event are those jets beyond the leading four in level-4 corrected E_T, but still having $E_T > 8$ GeV and $|\eta| < 2.0$. They are identified as not belonging to the top decay chain, but arising from initial state radiation, underlying event, or multiple interactions. This is, of course, an approximation, since the additional jets may in fact be top decay daughters, or may arise from final state radiation and therefore be relevant in reconstructing the top quark mass. These jets are corrected using level 5 generic corrections; however, they contribute to the reconstructed top mass only through their effect on the $\not\!\!E_T$ calculation.

The "unclustered energy" in an event consists of any energy seen in the calorimeter that is not associated with the primary lepton or a jet. The p_T of towers with $|\eta| < 3.6$ are included in the unclustered energy.[9] The "missing energy" is identified with the energy carried out of the detector by one or more neutrinos. The unclustered energy and missing energy are related to each other through the other measured physics objects in the event, since we assume that the $p\bar{p}$ system has $p_T = 0$.

In this analysis, the input to the MINUIT fit called unclustered energy is the sum of the raw unclustered energy, described above, and the energies of the additional jets. We add to the unclustered energy the energy that would have been subtracted from the leading four jets due to the underlying energy (level 6 generic corrections), and we subtract the energy that would have been added to those jets due to energy falling outside the jet cone (level 7 generic corrections). This is done to avoid double-counting of energy that is included in the jet energies after all corrections. The raw unclustered energy is then multiplied by a scale factor of 1.4, which is roughly the level 5 correction factor for 8 GeV jets. So the unclustered energy input to the fit is

$$U_T = 1.4 * \left(U_T^{raw} + \sum_{jet=1}^{4} E_T^{L6} - \sum_{jet=1}^{4} E_T^{L7} \right) + \sum_{\mathrm{add'l\,jets}} E_T^{jet}.$$

Each transverse component of this composite unclustered energy (U_x, U_y) is assigned an uncertainty of $0.4 \cdot \sqrt{\sum E_T^{unclus}}$. Various other approaches to correcting the unclustered energy and assigning resolution were tried, and no changes had any significant effect on the top mass resolution. We conclude that the $\not\!\!E_T$ calculation does not have a large effect on the χ^2 fit.

The neutrino energy, i.e. the missing energy, is always calculated from the other objects, including the composite unclustered energy. In practice, only the transverse momentum in the event balances, so only the neutrino transverse momentum p_T^ν is calculated at each stage in the fit, using the current values of lepton, jet, and unclustered transverse energies:

$$\vec{p_T^\nu} = -\left(\vec{p_T^\ell} + \sum \vec{p_T^{jet}} + \vec{U_T} \right) \tag{3.4}$$

The longitudinal momentum of the neutrino p_z^ν is a free (unconstrained) parameter in the fit. Its initial value is calculated using the initial value of the lepton four-vector and the

[9] Jets with $E_T > 8$ GeV but $|\eta| > 2.0$ are not considered as separate physics objects in this analysis, so their raw energy contributes to the unclustered energy like any other tower.

initial missing energy, and assuming their mother W has its pole mass. Since these conditions yield a quadratic equation, there are in general two solutions for the p_z^ν; a separate fit is done with each solution used as the initial value of p_z^ν. When the two fits land in different minima, we choose the one that provides the best fit using the χ^2 values as described below.

3.2 MINUIT fit

Given the inputs described above, the event-by-event fit for the reconstructed top mass proceeds as follows. MINUIT is used to minimize a χ^2 where the top mass is a free parameter. For each event this is done 24 times, corresponding to the 12 ways to assign the four leading jets to the four partons in $t\bar{t}$ decay, times the 2 solutions for the neutrino longitudinal momentum. For each combination, the following χ^2 is minimized:

$$\begin{aligned}\chi^2 &= \Sigma_{i=\ell,4jets}\frac{(p_T^{i,fit}-p_T^{i,meas})^2}{\sigma_i}+\Sigma_{j=x,y}\frac{(p_j^{UE,fit}-p_j^{UE,meas})^2}{\sigma_j}\\ &+ \frac{(M_{jj}-M_W)^2}{\Gamma_W^2}+\frac{(M_{\ell\nu}-M_W)^2}{\Gamma_W^2}+\frac{(M_{bjj}-M_t)^2}{\Gamma_t^2}+\frac{(M_{b\ell\nu}-M_t)^2}{\Gamma_t^2}. \end{aligned} \tag{3.5}$$

In the first term, σ_ℓ and σ_{jet} are the lepton and four leading jet p_T resolutions. In the second term, $p_{x,y}^{UE}$ and $\sigma_{x,y}$ are the components of the composite unclustered energy and their resolutions. These quantities have all been defined in section 3.1.

Each of M_{jj}, $M_{\ell\nu}$, M_{bjj}, and $M_{b\ell\nu}$ refers to the invariant mass of the sum of the four-vectors denoted in the subscript. For example, M_{jj} is the invariant mass of the vector sum of the W daughter jets. M_W and M_t are the pole masses of the W and top quark. M_W is 80.41 GeV/c^2, taken from the PDG,[10] and M_t is, of course, the free parameter that we will take as the reconstructed mass after the χ^2 is minimized. The fit is initialized with $M_t = 175$ GeV/c^2. Γ_W and Γ_t are the total width of the W boson and the top quark.[11] Γ_W is 2.06 GeV, again from the PDG, and Γ_t is 2.5 GeV.[12] Thus these terms provide constraints such that the W masses come out correctly, and the t and $\bar{t}$ masses come out the same (modulo the Breit-Wigner a.k.a. Gaussian distribution in both cases).

The jet-parton assignment (and p_z^ν solution) with the lowest χ^2 after minimization is selected for each event. The χ^2 of this combination is denoted $\chi^2_{\min}$, and the requirement $\chi^2_{\min} < 9$ is imposed. (When the context is unambiguous, we may use χ^2 and $\chi^2_{\min}$ interchangeably to denote the χ^2 of the selected combination for each event.) This value of the χ^2 cut was found to give the best expected statistical uncertainty on the top mass, as shown in

[10]Especially given that the mean of the fully reconstructed dijet mass from W daughters is less than 80.41 GeV/c^2 (see section 3.1.3), it is not clear that the PDG mass is the best constraint to use here. An interesting study would be to scan the value of the W mass constraint in the χ^2, leaving everything else identical. There is no reason this parameter should not be optimized in the same way we optimize other parameters like E_T^{jet} cuts or the χ^2 cut.

[11]The W and t have lineshapes described by a Breit-Wigner, not by a Gaussian. It is not clear what one should use for σ if one wants to approximate a Breit-Wigner by a Gaussian; currently we use the Breit-Wigner full width at half maximum. This could be investigated further—a complete solution would require throwing out the Gaussian approximation and using the complete Breit-Wigner lineshape.

[12]We don't know where this number came from. The commonly referenced theoretical top width is ≈ 1.5 GeV. We should be consistent what the generators use, if anything.

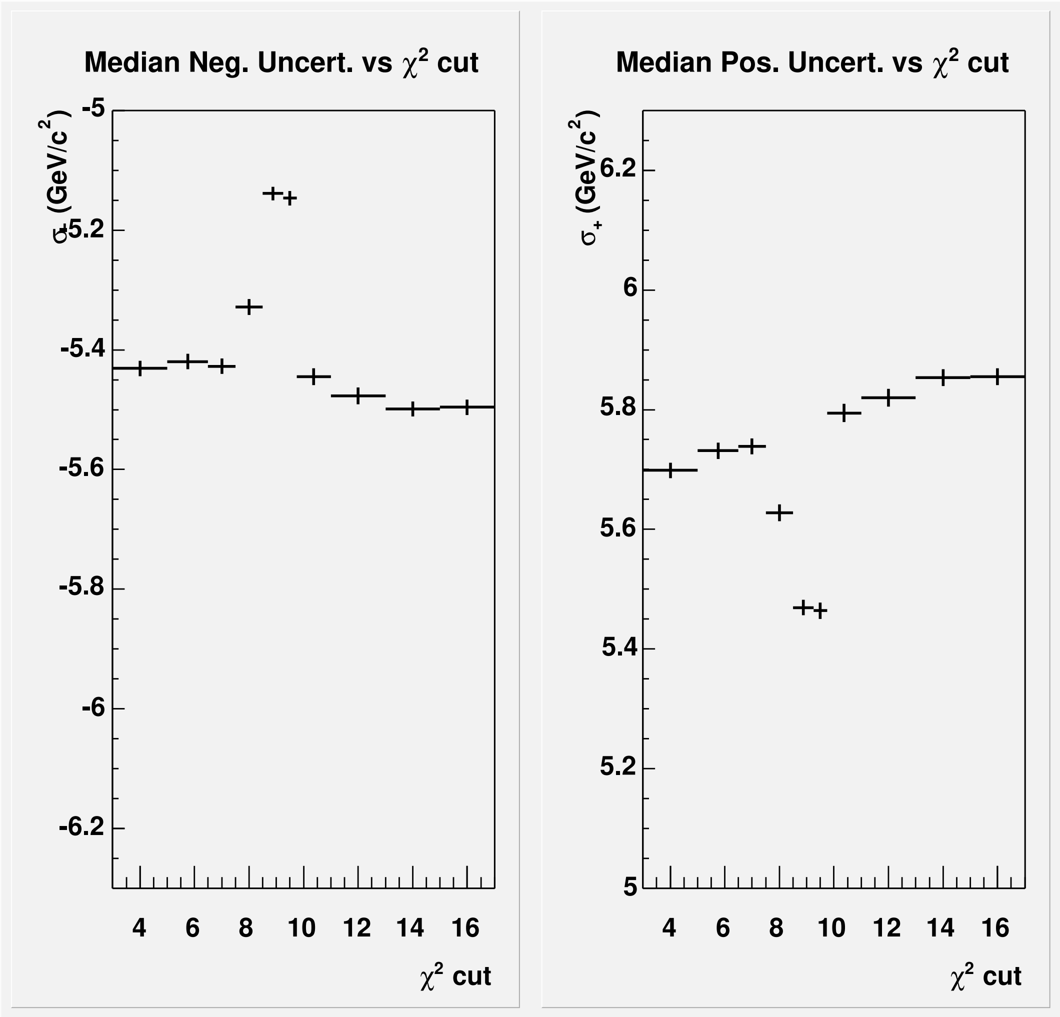

Figure 4: The expected statistical uncertainty on the top mass is given as a function of the χ^2 cut. The number of events per pseudoexperiment is changed for each value of the χ^2 cut, so that the effect of the cut efficiency on the fit statistics is taken into account.

Figure 4.[13] For this analysis, b-tagging information is taken into account simply by ignoring combinations that assign a tagged jet to a light quark at parton level.[14] So at this stage, after mass reconstruction, each event either has been rejected or can be described by a single value of this reconstructed mass variable. Indeed, the rest of the analysis can be performed with nothing more than a list of the reconstructed masses for events in various samples that have passed all selection cuts (including the χ^2 cut).

Figure 5 (top) shows the distribution of $\chi^2_{\rm min}$ for a 175 GeV/c^2 $t\bar{t}$ signal sample, and for

[13] The optimization study was performed using the current version of JF corrections, but with a slightly outdated version of the fitter. The study should be revisited but we expect the result to remain unchanged.

[14] Rather than this black and white distinction, a probabilistic approach may be preferable. One can imagine an extra term in the χ^2 that quantifies the probability that the assignment is correct, given tag information (which, in addition to SecVtx tags, could include other brands of tagging and other jet observables).

W+jets events (mistags), one important background sample. The signal events are more sharply peaked at low values of χ^2, but the separation is not overwhelming. The bottom part of Figure 5 gives the efficiency of the χ^2 cut as a function of the cut value. Our cut at 9 is $\sim 80\%$ efficient for signal and $\sim 70\%$ efficient for the background. Also shown are the ratio of signal efficiency to background efficiency (S/B) and the ratio of signal efficiency to the square root of the background efficiency ($S/\sqrt{B}$). The $\chi^2_{\mathrm{min}} < 9$ cut is also expected to distinguish between signal events where the leading four jets are associated with the top decay daughters, and those where they are not.

A typical reconstructed mass distribution for signal Monte Carlo (this is from the large 175 GeV/c^2 mass sample) is shown as the yellow histogram in Figure 6. Each event in the sample that passes both event selection and the $\chi^2_{\mathrm{min}} < 9$ cut contributes exactly one entry to this plot.[15] As expected, the distribution peaks near the generated mass of 175 GeV/c^2, but we neither seek nor expect an exact correspondence between the generated mass and, say, the mean of the reconstructed mass. The broader shape, beneath the relatively sharp peak at 175 GeV/c^2, is believed to comprise events where an incorrect assignment of jets to partons has been chosen in the fit. The green histogram in the same figure shows the reconstructed mass distribution for the correct jet-parton assigment (for events where the four leading jets are matched to the four partons from $t\bar{t}$ decay), and this distribution has much smaller tails.

For more details on the minimization procedure and inputs see CDF notes 1935 and 2200 [14, 15].

4 Extracting the Top Mass

Given an observable quantity that depends strongly on the mass of the top quark, namely the reconstructed mass, we can measure the top mass in a group of events by comparing their distribution of reconstructed masses to probability density functions with known dependence on the true top quark mass. This section describes that process.

Each event after selection contributes a single value to the reconstructed mass distribution. We use an unbinned likelihood fit, described in section 4.3, to extract the top mass. But first we need the probability density functions as a function of top mass, which are derived from Monte Carlo samples as described in section 4.1. Since we have background events in our sample that cannot *a priori* be distinguished from the signal, we need also p.d.f.'s for the background contribution. These are the subject of section 4.2.

[15] Since the efficiency of the SecVtx b tagger differs in data and Monte Carlo, the ratio of double- to single-tagged events will differ as well. In the future, we should scale the contributions of the two types of events in our signal templates. If N_1 is the number of single-tagged events in MC, N_2 is the number of double-tagged events in MC, and x is the scale factor $\epsilon_{data}/\epsilon_{MC}$, then the ratio will be correct for data if we use the scaling

$$\begin{aligned} N_2 &\rightarrow N_2 x^2; \\ N_1 &\rightarrow N_1 x + 2N_2 x - 2N_2 x^2. \end{aligned}$$

The point is moot if we fit separately the subsamples of single-tagged and double-tagged events.

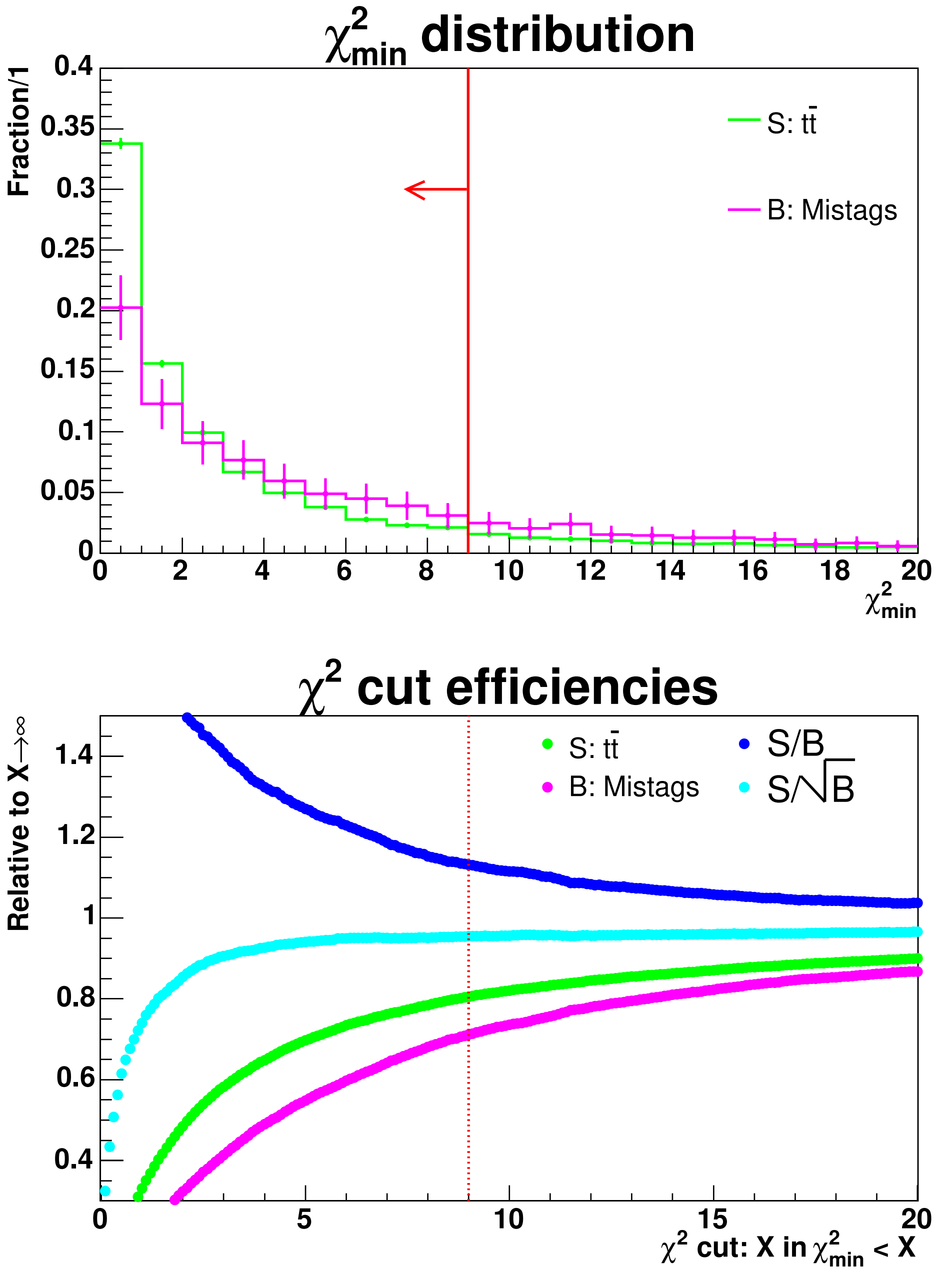

Figure 5: Top: the χ^2 distributions of signal and background Monte Carlo samples. Bottom: The efficiency of the χ^2 cut (relative to no cut) on signal and $Wb\bar{b}$ background samples. Also shown are S/B and $S/\sqrt{B}$, where S and B are the signal and background efficiencies, respectively. In both plots, the red line marks our applied cut $\chi^2_{\rm min} < 9$.

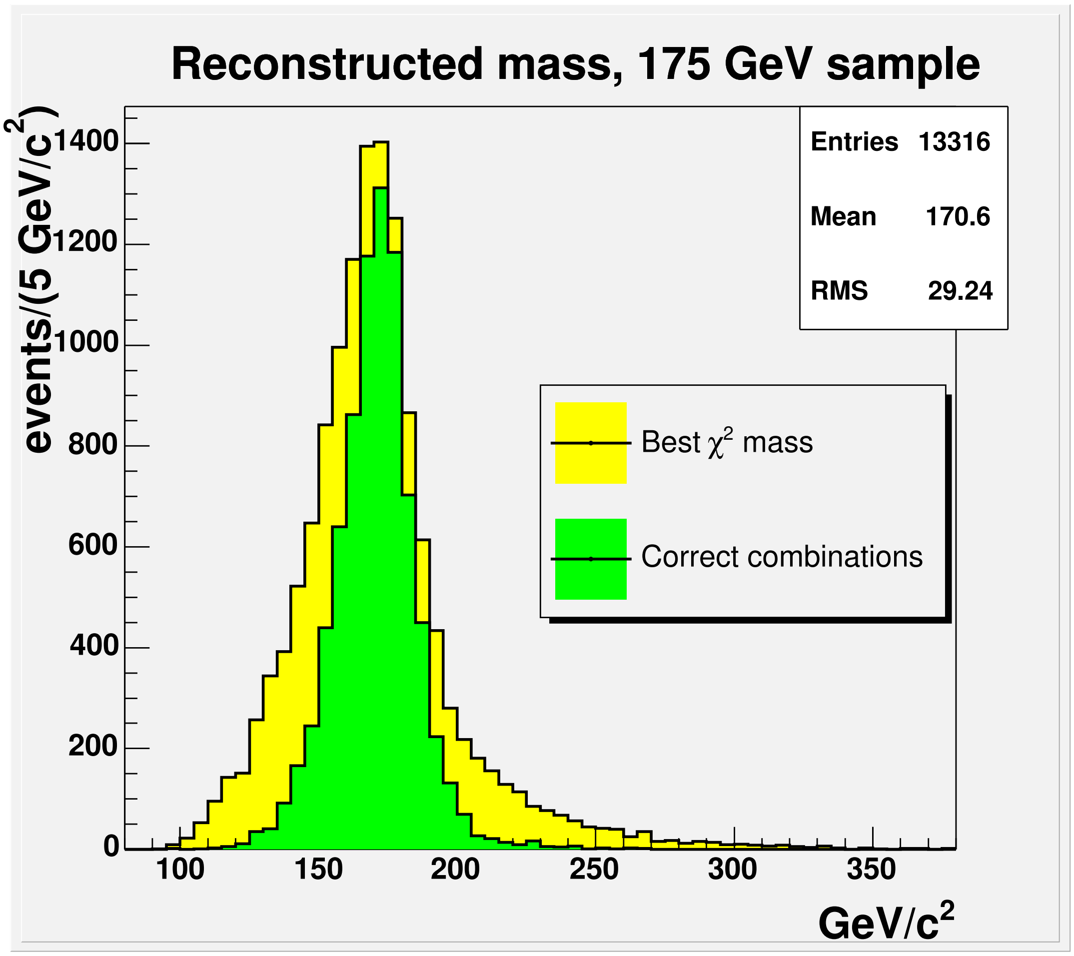

Figure 6: In yellow, the reconstructed mass distribution for the 175 GeV/c^2 HERWIG $t\bar{t}$ sample. Overlaid in green is the reconstructed mass distribution for the correct parton-jet assignment, in the subset of events for which the leading four jets are matched to the four partons from the $t\bar{t}$ decay.

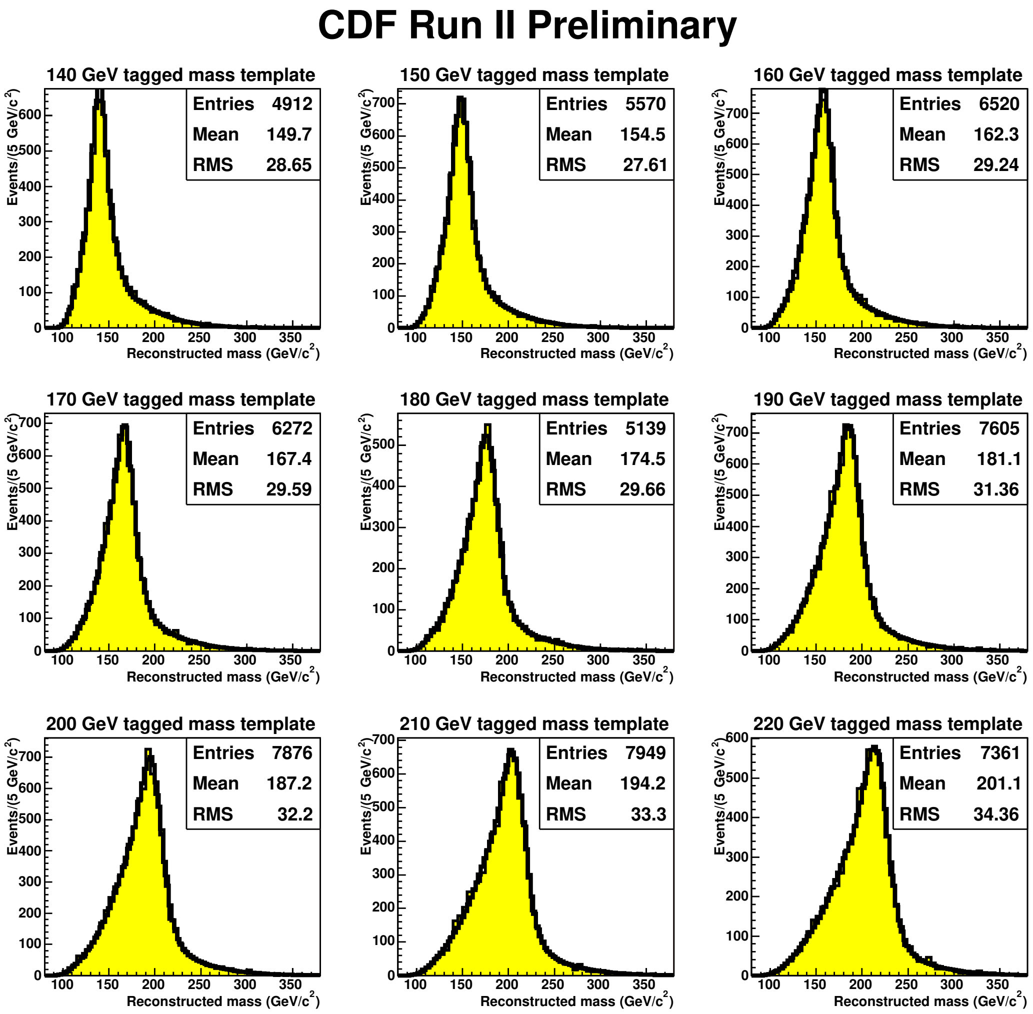

Figure 7: Selected Monte Carlo top mass templates with generated top mass between 140 GeV/c^2 and 220 GeV/c^2. Overlaid are curves from the parameterization whose form is given in Eq. 4.1 and whose fitted parameters are given in Table 5.

4.1 Monte Carlo Mass Templates

Signal mass templates are produced using 29 official Monte Carlo samples with the input top mass at $2.5 - 5$ GeV/c^2 intervals from 130 GeV/c^2 to 230 GeV/c^2. Figure 7 shows nine selected mass templates built using the events that pass the event selection criteria ($E_T^{j4} > 8$ GeV) described in section 2 and the $\chi^2_{\rm min} < 9$ cut described in section 3. In Figure 8 are shown the means, medians, and most probable values of all 29 mass templates as a function of the generated top mass, as well as their slopes from a linear fit.

From these templates we want to obtain p.d.f.'s that are a smoothly varying function of true top mass. We fit to an arbitrary parameterization that gives the probability to observe a particular reconstructed top mass given the true top mass. For a given true top mass, the parameterization consists of two Gaussians—intended to account for the well measured events—plus "that function which is integrated to get the Gamma function"—intended to

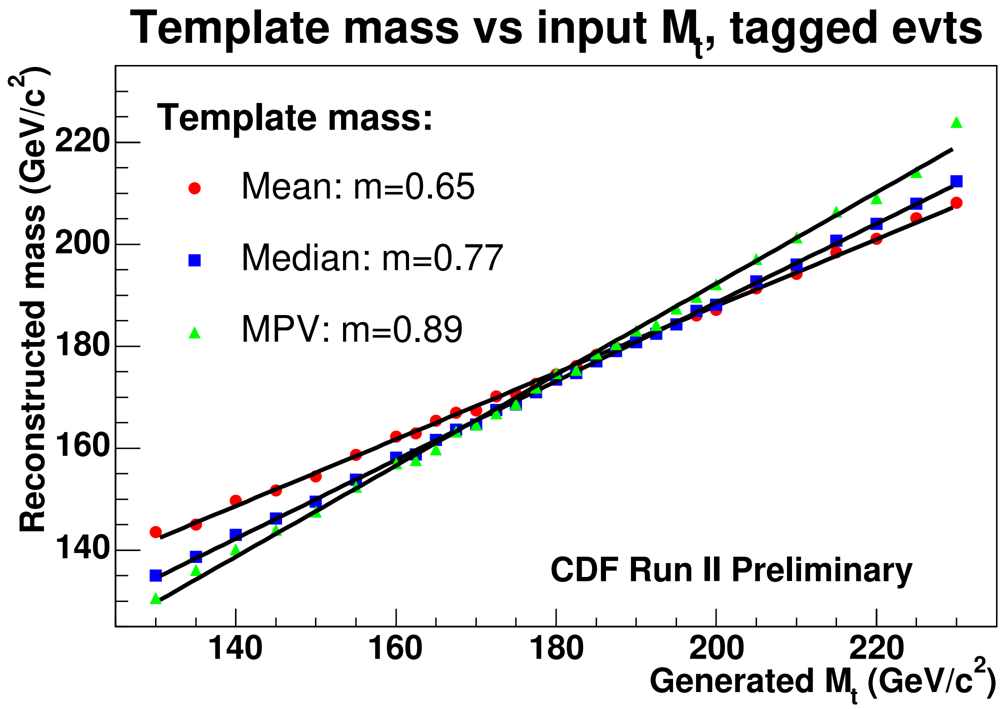

Figure 8: Mean, median, and most probable values of mass templates as a function of the generated top mass between 130 GeV/c^2 and 230 GeV/c^2. The lines are linear fits to the points; slopes are given in the legend.

account for events where the incorrect combination is chosen, or where the four leading jets do not match the four partons from the $t\bar{t}$ decay. The second Gaussian was added to the parameterization in order to fit better the current generation of large statistics Monte Carlo samples. We assume that the 9 parameters necessary to specify this combination of functions themselves depend linearly on the true top mass, so that the full set of p.d.f.'s is specified by 18 parameters. This assumption is certainly arbitrary as well, but seems to be reasonable in the limited range of top masses we consider. Thus the parameterization is as follows:

$$\begin{aligned} P_{sig}(m;M) &= \alpha_7 \cdot \frac{\alpha_2^{1+\alpha_1}}{\Gamma(1+\alpha_1)} \cdot (m-\alpha_0)^{\alpha_1} e^{-\alpha_2(m-\alpha_0)} \\ &\quad +\alpha_8 \cdot \frac{1}{\alpha_4\sqrt{2\pi}} \cdot e^{\frac{-(m-\alpha_3)^2}{2\alpha_4^2}} \\ &\quad +(1-\alpha_7-\alpha_8) \cdot \frac{1}{\alpha_6\sqrt{2\pi}} \cdot e^{\frac{-(m-\alpha_5)^2}{2\alpha_6^2}}; \end{aligned} \tag{4.1}$$

where

$$\alpha_i = p_i + p_{i+9} \cdot (M - 175), \tag{4.2}$$

M in GeV/c^2 refers to the true top mass, and m in GeV/c^2 refers to the reconstructed top mass. Note that the p.d.f.'s are normalized so that, for a given true top mass M, the integral over all reconstructed top masses m is unity.

A binned likelihood fit is used to extract the 18 parameter values. The full covariance matrix of uncertainties from this binned likelihood fit is saved and used to allow the parameters to vary in the final, unbinned likelihood fit to the data described in section 4.3. For the templates shown in Figure 7, the fit returns the parameters given in Table 5. Figure 9 shows the p.d.f.'s for true top mass between 130 GeV/c^2 and 230 GeV/c^2. The χ^2 is calculated between the MC samples and the prediction from the fit, after rebinning to ensure that each bin has at least five predicted events. The resulting χ^2 is 1365, with 1263 degrees of freedom, for a reduced χ^2 of 1.08.[16]

4.2 Monte Carlo Background Template

The source and number of background events in the tagged sample were studied for the $W + 3.5-$jet bin and the $W+ \geq 4-$jet bin by the top cross-section measurement group and documented in CDF note 6907 [16]. Table 6 summarizes their background estimates for the $W + 3.5-$jet sample and the $W+ \geq 4-$jet sample before and after accounting for the top contamination, but without the χ^2 cut in the mass reconstruction, which is an additional selection cut specific to the mass measurement. The dominant contributions (totaling about 75%) come from W+jets (mistags), non-W (QCD), and $Wb\bar{b}$.[17] We follow CDF 6907 in assuming 100% correlation for uncertainties in different jet bins of the same process, and in

[16]This corresponds to a very small probability for such a large number of degrees of freedom. So even with the addition of a second Gaussian in the parameterization, the limited power of our arbitrarily chosen function to describe the high-statistics templates is beginning to show.

[17]The improvements to the SecVtx algorithm (see footnote 4) may affect the relative contributions of backgrounds for which the b tag is a mistag of a light jet.

Table 5: The fitted parameters for the signal p.d.f.'s are given. The form of the parameterization is given in Equation 4.1.

Parameter (see Eq. 4.1)	Fitted value
p_0	87.9 ± 0.5
p_1	3.32 ± 0.08
p_2	0.0488 ± 0.0006
p_3	173.3 ± 0.2
p_4	8.2 ± 0.2
p_5	165.1 ± 0.3
p_6	17.2 ± 0.2
p_7	0.411 ± 0.006
p_8	0.179 ± 0.009
p_9	-0.15 ± 0.02
p_{10}	0.025 ± 0.003
p_{11}	$(-2 \pm 2) \times 10^{-5}$
p_{12}	0.956 ± 0.005
p_{13}	0.077 ± 0.005
p_{14}	0.748 ± 0.009
p_{15}	0.127 ± 0.005
p_{16}	-0.00035 ± 0.00014
p_{17}	0.0015 ± 0.0002
χ^2/n.d.o.f.	1365/1263

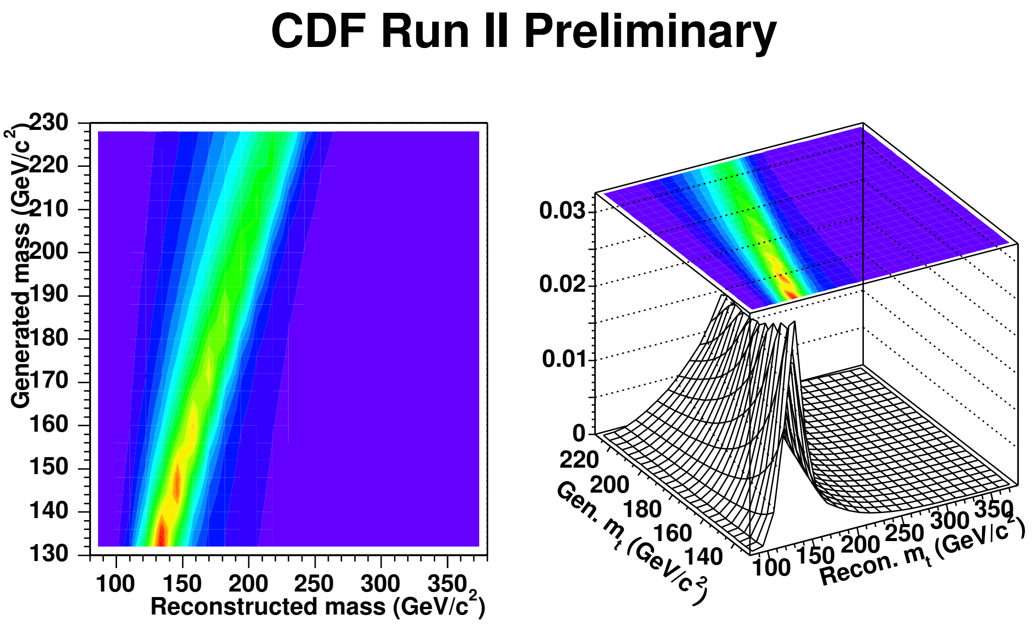

Figure 9: Visualizations of the fitted probability density functions for 130 GeV/c^2 < $\mathrm{M_{top}}$ < 230 GeV/c^2.

assuming no correlation for uncertainties on different processes, except for the W + heavy flavor backgrounds, which are correlated through the uncertainty on the heavy flavor fraction.

In modeling the background shape, which will be used in the final likelihood fit to reconstructed mass, we use the official top group Monte Carlo samples. Samples corresponding to all processes listed in Table 6 were reconstructed using the procedure in section 3, except WW/WZ because of its very small contribution to the total background. $Wc\bar{c}$ and Wc were shown to have the same reconstructed mass shape as $Wb\bar{b}$ within statistics. Given the relatively small statistics available for those two processes, and the larger statistics available for $Wb\bar{b}$, we have used the $Wb\bar{b}$ shape for all three contributions, as well as the small WW/WZ background.

Large single-top samples are available in the s channel and t channel separately. The s channel and the t channel contribute 60% and 40% of the single top background with our selection, respectively. Since the two channels have different kinematics, we expect the reconstructed mass distributions to be different. Even though the contributions are small, we make use of our ample statistics and treat the two channels as separate processes.

The most elusive background comes from QCD events, i.e. events with no real W to produce the isolated lepton and $\not\!\!E_T$. We looked at events in the data with non-isolated leptons, which are expected to be enriched in this type of background, but kinematically similar to our signal events. Within the limited statistics available, Figure 10 (left) shows that the reconstructed mass distribution of the QCD-enriched events is consistent with that of W+jets events. In order to improve the statistics, we also compare the W+jets template with a QCD-enriched template made without using a χ^2 cut and using all pre-tagged events where the most probable heavy-flavor jet (using jet probability) is required to be assigned to a b parton. These templates also appear to be very similar (Figure 10, right). A flattened

Table 6: The sources and numbers of background events in the $W + 3.5$-jet sample and the $W+ \geq 4$-jet sample, for 162 pb^{-1}. The quantities are shown before and after accounting for the top contamination.

Source	Initial estimate		Removing top contamination	
	$W + 3.5$ jets	$W+ \geq 4$ jets	$W + 3.5$ jets	$W+ \geq 4$ jets
W + jets (mistags)	1.8 ± 0.3	2.3 ± 0.5	1.6 ± 0.3	1.2 ± 0.3
$Wb\bar{b}$	1.2 ± 0.4	1.2 ± 0.5	1.0 ± 0.4	0.6 ± 0.3
$Wc\bar{c}$	0.5 ± 0.2	0.5 ± 0.2	0.4 ± 0.2	0.2 ± 0.1
Wc	0.6 ± 0.2	0.4 ± 0.2	0.5 ± 0.2	0.2 ± 0.1
WW/WZ	0.17 ± 0.03	0.12 ± 0.02	0.17 ± 0.03	0.12 ± 0.02
non-W (QCD)	1.7 ± 0.5	1.7 ± 0.5	1.7 ± 0.5	1.7 ± 0.5
Single top (S chan.)	0.18 ± 0.03	0.13 ± 0.02	0.18 ± 0.03	0.13 ± 0.02
Single top (T chan.)	0.12 ± 0.02	0.06 ± 0.02	0.12 ± 0.02	0.06 ± 0.02
Total	6.3 ± 0.9	6.4 ± 1.1	5.7 ± 0.8	4.4 ± 0.7

KS test gives a probability of 6.5% for the first plot, and 50.7% for the second. Given these similarities, we use the shape of the W+jets reconstructed mass template for the expected contribution from QCD.[18]

Thus we consider reconstructed mass distributions from the following processes:

- W + jets (mistags)
- $Wb\bar{b}$
- Single top in the s channel
- Single top in the t channel

The reconstructed mass template for the W+jets (mistag) sample is determined using the W + 4 parton sample—the E_T cut on partons is 8 GeV—and the mistag matrix. In particular, the b tags found in Monte Carlo are not used for this sample (and this sample alone). This is because the Monte Carlo b tagger is not trusted to model well the rate or kinematic dependences of fake tags. Instead, the mistag matrix is queried for each jet to determine the probability of getting a negative tag for that E_T, ϕ, η, N_{trk}, and ΣE_T. That probability is multiplied by 1.2 to account for the asymmetry in the L_{xy} of mistags, and the result is considered to be the probability to get a positive mistag on that jet. Next we consider each possible configuration of tags in the event. There are four single-tag configurations and six double-tag configurations. For each one we determine the best tag-consistent assignment of jets to partons, and fill the mass template with a weight corresponding to the probability of observing that tag configuration. The result is a weighted template for the

[18]This background could be controlled better. One idea is to apply additional cuts, such as the $\Delta\phi$ cut between $\not{E}_T$ and the leading jet, that will diminish the relative contribution of this poorly understood background.

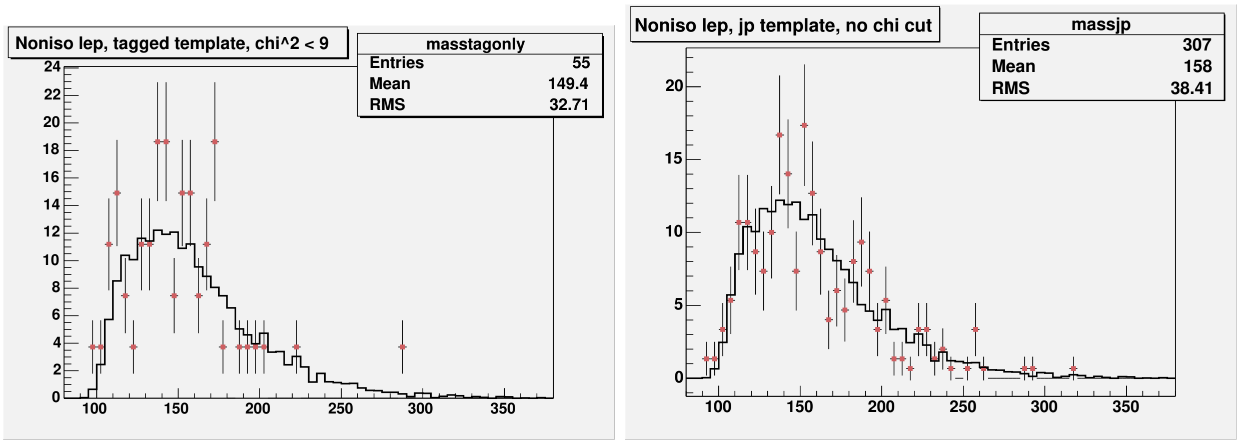

Figure 10: Comparison between W+jets templates (histograms) and data events with non-isolated leptons (points). The latter are thought to be enriched in non-W background. At left, the points are the default template, including the cut $\chi^2 < 9$. At right, the points are given improved statistics, both by eliminating the χ^2 cut, and by using the full pre-tagged sample, with jet probability to identify the most likely b jet.

mistag background. The reconstructed mass template for the $Wb\bar{b}$ and similar backgrounds is made using the $Wb\bar{b} + 2$ parton sample exactly as for the signal samples, and the single top templates are produced in the same way.

In order to estimate the number of background events in our mass fitting sample, we must account for the effect of the $\chi^2_{\min} < 9$ cut. The efficiency of this cut for background samples is around 60%–70% (see Table 7), taken directly from the fraction of events that pass the cut in our Monte Carlo samples. In the case of the mistag background, the uncertainty is inflated to account for possible differences in efficiency between mistag and QCD events. In the QCD-enriched data sample with non-isolated leptons, 55/68 tagged events survive the χ^2 cut, for an efficiency of $(81 \pm 5)\%$. We also have a small effect due to the requirement that a tag be on one of the leading four jets (CDF 6907 requires a tag on *any* tight jet). The efficiency for this requirement is also calculated from MC, and is given in Table 7 for ≥ 4-jet events; this requirement is by definition 100% efficient for W+3.5-jet events.

We do not allow each background contribution to vary independently in the final likelihood fit.[19] Instead, the eight contributions listed in Table 7 (3.5- and 4-jet contributions from each of four processes) are added with appropriate weights to create a combined background template, and the normalization of the combined shape is permitted to vary in the final likelihood fit (see section 4.3). Since the quantity that varies in the likelihood fit is the expectation value of the number of background events in the sample, we do not need to account for any counting error. The total number of background events is estimated to be 4.0 ± 0.6 in the $W + 3.5$ jet bin and 2.9 ± 0.5 in the $W+ \geq 4$ jet bin. The total background estimate for $W+ \geq 3.5$ jets is 6.8 ± 1.2. Detailed numbers are given in Table 7.

The mass templates for each process and the combined background mass template are shown in Figures 11 and 12. The systematic uncertainty due to background shape modeling

[19] This is one possible improvement, which may in addition give interesting information about the composition of our mass sample (though probably not much with current statistics).

Table 7: Top: the number of background events in each combined background sample. Middle: the efficiency of $\chi^2_{\rm min} < 9$ and requiring the tag on the leading four jets for each mass template. Bottom: the number of background events used in the mass fitting.

Background events without $\chi^2_{\rm min} < 9$			
Mass Template Source	Background Source	$W + 3.5$ jets	$W+ \geq 4$ jets
W + jets (mistags)	mistags, QCD	3.3 ± 0.6	2.9 ± 0.6
$Wb\bar{b}$	$Wb\bar{b}$, $Wc\bar{c}$, Wc, WW/WZ	2.1 ± 0.6	1.1 ± 0.4
Single top: s channel		0.18 ± 0.03	0.13 ± 0.02
Single top: t channel		0.12 ± 0.02	0.06 ± 0.02

Efficiency of cuts			
Mass template	$\chi^2_{\rm min} < 9$		Tag on leading 4 jets
source	$W + 3.5$ jets	$W+ \geq 4$ jets	$W+ \geq 4$ jets
W + jets (mistags)	0.716 ± 0.070	0.707 ± 0.070	0.973 ± 0.010
$Wb\bar{b}$	0.668 ± 0.011	0.692 ± 0.012	0.979 ± 0.004
Single top: s channel	0.598 ± 0.016	0.665 ± 0.018	0.994 ± 0.003
Single top: t channel	0.793 ± 0.026	0.564 ± 0.040	0.987 ± 0.009

Background events with $\chi^2_{\rm min} < 9$			
Mass Template Source	Background Source	$W + 3.5$ jets	$W+ \geq 4$ jets
W + jets (mistags)	mistags, QCD	2.4 ± 0.5	2.0 ± 0.5
$Wb\bar{b}$	$Wb\bar{b}$, $Wc\bar{c}$, Wc, WW/WZ	1.4 ± 0.4	0.7 ± 0.3
Single top: s channel		0.11 ± 0.02	0.09 ± 0.01
Single top: t channel		0.10 ± 0.01	0.03 ± 0.01
Total		4.0 ± 0.6	2.9 ± 0.5
		6.8 ± 1.2	

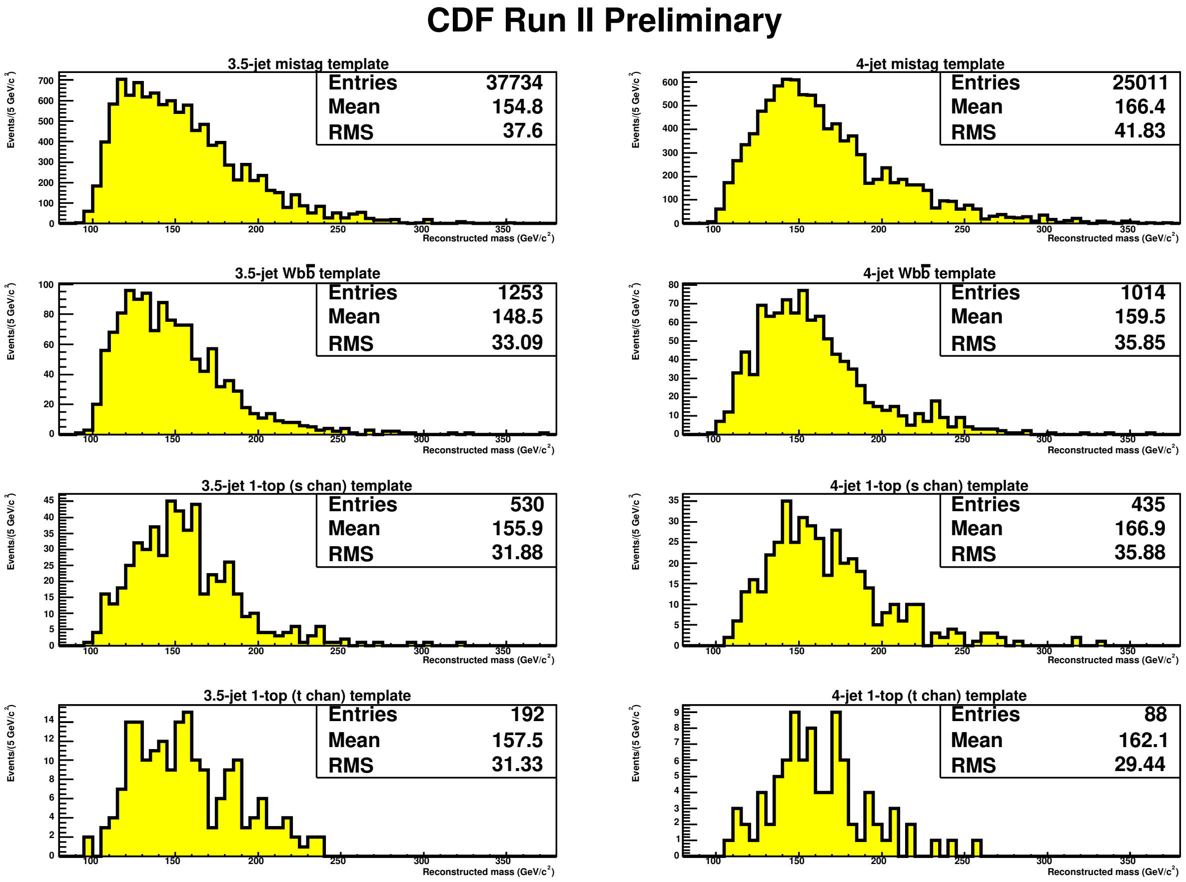

Figure 11: Reconstructed mass distributions for different background sources. On the left are the 3.5-jet templates, and on the right the 4-jet templates. From top to bottom: W+jets (mistags), $Wb\bar{b}$, single top (s channel), and single top (t channel).

will be obtained by comparing the fit masses when the mass template of each separate background process is used.

Finally, we determine the p.d.f. for the background reconstructed mass using a parameterization similar in spirit to that of the signal, but much simpler. First, there is obviously no dependence on top mass. Second, no narrow Gaussian peak is expected, so the full shape is modeled by "that function which is integrated to get the Gamma function." Specifically,

$$P_{bg}(m) = \frac{p_2^{1+p_1}}{\Gamma(1+p_1)} \cdot (m - p_0)^{p_1} e^{-p_2(m-p_0)}, \tag{4.3}$$

where m in GeV/c^2 is the reconstructed top mass. For our combined reconstructed mass template, shown in Figure 12, the fitted parameters are given in Table 8. After rebinning so that each bin has at least five predicted events, the χ^2 for the fit is 12, with 34 degrees of freedom.[20]

[20]The bin-by-bin uncertainties for the combined template may be incorrect, leading to an incorrect χ^2. The binned likelihood fit assumes a histogram filled with a constant weight.

Table 8: The fitted parameters for the background p.d.f. are given. The form of the parameterization is given in Equation 4.3.

Parameter (see Eq. 4.3)	Fitted value
p_0	94 ± 4
p_1	1.8 ± 0.5
p_2	0.045 ± 0.006
χ^2/n.d.o.f.	12/34

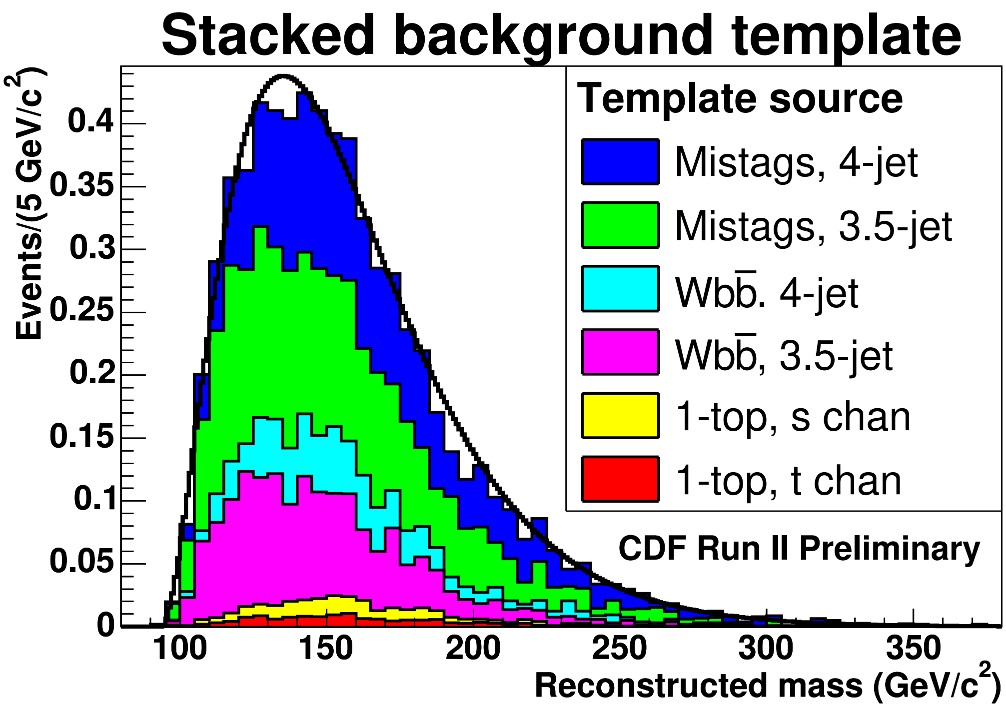

Figure 12: Reconstructed mass distribution of the combined backgrounds. The contributions from different background processes are stacked. Overlaid is the fitted curve (see Eq. 4.3) with parameters given in Table 8.

4.3 Likelihood

To measure the top mass, we compare the reconstructed mass distribution from data to a sum of p.d.f.'s from signal (section 4.1) and background (section 4.2) Monte Carlo using an unbinned extended likelihood fit.

There are 18 parameters in the parameterization of the signal p.d.f.'s as a function of $\mathrm{M_{top}}$, and 3 in the parameterization of the background p.d.f. All 21 of these are permitted to vary in the likelihood fit; they are constrained by the covariance matrices output from their independent binned likelihood fits.

The extended likelihood fit involves parameters for the expectation values of the number of signal and background events. It contains terms that treat the possible Poisson fluctuations of these quantities. In the absence of prior constraints, the best fit expectation values are the same as the best fit for the number of signal or background events in the sample, but this is no longer the case when for example the expected number of background events is constrained. The 22$^{\mathrm{nd}}$ parameter in the unbinned likelihood fit is the expectation value for the number of signal events, and the 23$^{\mathrm{rd}}$ parameter is the expectation value for the number of background events. The former is unconstrained, and the latter is constrained by a simple Gaussian. We also perform fits where the background fraction is not constrained. In this case (and technically even in the constrained case), the best fit may have an unphysical background fraction, i.e. $f_{bg} < 0$ or $f_{bg} > 1$.[21]

Finally, the true top mass is the final (and most interesting!) parameter. It has no constraint. Its initial value is 175 GeV/c^2. The likelihood is maximized with respect to all 24 parameters using the MINUIT package.

The likelihood is given by:

$$\mathcal{L} = \mathcal{L}_{shape} \times \mathcal{L}_{bg} \times \mathcal{L}_{params}; \tag{4.4}$$

$$\mathcal{L}_{shape} = \frac{e^{-(n_s+n_b)}(n_s+n_b)^N}{N!} \prod_{i=1}^{N} \frac{n_s P_{sig}(m_i;\mathrm{M_{top}}) + n_b P_b(m_i)}{n_s+n_b}; \tag{4.5}$$

$$-\ln \mathcal{L}_b = \frac{(n_b - n_b^{exp})^2}{2\sigma_{n_b}^2}; \tag{4.6}$$

$$-\ln \mathcal{L}_{params} = \sum_{i=0}^{17}\sum_{j=0}^{17} \frac{1}{2}(\delta p_i^{sig} C_{ij}^{sig} \delta p_j^{sig}) + \sum_{i=0}^{2}\sum_{j=0}^{2} \frac{1}{2}(\delta p_i^{b} C_{ij}^{b} \delta p_j^{b}); \tag{4.7}$$

where the last two terms are given as the negative log likelihood for simplicity. N is the total number of events observed in the data, m_i is the reconstructed mass of the ith event, P_{sig} is the signal p.d.f. defined in Equation 4.1, P_b is the background p.d.f. defined in Equation 4.3, $\mathrm{M_{top}}$ is the value of the true top mass parameter, C is the inverted error matrix from either of the binned likelihood fits for the p.d.f. parameters, and δp_i is the difference between the fitted ith parameter and the input, for signal or background.

We note that since we fit for both $\mathrm{M_{top}}$ and n_s, the expectation value of the number of signal events, we could extract the top mass and the $t\bar{t}$ cross-section simultaneously (given the efficiency of our χ^2 cut on signal events, plus various other quantities already available).

[21] Is it reasonable to allow this in our likelihood function?

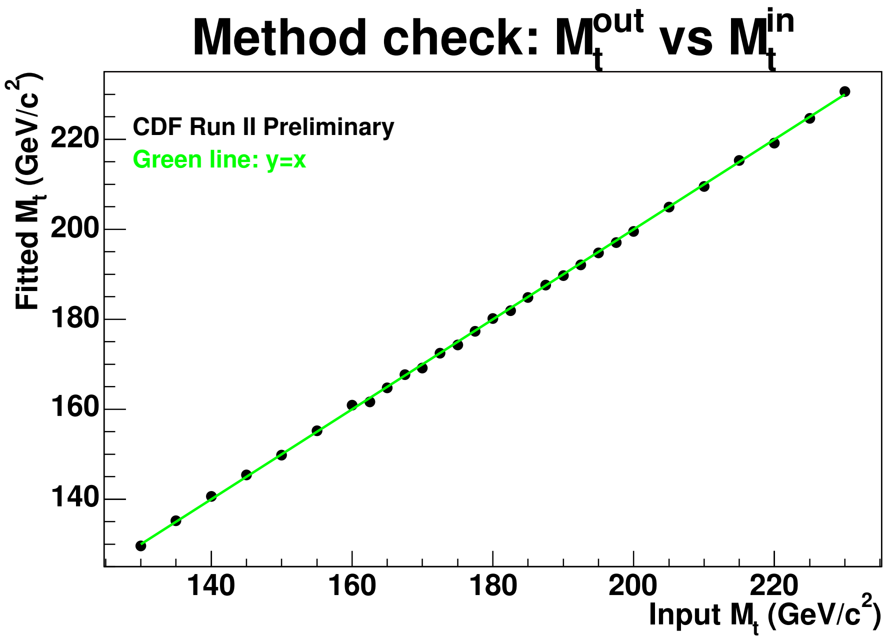

Figure 13: The returned (fit) top mass as a function of the input top mass. The line is drawn with slope of 1. Pseudoexperiments with 28 events each were performed, and the median of those pseudoexperiments is plotted here.

It would be interesting to do this exercise and see the cross-section value we observe, as well as its correlation with the top mass.

We check the fitting procedure on our Monte Carlo samples. Checking whether the likelihood fit returns the correct mass for a wide range of the input top masses is performed by comparing the fit mass using pseudoexperiments with the input top mass. (See Appendix A for details on the generation of pseudoexperiments.) We use 28-event pseudoexperiments, with a background constraint of 7.0 ± 0.8 events. As illustrated in Figure 13, the slope of the linear fit between the input and fit top mass is consistent with 1. The centers and widths of the associated pull distributions are checked in Figure 14. The pull widths are consistently larger than one. We believe this is an unavoidable problem with trying to describe non-Gaussian errors with a single "1σ" uncertainty. However, we would like our quoted $\pm 1\sigma$ statistical uncertainties to cover the true mass value (neglecting systematic effects) 68% of the time. To achieve this effect, we scale the raw uncertainties by an appropriate factor. Please see Appendix B for more details.

4.4 Expected Statistical Uncertainty

The raw expected statistical uncertainty (before scaling as described in Appendix B) on the top mass from 32 top candidate events with 7.0 ± 0.8 expected background events is estimated from pseudoexperiments. Figure 15 shows the raw expected uncertainty as a function of the top mass for both the default measurement ($\geq 3.5-$jet events) and the 4-jet-only measurement. The default measurement is expected to perform slightly better across the board.

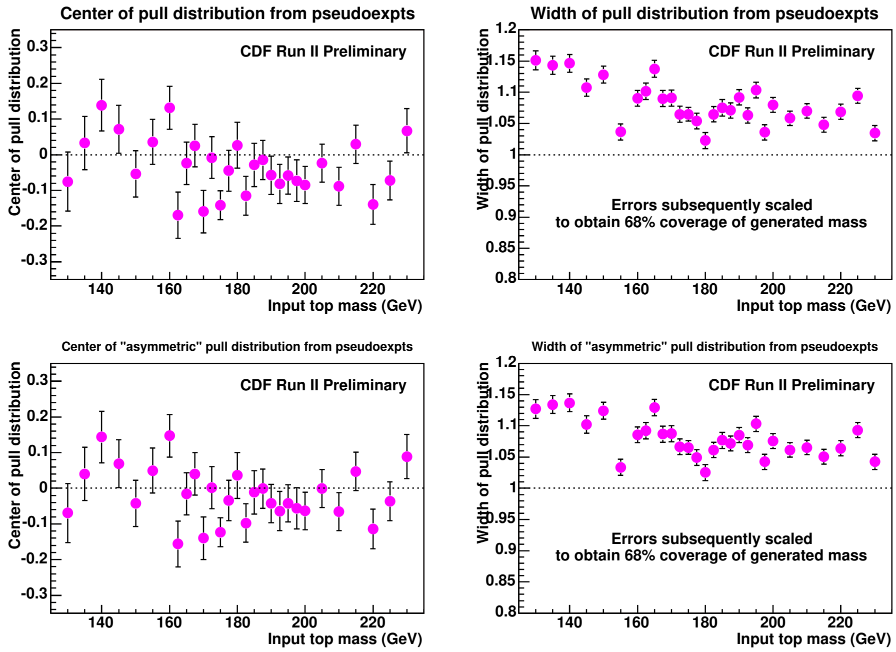

Figure 14: The center (left) and the width (right) of the mass pull distribution from 28-event pseudoexperiments ($\geq 3.5-$jet events) as a function of the input top mass. Top plots use a symmetrized error, while the bottom plots make use of the reported asymmetric errors.

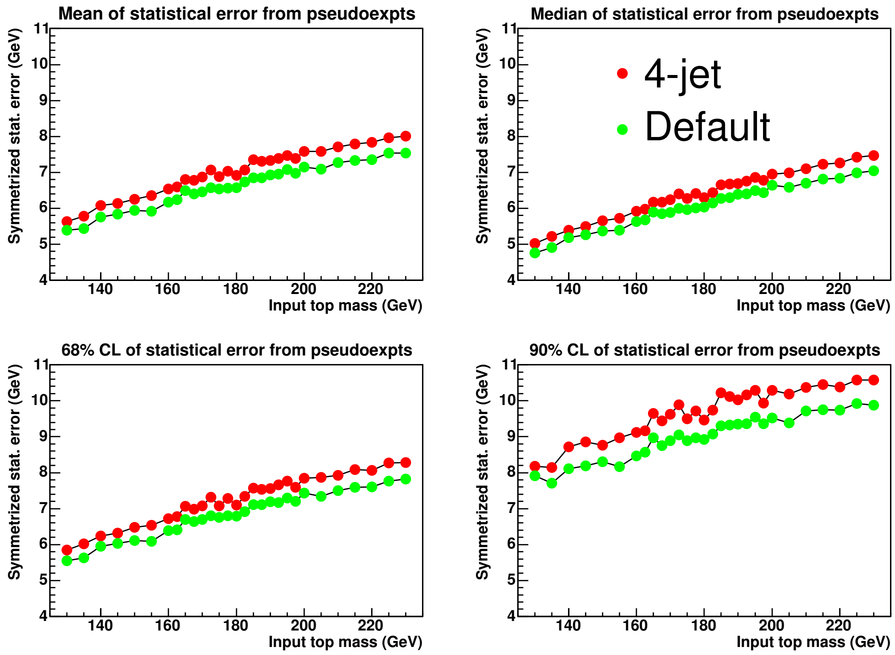

Figure 15: The estimated raw statistical uncertainty as a function of the input top mass using mean, median, 68% CL, and 90% CL. From 10,000 28-event pseudoexperiments. The blue (lower) curve is for the default measurement ($\geq 3.5-$jet events), and the purple (upper) curve is for the measurement using only 4-jet events (19-event pseudoexperiments).

5 Results from the data

Figure 16 (top) shows the reconstructed mass distribution from the data with ≥ 3.5 jets, compared to a combination of the parameterized signal template at the fit mass and the combined background Monte Carlo template when the background normalization is constrained. The likelihood curve as a function of top mass is also shown in the inset. The extracted top mass is

$$\mathrm{M_{top}} = 174.9\ ^{+6.7}_{-7.2}\ \text{(stat.) GeV}/c^2.$$

We check the KS probability for the data against the fitted signal and background templates. Normalizing the probability using sets of events drawn from the fitted templates, as recommended by Igor Volobouev, we find a probability of 21.9% for the data. When a finer binning is used (3 GeV/c^2 instead of 15 GeV/c^2), we find a probability of 34.4%.

We also perform the fit without the background constraint as a check. In this case, shown in the bottom plot of Figure 16, the fitted mass is

$$\mathrm{M_{top}} = 177.7\ ^{+9.2}_{-8.3}\ \text{(stat.) GeV}/c^2.$$

In this case the normalized KS probabilities are 76.4% for 15 GeV/c^2 binning, and 89.9% for 3 GeV/c^2 binning. The number of background events favored by the fitter in the unconstrained fit is 16.6 $^{+8.2}_{-7.3}$, more than one sigma higher than the estimate of 6.8 ± 1.2. After scaling to achieve 68% coverage of the true mass value, as described in Appendix B, the default measurement with statistical error becomes

$$\mathrm{M_{top}} = 174.9\ ^{+7.1}_{-7.7}\ \text{(stat.) GeV}/c^2.$$

The fitted top mass and background values are summarized in Table 9.

We check that the statistical uncertainty seen in the data is consistent with expectations for our measured mass. Figure 17 shows the expected positive and negative uncertainty distributions for an input top mass of 175 GeV/c^2, where the arrows indicate the statistical uncertainties in the data. About 66% of the positive errors are smaller than our observed positive error of +7.1 GeV/c^2, and about 80% of the negative errors are smaller (in magnitude) than our observed negative error of −7.7 GeV/c^2. Figure 18 shows the same quantities in two dimensions so that the correlations are apparent. In Figures 17 and 18, the scaled uncertainties are used.

Finally, we perform the 4-jet likelihood fit to the 19 such events in the data. The extracted top masses with and without the background constraint are

$$\mathrm{M_{top}} = 179.4 \pm 6.2\ \text{(stat.) GeV}/c^2,$$

and

$$\mathrm{M_{top}} = 179.5\ ^{+6.6}_{-6.2}\ \text{(stat.) GeV}/c^2,$$

respectively. The reconstructed mass distribution and the fit results are shown in Figure 19 and Table 9. Although the statistical uncertainty on the 4-jet sample happens to be smaller than that of the 3.5-jet sample, the 3.5-jet result is the primary measurement, and the 4-jet result is considered a check.[22]

[22] As mentioned in footnote 2, optimization of the analysis with respect to the fourth jet cut will be considered in the future.

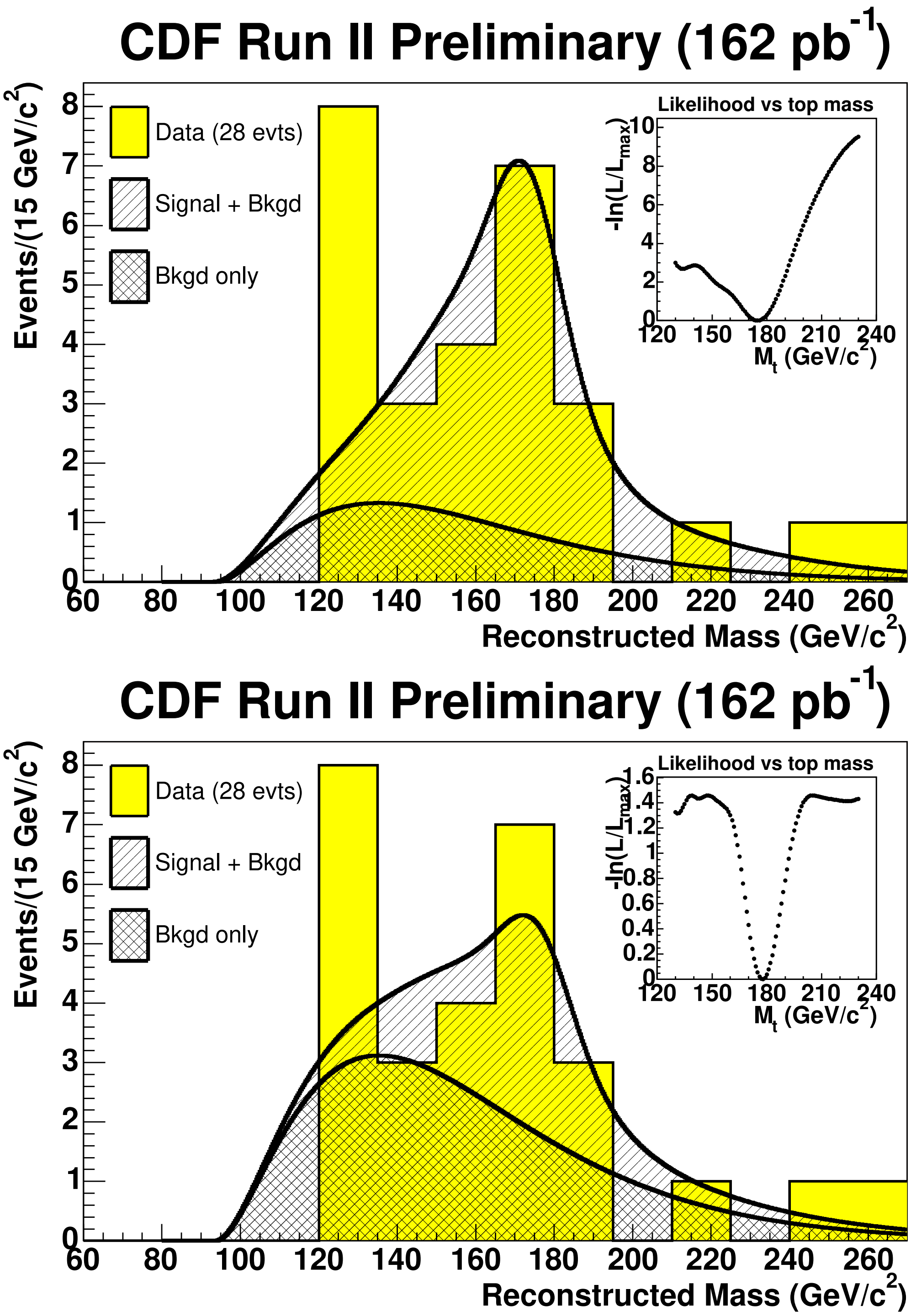

Figure 16: The reconstructed mass distribution plotted with the expected distributions from the Monte Carlo signal template at the fit mass and the background template for the $W+\geq 3.5$ jet sample. The background normalization is constrained in the upper plot and not constrained in the lower plot. In the lower plot, the points on the likelihood curve (inset) for which 139 GeV/$c^2 \leq \mathrm{M_{top}} \leq$ 147 GeV/c^2 and 206 GeV/$c^2 \leq \mathrm{M_{top}}$ are best fit with $f_{bg} > 1$.

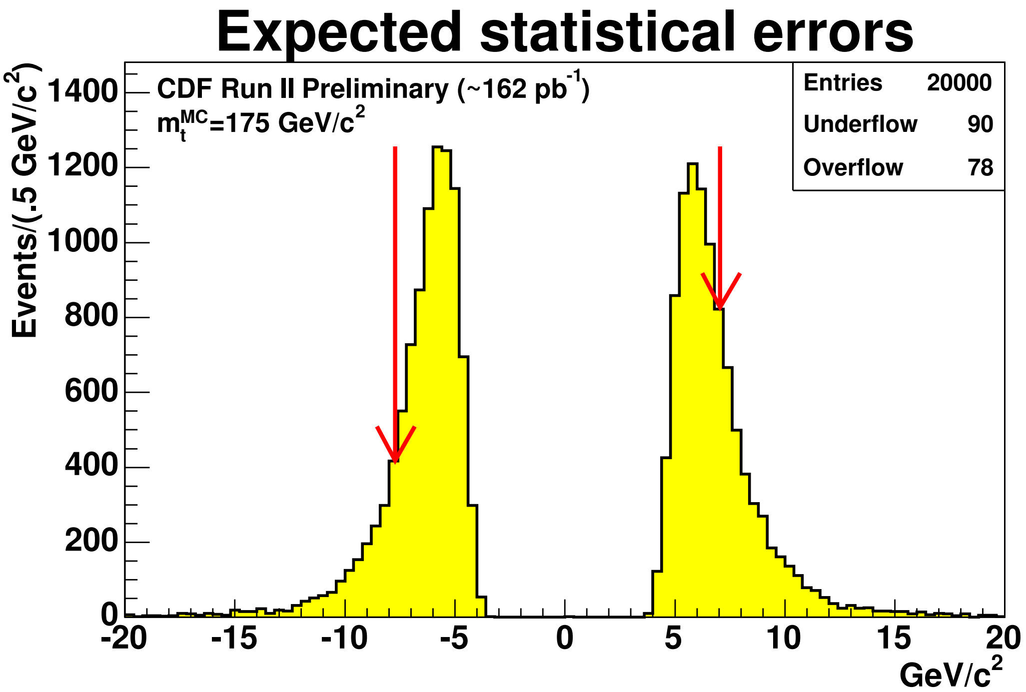

Figure 17: The positive and negative scaled statistical uncertainty distributions from 10,000 28-event pseudoexperiments for an input top mass of 175 GeV/c^2. The red arrows indicate the statistical uncertainties in the data.

Table 9: Results of likelihood fit with and without background constraint. The measurement in bold is the primary result for this analysis. In the last column, the statistical uncertainties are scaled to provide 68% coverage of the true mass value (see Appendix B).

Category	Background (events)		$M_{top}(GeV/c^2)$	$M_{top}(GeV/c^2)$
	input	output		(scaled errors)
$W+\geq 3.5$ jets	6.8 ± 1.2	7.1 ± 1.2	$174.9\ ^{+6.7}_{-7.2}$	$\mathbf{174.9\ ^{+7.1}_{-7.7}}$
	no constraint	$16.6\ ^{+8.2}_{-7.3}$	$177.7\ ^{+9.2}_{-8.3}$	
$W+\geq 4$ jets	2.9 ± 0.5	2.9 ± 0.5	179.4 ± 6.2	
	no constraint	$3.2\ ^{+6.5}_{-5.5}$	$179.5\ ^{+6.6}_{-6.2}$	

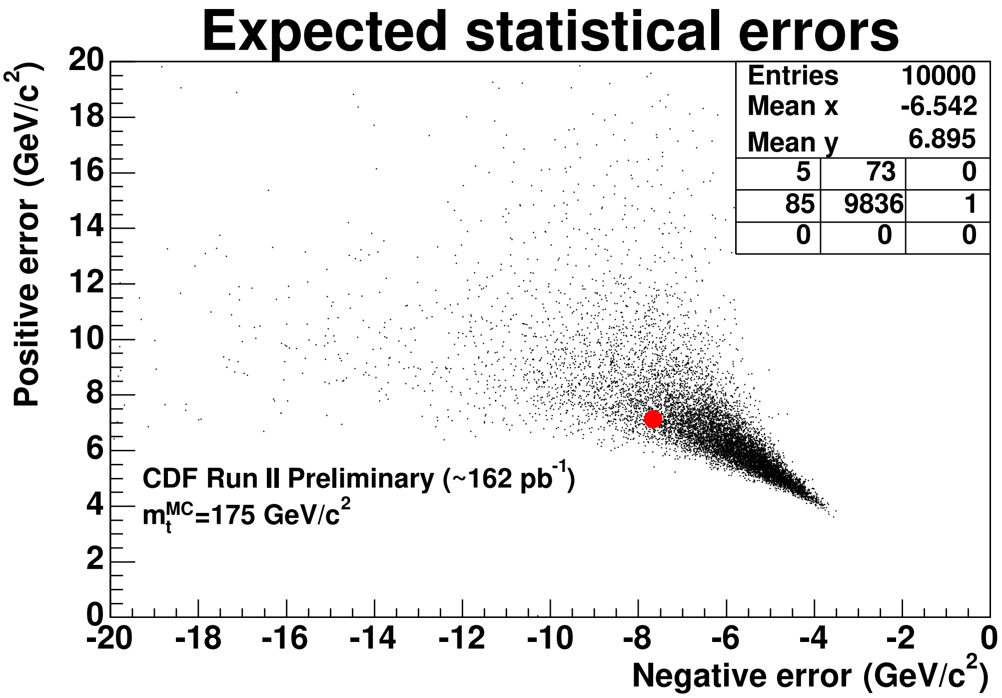

Figure 18: The positive vs negative scaled statistical uncertainty from 10,000 28-event pseudoexperiments for an input top mass of 175 GeV/c^2. The red point indicates the positive and negative statistical uncertainties in the data.

6 Systematic Uncertainties

In the limit of perfect Monte Carlo generation and perfect detector simulation, this method would have no systematic errors. A more optimal event-by-event mass reconstruction would produce a measurement with better statistical resolution, but *any* shifts or effects in the reconstructed mass distribution would be, on average, the same in Monte Carlo and data, so that no systematic effects could be present. Of course, that condition does not obtain. But it is helpful to understand that all systematics are, at their root, due to differences between the data and our Monte Carlo description both of physical processes and of our detector.

We have considered the following sources of systematic uncertainties on the top mass: jet energy scale/jet fragmentation, jet resolution, the generated top p_T distribution, our understanding of the reconstructed mass shape in the background events, the amount of initial and final state radiation, parton distribution functions, and the SecVtx b-tagging scale factor.

Systematic uncertainties are estimated by looking at simulated Monte Carlo samples, in order to avoid biases due to the particular set of events in the data. For each source of systematic uncertainty, we vary quantities associated with the uncertainty source by $\pm 1\sigma$, and produce new 175 GeV/c^2 $t\bar{t}$ signal and background Monte Carlo templates by performing event selection and mass reconstruction on the modified samples. We draw events for pseudoexperiments from these new templates, but the signal and background p.d.f.'s are always unchanged. We then find the shift in the median fitted top mass for a large ensemble of

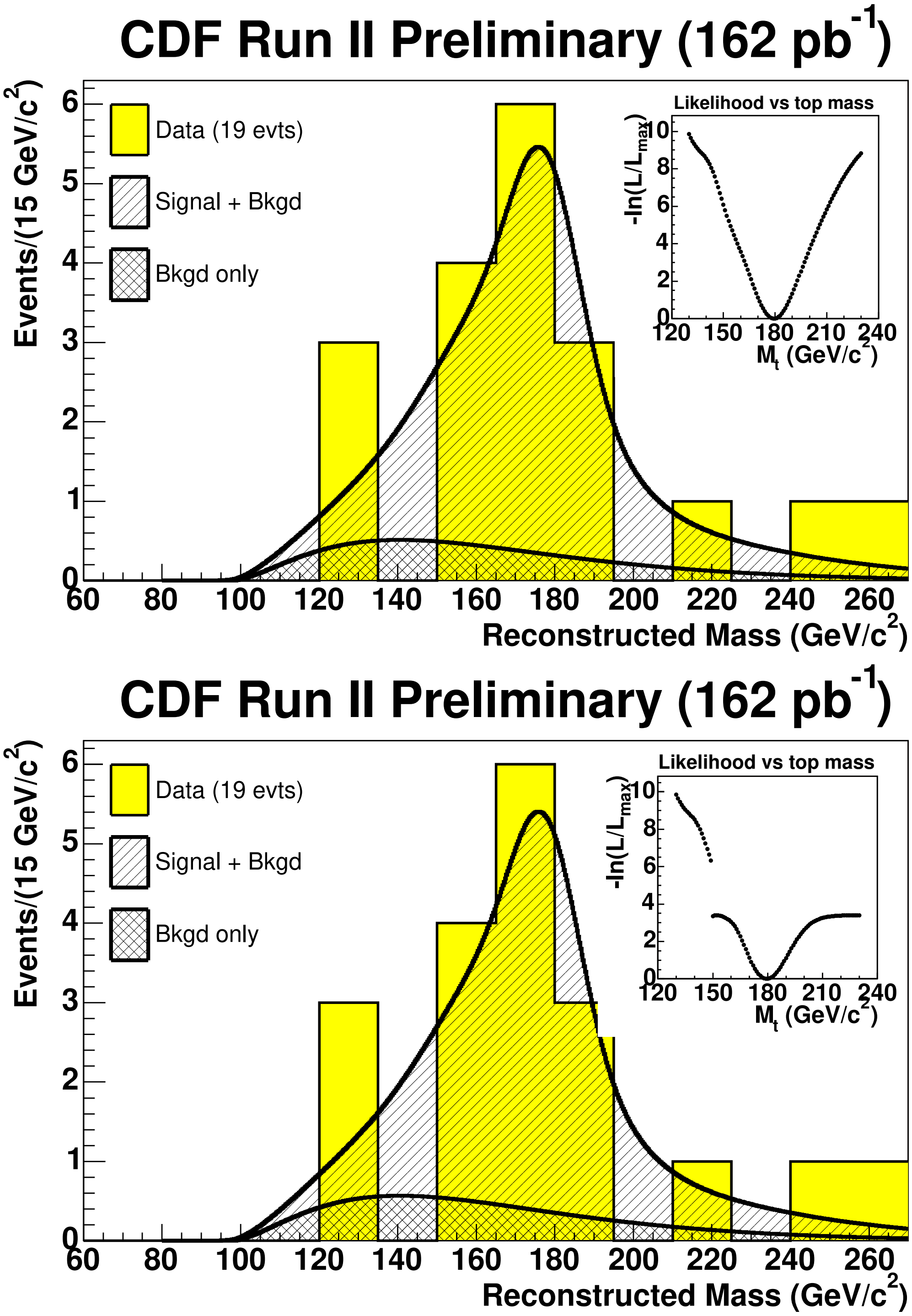

Figure 19: The reconstructed mass distribution plotted with the expected distributions from the Monte Carlo signal template at the fit mass and the background template for the $W+\geq 4$ jet sample. The background normalization is constrained in the upper plot and not constrained in the lower plot. In the lower plot, the points on the likelihood curve (inset) for which 150 GeV$/c^2 \leq \mathrm{M_{top}} \leq 152$ GeV$/c^2$ are best fit with $f_{bg} > 1$.

Table 10: Systematic uncertainties on the relative jet corrections for data and simulation.

η range	data	simulation
$\|\eta\| < 0.2$	3%	1%
$0.2 < \|\eta\| < 0.6$	0.5%	1%
$0.6 < \|\eta\| < 1.0$	2%	1%
$1.0 < \|\eta\| < 1.4$	4%	7%
$1.4 < \|\eta\| < 2.0$	2%	6%
$\|\eta\| > 2$	7%	7%

pseudoexperiments. Please see Appendix A for details regarding pseudoexperiments, including a discussion of the uncertainties we quote for the systematic shifts. The uncertainty on a given systematic shift is added in quadrature to the shift to obtain the quoted systematic error.

Unless otherwise noted, all systematics described here have been estimated using 28-event pseudoexperiments with background of 7.0 ± 0.8.

6.1 Jet energy scale and jet fragmentation

The procedure to evaluate the jet systematics is as follows.

6.1.1 Uncertainties on the jet energy

The details of the jet corrections and the sources and amounts of systematic uncertainties are documented in CDF note 6565 [17], and they are briefly described below:

- The η dependence in calorimeter response with respect to the central calorimeter is removed by applying corrections ("level 1") derived from the dijet balancing procedure and is tested by the photon-jet balancing in data and simulation. The uncertainties take into account residual spline-interpolation effects, biases in the di-jet balancing procedure, especially in the crack region, variation of plug calorimeter response with them, differences seen in the photon-jet balancing, and half the differences between the corrections for data and simulation. Table 10 summarizes the uncertainty which depends on η.

- The corrections for the central calorimeter stability is included in "level 2" and an uncertainty of 1% is assigned.

- Another systematic uncertainty is associated with the "level 3" corrections for the central calorimeter responses. The difference between run I and run II is studied using the photon-jet balancing (jets in the central region) and is measured to be 5%, out of which $> 2\%$ difference comes from the difference in the CEM scale definition and the difference in the material before the tracking volume. The remaining 3% is taken as a systematic uncertainty in data.

Table 11: Uncertainties on the jet corrections and the top mass differences associated with the uncertainties. The items with ** are expected to be different between `v4.9.1hpt1` and `v4.11.1 REMAKE`.

Source of Corrections		ΔM_{top} (GeV/c^2)		
Level	Description	`v4.9.1hpt1`	`v4.11.1 REMAKE`	
		≥ 3.5 jets	≥ 3.5 jets	≥ 4 jets
1 (sim)	η-Dependent Calibration **	3.77 ± 0.24	2.40 ± 0.11	2.53 ± 0.11
1 (data)	η-Dependent Calibration **	0.91 ± 0.24	1.74 ± 0.11	1.89 ± 0.11
2 (data)	Calorimeter Stability	0.99 ± 0.24	0.88 ± 0.11	1.11 ± 0.11
3 (sim)	Raw Scale (central) **	4.45 ± 0.24	3.57 ± 0.11	3.60 ± 0.11
3 (data)	Raw Scale (central) **	4.87 ± 0.24	2.72 ± 0.11	2.82 ± 0.11
5	Absolute Scale	2.17 ± 0.24	2.20 ± 0.11	2.34 ± 0.11
7	Out-of-cone: up to cone 1.0	1.21 ± 0.24	1.72 ± 0.11	1.79 ± 0.11
	Out-of-cone: outside cone 1.0	1.15 ± 0.24	1.47 ± 0.12	1.49 ± 0.11
Total		7.9 ± 0.7	6.3 ± 0.3	6.6 ± 0.3

A maximal difference of 5% between data and simulation is found. An uncertainty of 4% is estimated for the simulation by subtracting the data uncertainty (3%) in quadrature.

- The "level 5" corrections account for the calorimeter non-linearity, fragmentation, and underlying event.
- The final step in the generic corrections corrects for energy that lands outside the jet cone, thus, energy between $R = 0.4$ and $R = \infty$ ("level 7"). The out-of-cone energy is due to fragmentation (or final state radiation in the limit of one hard radiated gluon) and to particles swept out by the magnetic field. The uncertainty on this is estimated in two parts, one between $R = 0.4$ and $R = 1.0$ and the other between $R = 1.0$ and $R = \infty$.

The systematic uncertainties on the jet energy scale and fragmentation are summarized in Table 11.

6.1.2 Uncertainties on the top mass due to the jet energy systematics

For each systematic uncertainty defined by the jet corrections group, we apply a systematic shift to the jets in both the positive ($+1\sigma$) and negative (-1σ) directions. In each case, a mass fit is performed on every event in a given MC sample using the shifted jets. Thus the mass fitter is run $2 \times N_{syst}$ times on each event, where N_{syst} is the number of systematic uncertainties due to the jet energy scale.

For each shift (say, the uncertainty due to the level 3 corrections, -1σ), a reconstructed mass distribution is generated using all standard analysis cuts. A large number of pseudo-experiments are performed, drawing events from that shifted distribution. The number of events in each pseudoexperiment, and the background constraint, is the same as in the fit to the data events.

Each systematic uncertainty is defined as half the difference between the medians of the results of the $+1\sigma$ and the -1σ pseudoexperiments.

For level 1–3 corrections, the systematics uncertainties are different, and independent, for Monte Carlo and data jets. In order to estimate the uncertainty due to data jet systematics, we need to apply those data jet systematic shifts to Monte Carlo jets. We ask for three jet corrections for each jet: version 0 (MC), syscode 0 (default); version 4 (data), syscode e.g. 2 (cal. stability, $+1\sigma$); version 4 (data), syscode 0 (default). Then define the shift Δ as the difference between the latter two corrections. Then apply the correction ("corr" + Δ), where "corr" is the first correction above, to the default MC correction. Each jet is corrected thusly, and the rest of the procedure is as above.

The out-of-cone and splash-out uncertainty need to be treated differently since they are defined only for level 7 corrected jets and we use now level 5 corrected jets. We take the absolute difference in p_T of the fully corrected jets and add it to the level 5 corrected jets. This is expected to slightly overestimate the systematic uncertainty, but the effect is small and doesn't affect the total jet systematic uncertainties.

Table 11 lists the uncertainties for this analysis as well as the uncertainties that we measured with the pre-shutdown data and the offline version `4.9.1hpt1`. The total systematic uncertainty in the top mass due to jet energy determination is estimated to be 6.3 ± 0.3 GeV$/c^2$ for the measurement using the $W+ \geq 3.5$ jet sample. With the $W+ \geq 4$ jet sample, the uncertainty is estimated to be 6.6 ± 0.3 GeV$/c^2$, slightly larger than the uncertainty for the ≥ 3.5-jet sample. As illustrated in Figure 20 (top), there seems to be a small correlation between the uncertainty and ΣE_T^{4j}. The ΣE_T^{4j} of the ≥ 4-jet sample is higher than that of the ≥ 3.5-jet sample.

6.2 Generators

The estimation of the generator effect is performed using Pythia and Herwig generators. When the 175 GeV$/c^2$ Herwig and Pythia $t\bar{t}$ samples are used to produce pseudoexperiments, the returned top mass difference between them is found to be 0.3 ± 0.3 GeV$/c^2$ (see Table 12). We assign this to be the uncertainty due the generators. Note that this uncertainty is probably correlated with the jet fragmentation uncertainty (cf. level 5 and level 7 jet uncertainties).

6.3 Initial state radiation

The initial state radiation effect is studied using Rick Field's Pythia tune A, as well as Pythia with ISR enhanced and reduced as recommended by the top mass group. The results are summarized in Table 12. Since the median top mass from the default Pythia sample is not between the median top mass from the "less ISR" and the "more ISR" samples, we use the largest difference, 0.3 ± 0.3 GeV$/c^2$, as the systematic.

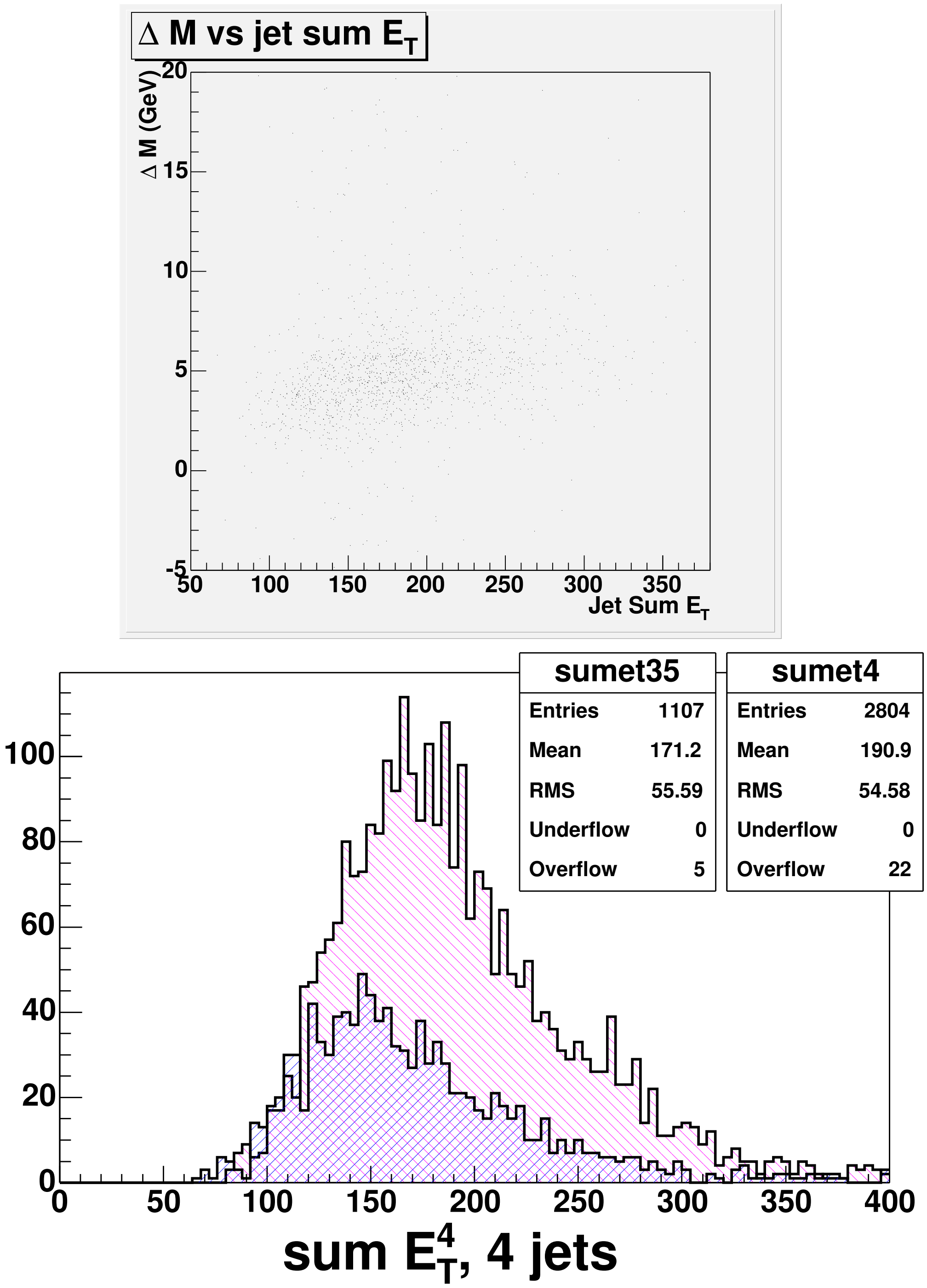

Figure 20: Upper plot: the uncertainty in top mass due to syscode-3 jet energy corrections as a function of ΣE_T of 4 jets. Lower plot: the ΣE_T distributions are compared between the $W + 3.5$ jet sample and the $W+ \geq 4$ jet sample.

Table 12: The top mass shift for various signal templates relative to a default are listed. We include the results from the DLM analysis for comparison [18].

Source		Dataset	ΔM_{top} (GeV/c^2)		
			Template		DLM
			≥ 3.5 jets	≥ 4 jets	$= 4$ jets
Gen	**Pythia - Herwig**	ttopei - ttopli	$+0.3 \pm 0.3$	$+0.2 \pm 0.3$	$+0.6 \pm 0.2$
PDF	**MRST72 - CTEQ5L** (diff. group)	ttop3e - ttopei	0.0 ± 0.3	-0.2 ± 0.3	-1.0 ± 0.2
	MRST75 - MRST72 (α_s var.)	ttop4e - ttop3e	$+0.2 \pm 0.3$	$+0.6 \pm 0.3$	$+0.7 \pm 0.2$
	CTEQ6M - CTEQ5L (NLO - LO)	ttop7e - ttopei			-0.3 ± 0.2
ISR	Tune B - Tune A	ttop5e - ttopei	$+0.6 \pm 0.3$	$+0.5 \pm 0.3$	-0.2 ± 0.2
	Less ISR	ttopbe - ttopei	$+0.3 \pm 0.3$	$+0.3 \pm 0.3$	-0.2 ± 0.2
	More ISR	ttopce - ttopei	$+0.3 \pm 0.3$	$+0.6 \pm 0.3$	$+0.3 \pm 0.2$
FSR	α_s var.	ttop6e - ttop3e	$+1.2 \pm 0.3$	$+1.4 \pm 0.3$	$+0.8 \pm 0.2$
	NLO corr. off -on	ttopae - ttopei	-1.4 ± 0.3	-1.5 ± 0.3	-1.0 ± 0.2
	Less FSR	ttopde - ttopei	$+0.7 \pm 0.3$	$+0.7 \pm 0.3$	-0.4 ± 0.2
	More FSR	ttopee - ttopei	$+0.8 \pm 0.3$	$+1.0 \pm 0.3$	$+0.5 \pm 0.2$
Spin	off - on	ttopge - ttopli	$+0.6 \pm 0.3$	$+0.8 \pm 0.3$	$+0.7 \pm 0.2$

6.4 Final state radiation

The final state radiation effect is studied by varying the amount of final state radiation in the event as recommended by the top mass group. The results are summarized in Table 12. Since the median top mass from the default Pythia sample is not between the median top mass from the "less FSR" and the "more FSR" samples, we use the largest difference, 0.8 ± 0.3 GeV/c^2, as the systematic.

6.5 Parton distribution functions

The effect of PDFs is studied using the reweighting technique [19]. In contrast to previous versions of this analysis, we do not reconstruct samples independently generated and simulated using various PDFs. Instead, one single sample is used (the standard HERWIG 175 GeV/c^2 sample `ttopli`), and reconstructed mass templates for each PDF are generated by weighting the mass for each event by the probability for that event to proceed according to the given PDF (relative to the default PDF).

We generate 46 reconstructed mass templates, where the PDFs used are

0 – CTEQ5L Our default PDF. The relative weight for every event is identically 1.

1 – MRST72 Leading order PDF using more or less the same data as our default but fitted by a different group. No significant difference is expected relative to the default, but if a difference is found, it should be taken as a systematic.

2 – MRST75 Same as previous, but using different value of α_s, corresponding to $\Lambda_{QCD} =$ 300 MeV vs $\Lambda_{QCD} = 228$ MeV for previous. The difference between these two PDFs is taken as a systematic.

3 – CTEQ6L More recent fit from CTEQ group, still leading order.

4 – CTEQ6L1 ???

5 – CTEQ6M This is the next-to-leading order PDF from the CTEQ group. Using a leading order matrix element, as the one found in HERWIG, in conjunction with this PDF will not give a correct description of event rates. However, we assume in the following that the *relative* behavior of various NLO PDFs is accurately modeled even though we use a LO matrix element.[23]

6–45 – CTEQ6M uncertainty PDFs These PDF sets encode the uncertainty in the CTEQ6M PDF. The possible variations are separated into contributions from 20 independent eigenvectors. Each eigenvector has a "$+1\sigma$" and a "-1σ" set, so for example sets 5 and 6 correspond to the $\pm 1\sigma$ variations of eigenvector 1, and sets 45 and 46 to $\pm 1\sigma$ of eigenvector 20.

[23] This assumption breaks down at some point since, for example, the contribution from gluon-gluon fusion in NLO is 2-3 times as important as in LO. Thus contributions to the systematics due to uncertainty in the gluon distribution may be underestimated since we use a LO matrix element.

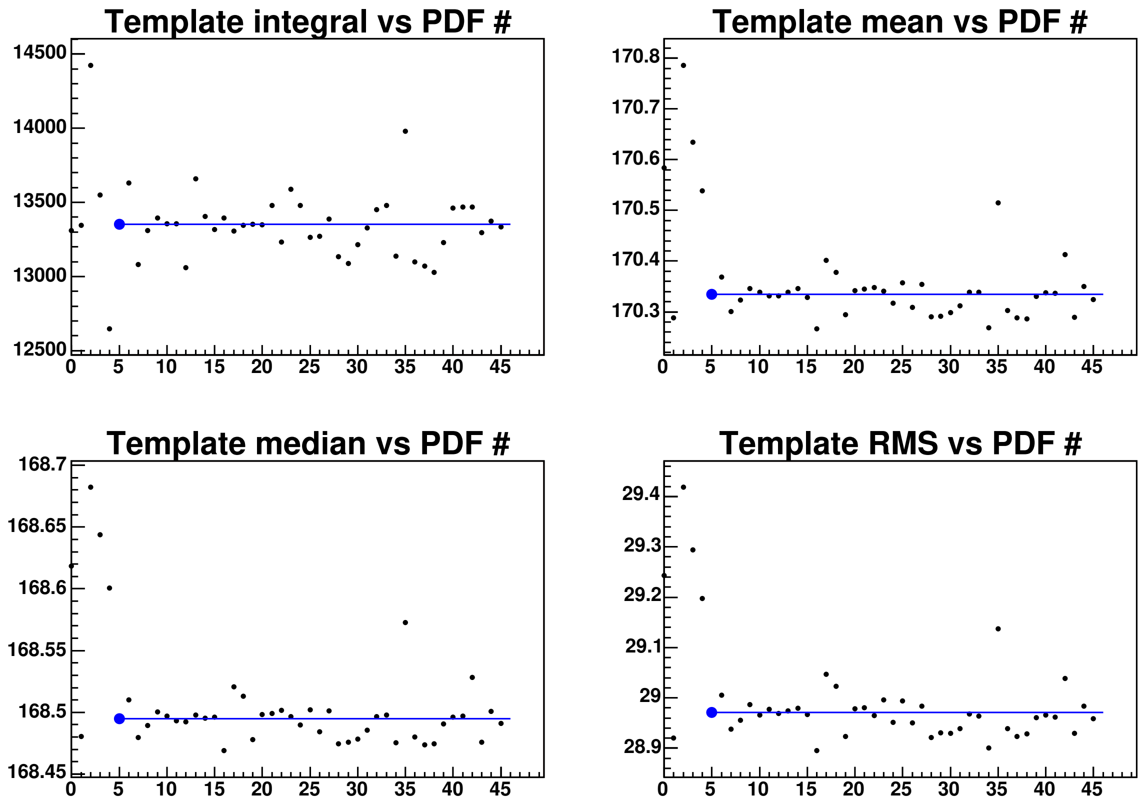

Figure 21: The integral (top left), mean (top right), median (bottom left), and RMS (bottom right) for each reweighted template are plotted vs PDF number. The central value NLO PDF (#5) is highlighted in blue, and a blue line is drawn through the 40 systematic PDFs at its value.

Interesting quantities from the resulting 46 templates are shown in Figure 21. Each plot shows some information about the reweighted templates vs PDF number, and in each plot the central value NLO PDF (#5) is highlighted in blue, and a blue line is drawn through the 40 systematic PDFs at that value. The integral (top left) gives information about the change in the overall cross-section (folded in with our selection cuts). Again, our generator uses LO PDFs with a LO matrix element, so the comparison with NLO PDFs is not too meaningful. But throughout this exercise, we're assuming that at least the differences between NLO PDFs can be trusted. The mean (top right), median (bottom left), and RMS (bottom right) of the templates track each other closely, but not exactly. A simple mechanism for change in the template, such as a linear slope in PDF probability vs reconstructed mass, is equivalent to rescaling the x axis, and would cause these three quantities to move together.

Note the y-axis scale in Figure 21. The differences are quite small. The largest effect in the CTEQ systematics is expected *a priori* for eigenvector #15, corresponding to PDFs 34 and 35. This is the systematic dealing with the gluon distribution at high x. Indeed, the difference in the template medians is largest for this eigenvector, but it is only of the order of 0.1 GeV/c^2. Slightly larger differences are observed between PDF sets 0, 1, and 2.

Next we perform pseudoexperiments using each reweighted template as the signal input, in order to estimate the systematics. The background input template is always our default.[24] Now, an important advantage of the reweighting technique is that it removes most of the difference between the templates that can be attributed to statistical fluctuations, so that we expect the largest contribution to the uncertainty on our systematics to come from the pseudoexperiment statistics. Accordingly, we run a large number of pseudoexperiments, 50,000, for each reweighted template.

Since the RMS for the distribution of fitted masses from the pseudoexperiments is typically 7.9 GeV/c^2, we expect an uncertainty on the mean of that distribution of $7.9/\sqrt{50000} = 0.035$ GeV/c^2. Thus we expect an uncertainty on the difference between two medians of $\sqrt{2} * 0.035 = 0.050$ GeV/c^2, and an uncertainty on half the difference of $0.050/2 = 0.025$ GeV/c^2. The latter quantity is the systematic quoted for each eigenvector:

$$\frac{\text{Med}[+\sigma] - \text{Med}[-\sigma]}{2}.$$

So even if we observe 0 difference between the $+\sigma$ and $-\sigma$ templates for each eigenvector, our prescription of adding the uncertainty in quadrature with the observed shift would yield 0 ± 0.025 GeV/c^2 for each of 20 eigenvectors, or a 0.112 GeV/c^2 total PDF eigenvector uncertainty. Of course, even if there were no real differences, we would still expect typical differences of the same order due to the statistical fluctuations, so that the expected uncertainty for each eigenvector would be 0.025 ± 0.025 GeV/c^2, for a total uncertainty of 0.158 GeV/c^2.

The medians and means of the pseudoexperiment masses for each PDF are shown in Figure 22. The left plots show the actual distribution of medians (top) and means (bottom) from the 50,000 pseudoexperiments for the 40 CTEQ systematic PDFs. The RMS on the means and medians is $\sim 0.038 \pm 0.004$ GeV/c^2, not much larger than the 0.035 GeV/c^2 we expect, so whatever real effects there are in the CTEQ systematics are small.

On the right in Figure 22 are the medians and means of the pseudoexperiment masses vs PDF number. The default NLO PDF (#5) is highlighted in blue, and the pairs of $\pm\sigma$ PDFs for each eigenvector are joined by thin black lines. (The blue point may seem "far" from the others, but it is less than 2σ away from the mean of the remaining PDFs.) At the far right is a red line indicating the typical difference expected from statistics alone (0.050 GeV/c^2). Adding half the difference between each pair in quadrature gives a central shift in the top mass due to the CTEQ PDF systematics of 0.132 GeV/c^2. Since the systematic on each eigenvector has an uncertainty of 0.025 GeV/c^2, we have a total systematic on the top mass due to the CTEQ PDF systematics of $\sqrt{0.132^2 + 20 \times 0.025^2} = 0.173$ GeV/c^2. As expected, the largest contribution of ~ 0.14 GeV/c^2 comes from eigenvector #15.[25]

Finally we estimate the remaining PDF uncertainties: the pseudoexperiments using PDF numbers 1 and 0 give a difference of -0.026 ± 0.050 GeV/c^2, while PDF numbers 2 and 1

[24] A more complete study would include the effects of the different PDFs on the background distributions as well.

[25] It has been suggested that we double the effect of eigenvector #15 in our systematic to account for the difference in the contribution of $gg \to t\bar{t}$ to the total $t\bar{t}$ cross-section at LO and NLO. However, it has also been pointed out that the CTEQ PDF systematics correspond not to $\pm 1\sigma$, but to $\sim 90\%$ confidence. Since we treat the resulting uncertainties on the top mass as $\pm 1\sigma$ uncertainties, these two concerns at least partially cancel.

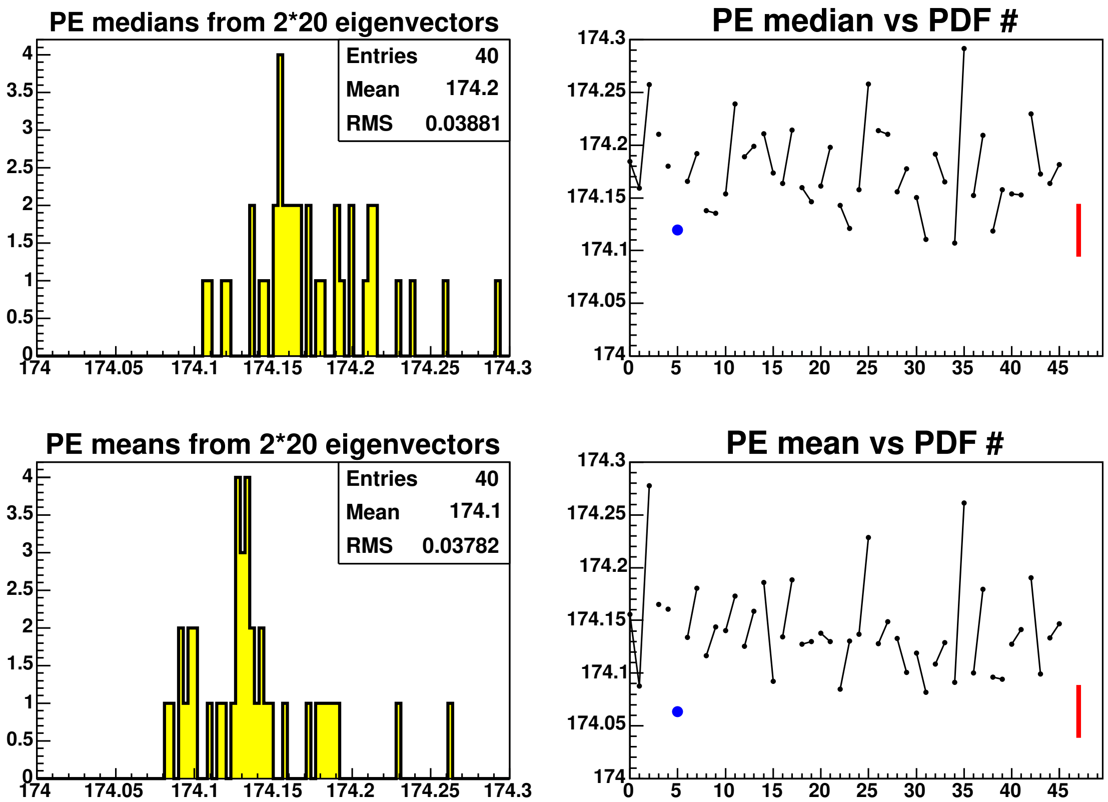

Figure 22: Results used for PDF systematic, from 50,000 pseudoexperiments for each reweighted template. The top left plot histograms the median mass from pseudoexperiments for the 40 CTEQ systematic PDFs. The top right plot shows the median mass from pseudoexperiments vs PDF number for all 46 PDFs. The bottom plots use the mean mass rather than the median.

Table 13: The mean and sigma of Gaussian fits to $(E_T^{jet} - E_T^{\gamma})/E_T^{jet}$ distributions in the photon-jet sample. Jets are reconstructed using the cone of 0.4.

Jet corrections		Data	MC
none	Mean	-0.385 ± 0.002	-0.299 ± 0.003
	Sigma	-0.201 ± 0.001	$+0.169 \pm 0.002$
Level 7	Mean	$+0.002 \pm 0.002$	$+0.053 \pm 0.003$
	Sigma	$+0.241 \pm 0.001$	$+0.214 \pm 0.002$

have a difference of 0.099 ± 0.050 GeV/c^2. Thus we take systematics due to PDF group and PDF α_s of 0.056 GeV/c^2 and 0.111 GeV/c^2, respectively.[26]

Adding the three sources of PDF systematics in quadrature gives a total PDF uncertainty of 0.213 GeV/c^2. This is a large reduction from our previous (statistics-dominated) PDF uncertainty of 1.5 GeV/c^2.

6.6 Jet resolution

The simulation does not model the jet resolutions well. As illustrated in the γ-jet balance studies (see Table 13), the simulation underestimates the resolution by about 15% on average in this data sample. We estimate a possible bias in the top mass measurement by smearing the MC jets in the pseudoexperiment samples by an extra 15%. (Thus jets with 20% energy resolution will have $\sqrt{(20\%)^2 + (15\%)^2} = 25\%$ resolution after the smearing.) See Figure 23 for plots of the smearing effect and the change in the reconstructed mass template. Using the full machinery of pseudoexperiments, the top mass shift due to the extra smearing is found to be -0.4 ± 0.1 GeV/c^2. We take this as an uncertainty due to the jet energy resolution. This uncertainty was estimated using 25-event pseudoexperiments corresponding to the 108 pb^{-1} analysis.

We also checked the effects of the jet resolutions in the fitting procedure by scaling jet resolutions (σ_{jet} in Equation 3.5) by factors between 0.5 and 2. The top mass shift between the scale factor of 0.5 and that of 2 in the fitting is found to be 0.4 ± 0.1 GeV/c^2.

Finally, we determined the jet resolutions using RMS in the jet response after the top-specific corrections, instead of using 68% CL (our default), and used them in the mass fitting. A mass difference of 0.4 ± 0.1 GeV/c^2 was observed. Both of these checks are consistent with the quoted systematic.

6.7 Top p_T distribution

As described in section 3.1.3, the top-specific corrections depend on the p_T spectrum of jets, thus the p_T spectrum of top. It is possible that the Herwig and Pythia modeling of

[26] As mentioned above, it may be preferable not to take a systematic due to the difference between CTEQ and MRST PDFs, as long as no significant shift is observed. This will be taken into consideration in the future.

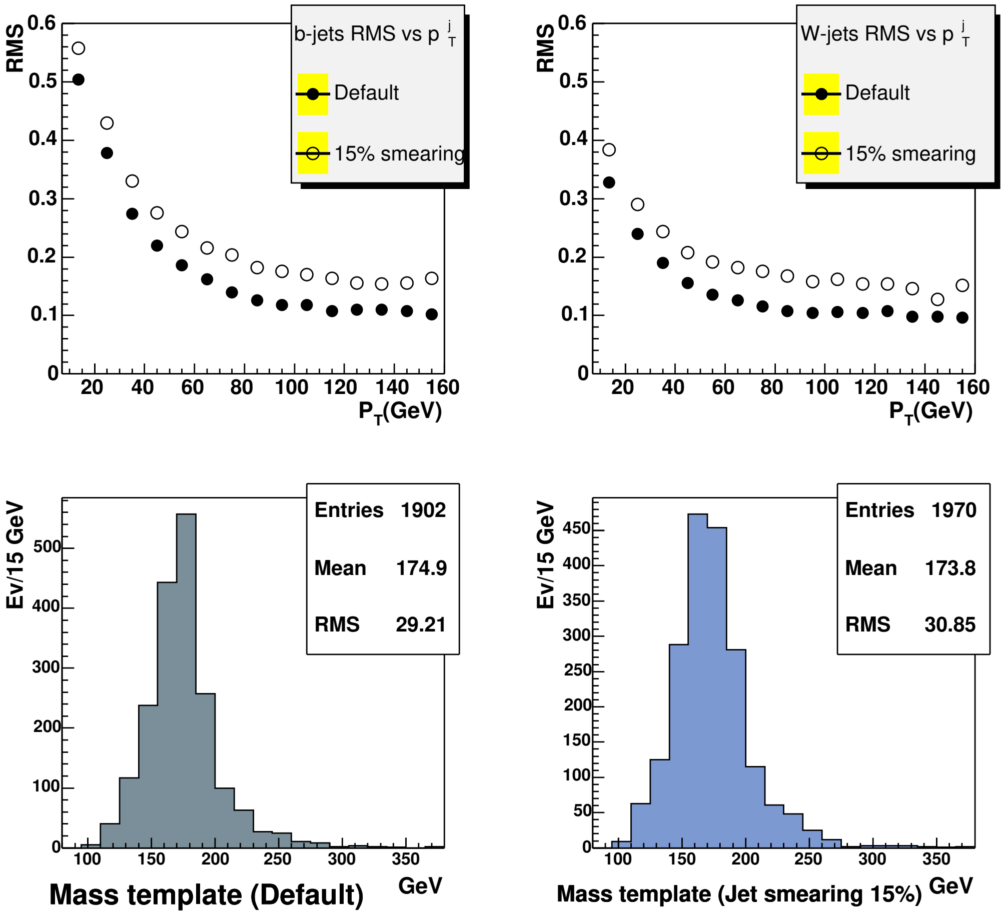

Figure 23: Upper plot: jet response as a function of p_T^{jet} for b jets and W jets after generic corrections applied, for the default jets (full circles) and the jets with extra 15% smearing (open circles). Lower plot: the reconstructed mass distributions with the default simulation (left) and the simulation with extra 15% smearing on jet energies (right).

Table 14: Top mass differences when the background shape is varied, but the same normalization is used. We vary the shape by using each background template separately in the fit, rather than combining them.

Background Shape	ΔM_{top} (GeV/c^2)	
	≥ 3.5 jets	≥ 4 jets
Combined	0 (default)	0 (default)
W + jets	$+0.2 \pm 0.1$	-0.64 ± 0.12
$Wb\bar{b}$	-0.6 ± 0.1	-0.98 ± 0.12
Single top (s channel)	$+0.1 \pm 0.1$	-0.51 ± 0.12
Single top (t channel)	$+0.4 \pm 0.1$	-0.79 ± 0.11
Total	0.5 ± 0.1	0.5 ± 0.1

the top p_T distribution is incorrect. We studied this possibility by constraining the top p_T distribution using the CDF run I measurement [20]. The variation in the hadronic top mass (the invariant mass of one of the top quarks which decays to two light-quarks and one b quark) is measured to be 0.4 ± 0.4 GeV/c^2. Although this is statistically insignificant, we take it as a systematic on the MC modeling of the top p_T distribution. Note that this systematic is estimated without the full machinery of pseudoexperiments.

6.8 Background shape

The uncertainty due to the background reconstructed mass shape comes in two parts. The first is due to variations in the relative normalizations of the individual background processes, since in our method the overall background normalization is allowed to float, but the relative normalizations are fixed. The second part is due to variations in the Q^2 used for the background event generation.

The relative normalization uncertainty is studied by using each of the $Wb\bar{b}$, W + jets (mistags), and single top mass templates (see Figure 11) as the background template in pseudoexperiments, rather than combining them as for the default measurement. The 3.5-jet and 4-jet templates for each process are combined in the expected fractions. The shifts in the top mass are summarized in Table 14. We assign half of the largest difference, 0.5 ± 0.1 GeV/c^2, to be the uncertainty due to the background shape. This is a conservative estimate that also covers various possible problems with the background modeling.

The uncertainty due to the Q^2 used in the background simulation is estimated using $Wb\bar{b} + 1$p samples generated using four different Q^2 values. The samples and the resulting top mass shifts are given in Table 15. We assign half of the largest difference, 0.5 ± 0.3 GeV/c^2, as the systematic uncertainty.

6.9 Additional MC modeling checks

Another set of the top-specific corrections are extracted using the Pythia generator. The difference in the hadronic top mass between Herwig- and Pythia-based top-specific corrections

Table 15: Median top masses from pseudoexperiments when the background shape is taken from $Wb\bar{b} + 1\text{p}$ samples generated using different Q^2.

Q^2	$\mathrm{M_{top}}$ (GeV/c^2)	
	≥ 3.5 jets	≥ 4 jets
$(2M_W)^2$	174.4 ± 0.2	174.75 ± 0.25
M_W^2	173.8 ± 0.2	174.35 ± 0.27
$(M_W/2)^2$	173.7 ± 0.2	173.72 ± 0.25
$M_W^2 + (p_T^W)^2$	174.7 ± 0.2	174.61 ± 0.26
$\Delta\mathrm{M_{top}}$	0.5 ± 0.3	0.5 ± 0.3

is measured to be 0.1 ± 0.1 GeV/c^2. When the full machinery of the pseudoexperiments is used, the difference becomes 0.5 ± 0.1 GeV/c^2. The above checks are correlated with uncertainties due to initial state radiation and generators; we don't assign a separate systematic for these differences.

6.10 SecVtx b tagging

We use the run I estimate of the uncertainty due to the SecVtx b-tagging scale factor energy dependence: 0.1 GeV/c^2.[27] We exclude that part of the run I b-tagging uncertainty due to SLT tags.

In the default measurement, we do not correct the ratio of single- to double-tagged events in our templates for the data/MC tagging efficiency scale factor (see footnote 15). For now, we check the effect of this omission in the following ways. First, we fit the data using corrected signal templates. There is no change from our default measurement or errors, at least at the quoted precision (0.1 GeV/c^2). Second, we perform pseudoexperiments in which we fit generated events using both the default and the corrected signal templates. The mean pseudoexperiment-by-pseudoexperiment shift between the two fits is ~ 0.1 GeV/c^2, which is roughly the same size as our quoted b-tagging systematic, and negligible compared to other systematics.

6.11 Summary of systematic uncertainties

The systematic uncertainties are summarized in Table 16. The total systematic uncertainty is estimated to be 6.7 GeV/c^2.

7 Other Checks

This section contains various checks and studies performed with the aim of validating our understanding of the data, including the goodness of our Monte Carlo modeling.

[27] We should reevaluate this uncertainty using the run II b tagging.

Table 16: Summary of systematic uncertainties $W+ \geq 3.5$ jets and and $W+ \geq 4$ jets analyses. The numbers in the parentheses are taken from the $W+ \geq 3.5$ jets analysis.

Source of Systematics	ΔM_{top} (GeV/c^2)	
	$\geq$ 3.5 jets	$\geq$ 4 jets
Jet Energy	6.3	6.6
ISR	0.4	0.6
FSR	0.9	1.0
PDFs	0.2	(0.2)
Generators	0.4	0.4
Background Shape	0.8	0.8
Other MC modeling (Jet Resolution, p_T^{top})	0.7	(0.7)
b tagging	0.1	(0.1)
Total	6.5	6.8

Most of the studies were performed with 108 pb^{-1} of data. Any results using the full 163 pb^{-1} will be noted.

7.1 Subdivision of top mass sample

The statistical sensitivity of this analysis can be improved in principle by dividing the top mass sample into subsamples with different signal and background mass shape and background event estimation. This strategy was employed for the Run I analysis where 4 subsamples were used based on the b-tagging information [1].

We have tried two possibilities: firstly, we treated separately the single and double-tag events, and secondly the 3.5 and 4-jet events. These results are only treated as cross-checks so far, but are considered for the extracting the final result in the future.

The double-tag background estimate is taken from CDF Note 6907 [16]. We assume the same χ^2 cut efficiency for double-tag events as for $\geq$ 1-tag events (see Table 7), for a total of 0.36 $\pm$ 0.07 expected double-tag background events. We substract this amount from the $\geq$ 1-tag expected background and get 6.6 $\pm$ 0.8 expected single-tag background events. The expected background events for 3.5 and 4-jets separately is given in Table 7. For each of these subsamples, the signal and background templates have been extracted separately and a likelihood function has been defined as in Section 4. The likelihoods of the associated subsamples are multiplied to get a combined answer.

To test the fitting procedures, pseudo-experiments have been generated. The same ratio of 1/2-tags events and 3.5/4-jets events used to create the default templates have been used as input for the pseudo-experiments to do a fair comparison. The 68% C.L. of the expected uncertainties are shown in Table 17. The expected improvement is of the order of a few percent.

The fitting procedure has been applied to data. The results are shown in Table 18. The 1/2-tag result is understandably very close to the default one, since only two double-tag events are seen in the data. The 3.5/4-jets separation gives a central value slightly

Table 17: 68% C.L. of expected statistical uncertainty from background contrained fit for various fitting procedures

Fitting procedure	Expected Uncert. (GeV/c^2)
Default	6.46 ± 0.14
1/2-tag separate	6.33 ± 0.13
3.5/4-jets separate	6.37 ± 0.13

Table 18: Constrained fit results on data events for separate fit of 1/2-tag events and 3.5/4-jet events

Fitting procedure	Result (GeV/c^2)
Default	$174.9\ ^{+6.7}_{-7.2}$
1/2-tag separate	$174.4\ ^{+6.7}_{-7.3}$
3.5/4-jets separate	$177.5\ ^{+6.5}_{-6.6}$

larger with significantly smaller uncertainties, probably since the 3.5- and 4-jet events are so differently distributed in data, and the 4-jet events are given more weight in the fit since they have sharper mass templates. The mass distributions fitted individually for the single-tag, double-tag, 3.5- and 4-jet subsamples are shown in Figure 24.

7.2 Alternative top-specific corrections

We checked the stability of the mass extraction by using slightly different top-specific corrections which were used in Winter '03 top mass measurement with no b tag [21]. The differences between these two corrections are described in CDF Note 6794 [13]; briefly, they are

- Jet/event selection (isolated jets, dilepton sample for b jets in GG)
- η-dependent corrections in JF
- Jet resolutions taken from RMS of response in GG
- Jet corrections taken from mean of response in GG

A complete analysis is done with the alternative top-specific corrections using pseudoexperiments, including remaking the MC templates and p.d.f.'s. To observe the expected differences between the two sets of corrections for a given set of events, we need to know the pseudoexperiment-by-pseudoexperiment difference in M_{top}. We select a sample of events for each pseudoexperiment, two top-specific corrections (default and alternative) are applied to the sample, and the two corresponding fit top masses are extracted. The extracted top distributions from 2000 pseudoexperiments are shown in Figure 25 for the default (top left)

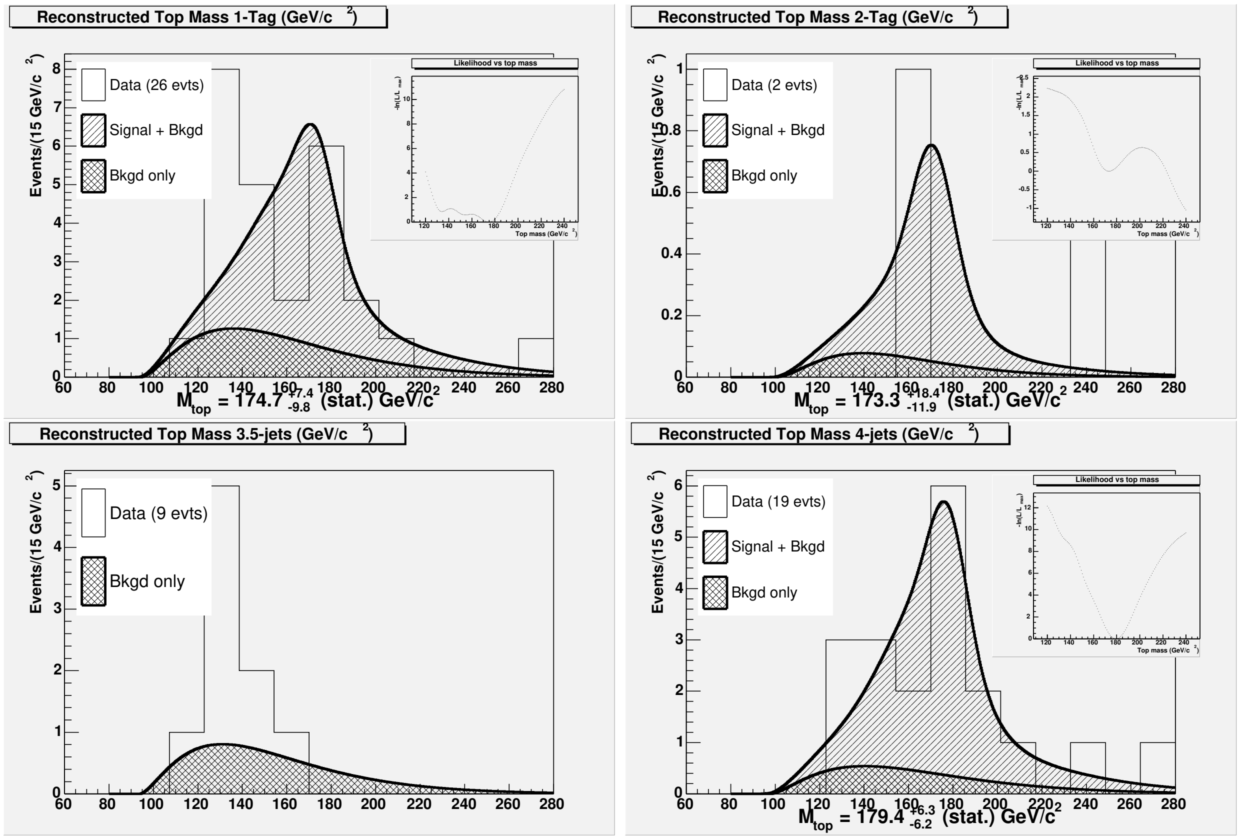

Figure 24: Fitted data mass distribution for single-tag events (top left), double-tag events (top right), and 4-jet events (bottom right). The fit does not converge for the 3.5-jet data distribution (bottom left); for 3.5-jet events, the data mass distribution is shown along with the background shape using the central value for the background normalization.

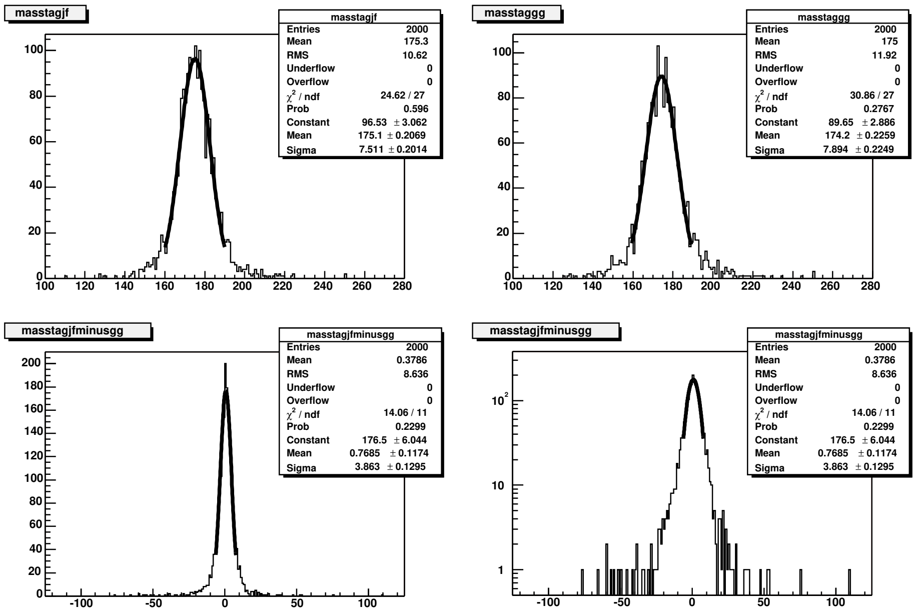

Figure 25: Top plots: the extracted mass distributions from 2000 pseudoexperiments using this analysis's top-specific corrections (top left) and the alternative corrections (top right). Bottom plots: top mass difference distribution from 2000 pseudoexperiments in the linear scale (bottom left) and the logarithmic scale (bottom right).

and alternative (top right) top-specific corrections. This figure also shows the fit mass difference between the two corrections from 2000 pseudoexperiments: the bottom left plot in the linear scale and the bottom right plot in the logarithmic scale. The average and width of the mass difference distribution are 0.7 GeV/c^2 and 3.8 GeV/c^2, respectively.

A complete analysis is also done with the alternative top-specific corrections for the data. Figure 26 (top) demonstrates the reconstructed mass difference for each event. The fitted top mass is found to be 2.2 GeV/c^2 lower than the default measurement, which is consistent with what we expect from the pseudoexperiment studies.

7.3 W mass in the hadronic decay mode

An important intermediate handle we have in any $t\bar{t}$ event is the well known W mass. If we pick the right jet-parton assignment, and the jets are corrected properly, we expect to find the invariant mass of the two W daughter jets equal to the W mass. Figure 27 (center) shows the invariant mass distributions of W daughter jets where the jets are assigned by the mass fitter and the jet energies include the top-specific corrections but not the W mass constraint. The agreement between the data and the signal + background combined sample is reasonable, but the statistics are poor. We increased statistics by removing the b-tagging requirement. The agreement is good and the results are shown in Figure 27 (right). We also show the distributions for double-tagged events, where the statistics are even more limited (Figure 27 left). For the comparison between data and Monte Carlo, we use a combination of signal and background MC in the ratios 95/5, 75/25, and 25/75 for two tag, at least

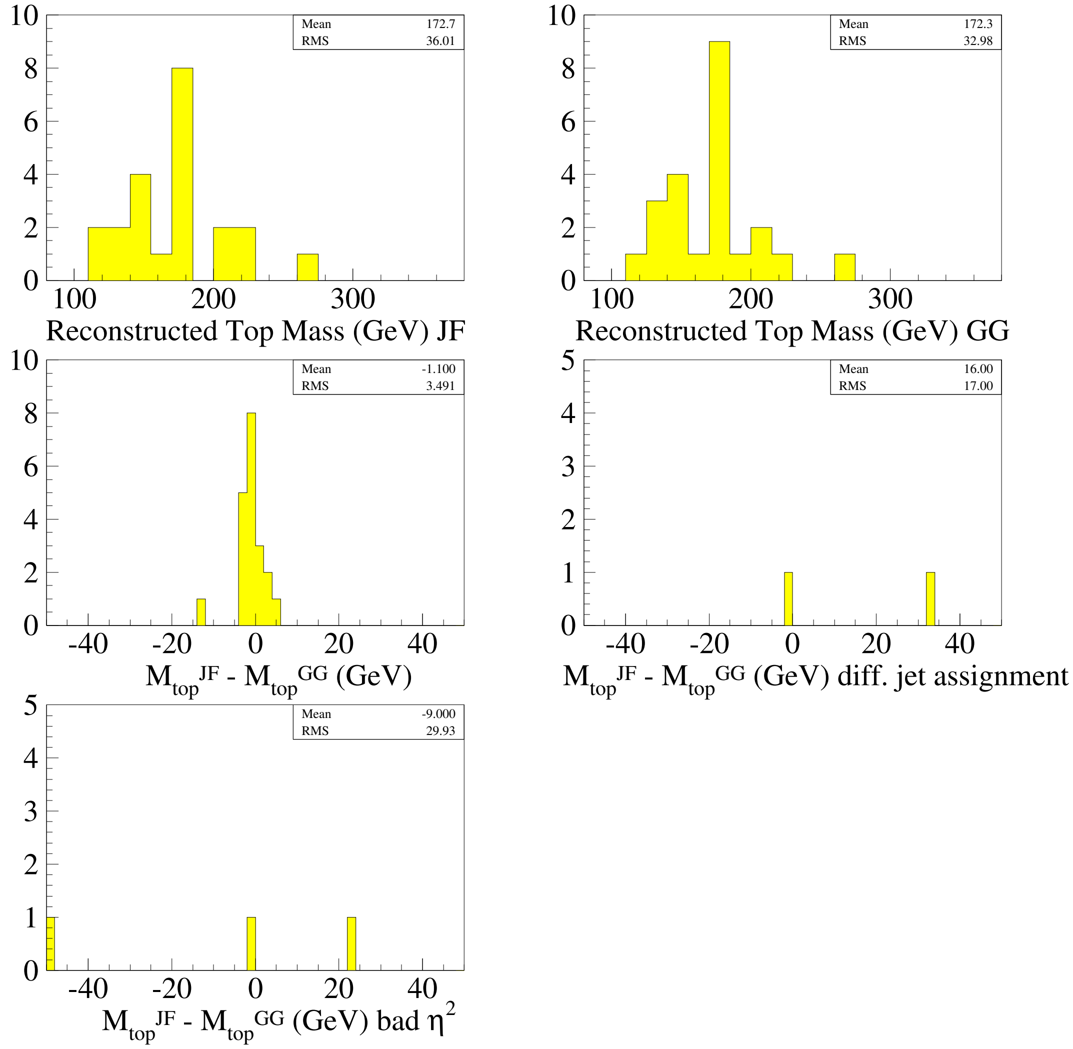

Figure 26: Reconstructed mass distributions for 108 pb^{-1} with the default top-specific corrections (top left) and the alternative corrections (top right). Event-by-event mass differences between these two corrections for events with $\chi^2_{\rm min} < 10$ and the same jet assignment (middle right), events with different jet assignments (middle right), and events with $\chi^2_{\rm min} > 10$.

one tag, and all events, respectively. For all three subsamples, a KS test implies consistent distributions.

7.4 Lepton η dependence

In this analysis we assumed that the lepton trigger efficiencies were flat in η and the total integrated luminosity for CMX muons is the same as that of central electrons and CMUP muons. We compared the reconstructed mass distributions between the electron sample and the muon sample, and between the CMUP sample and the CMX sample. As illustrated in Figure 28, the average of the mass templates varies by $1 \sim 2$ GeV/c^2, which is an extreme case. If there is a bias in the top mass shape as a function of η or between electrons and muons, we would have a bias, which is a small fraction of 1 GeV/c^2 in the measurement.

7.5 Kinematic distributions

We compare various kinematic distributions for the data with the Monte Carlo predictions for combined signal and backgrounds. The top mass analysis in the lepton+jets channel requires a good understanding of various objects such as leptons, b jets, light jets, and neutrinos. Furthermore, kinematic distributions of reconstructed top and $t\bar{t}$ objects provide useful information about the properties of the top quark. This information could be used to check whether the top properties are consistent with Standard Model predictions.

Figure 29 shows the p_T and η distributions of the lepton (electron or muon) and Figure 30 shows the E_T distribution of the leading jet and $\not\!\!E_T$ distribution. The data are compared with the Monte Carlo simulation with 175 GeV/c^2 top signal and background combined.

The H_T distribution is shown in Figure 31. H_T is defined as

$$H_T = p_T^{e,\mu} + \not\!\!E_T + \Sigma_i E_T^{i-th\ jet}, \tag{7.1}$$

where jets include all the jets with $E_T > 8$ GeV and $|\eta^{jet}| < 2$. In these distributions, jets and $\not\!\!E_T$ are the quantities used for event selection (see Section 2). Also shown in Figure 31 is the distribution of number of jets in the event ($E_T > 8$ GeV).

Figure 32 shows the p_T and η distributions of reconstructed top quarks. The jet assignments are taken from the best χ^2 combination in the top mass fitting. Thus the top-specific corrections as well as the W mass constraint are applied to the jets.

The p_T distribution of the reconstructed $t\bar{t}$ system is shown in Figure 33. As above, the jet assignments are taken from the best χ^2 combination in the top mass fitting.[28]

Finally, the mass of the reconstructed $t\bar{t}$ system is shown in Figure 34. All these distributions show reasonable agreement between data and the Standard Model predictions.

7.6 χ^2 check

Figure 35 compares the $\chi^2_{\min}$ distribution in the mass reconstruction between the data and the signal + background samples. The data and the expectation are in good agreement.

[28] It has been suggested that we also compare the distributions of p_z of the $t\bar{t}$ system.

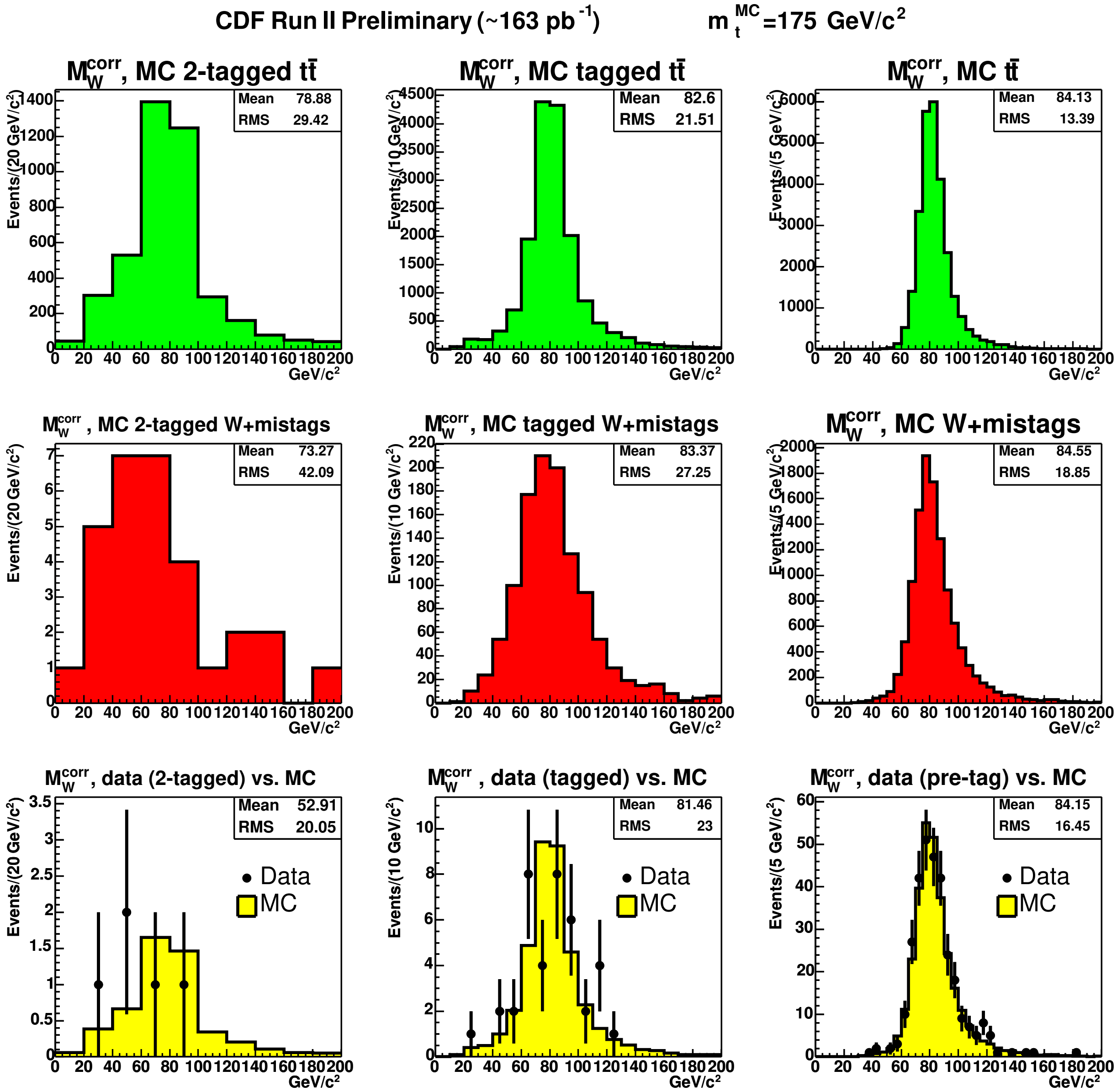

Figure 27: The invariant mass distributions of $W \to q\bar{q}'$ jets where the jet assignment is determined by the top mass fitter and jet energies include top-specific corrections without the M_W constraint. The left plots are for events with two b tags, center plots show events with at least one b tag, and the right plots do not require any b tag in event selection or when choosing the jet assignment. Top, middle and bottom plots present the top signal, background (W + jets), and data plotted against Monte Carlo. We use a combination of signal and background in the ratios 95/5, 75/25, and 25/75 for left, middle, and right, respectively.

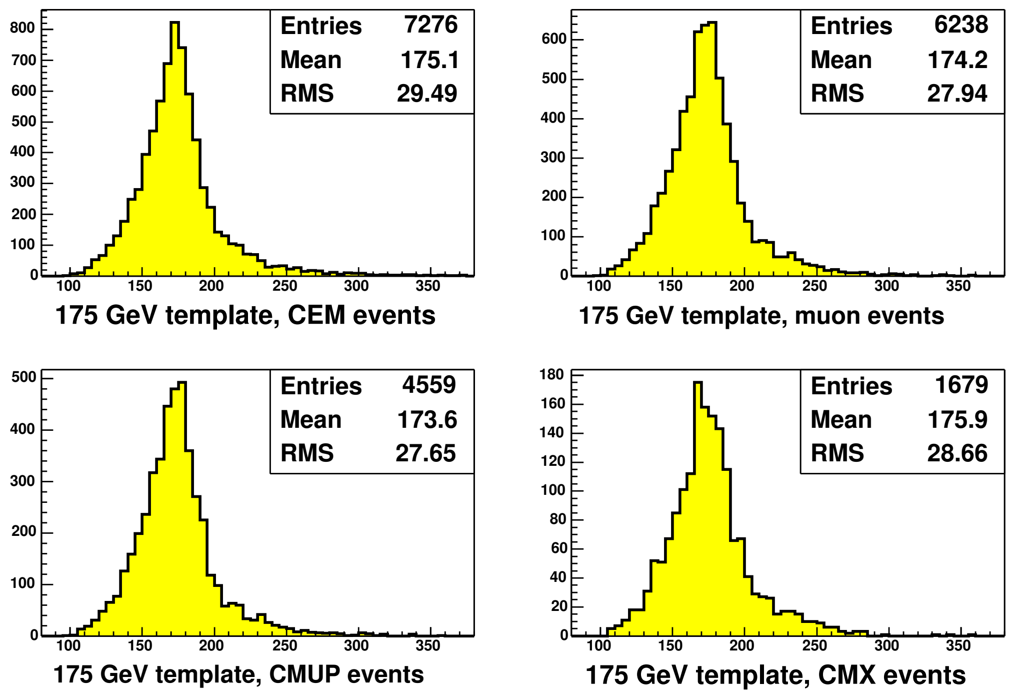

Figure 28: Reconstructed mass distributions of top events with all electrons (top left), all muons (top right), CMUP muons (bottom left), and CMX muons (bottom right).

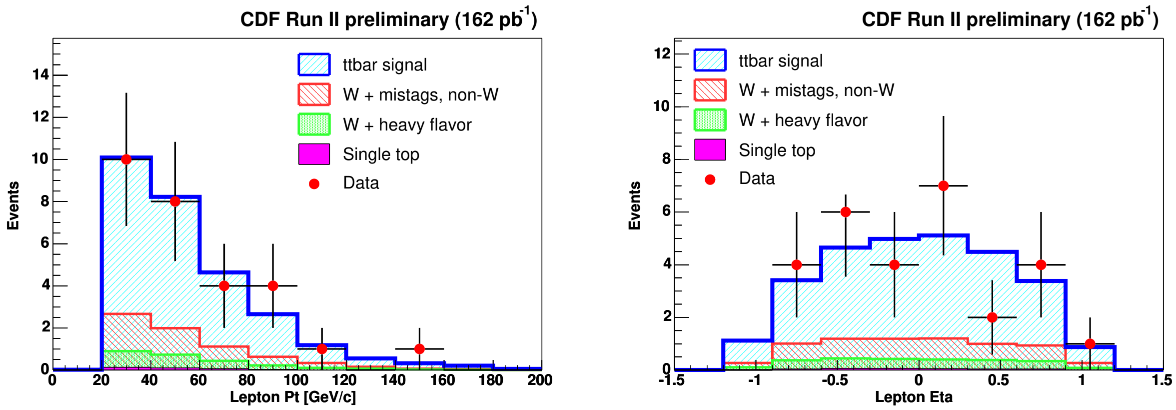

Figure 29: p_T (left) and η (right) distributions of the lepton (e or μ) for $W+\geq 3.5$ jet events.

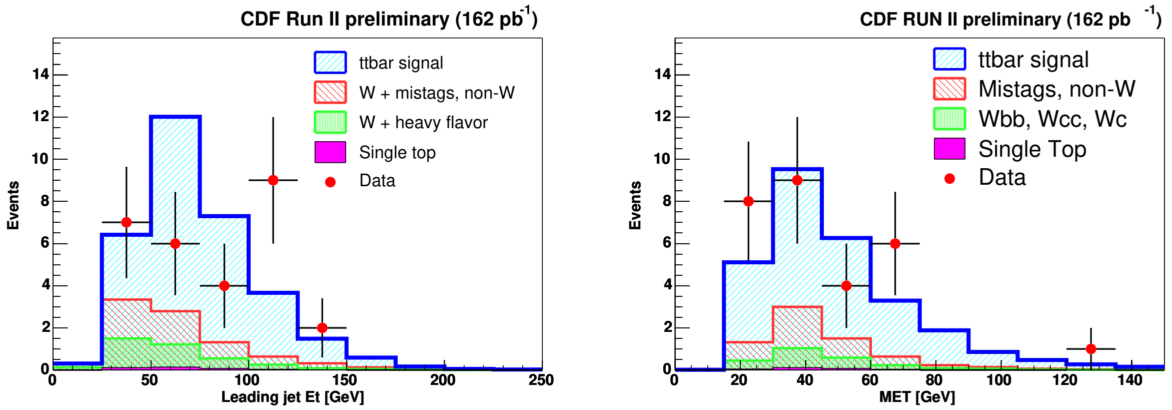

Figure 30: E_T of the leading jets (left) and $\not{E}_T$ (right) for $W+\geq 3.5$ jet events.

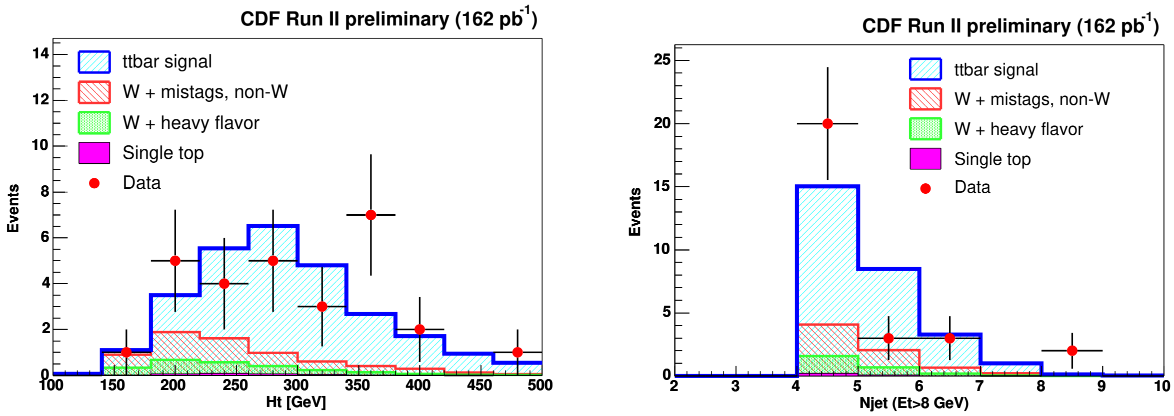

Figure 31: H_T distribution (left) and number of tight + loose jets (right) for $W+\geq 3.5$ jet events.

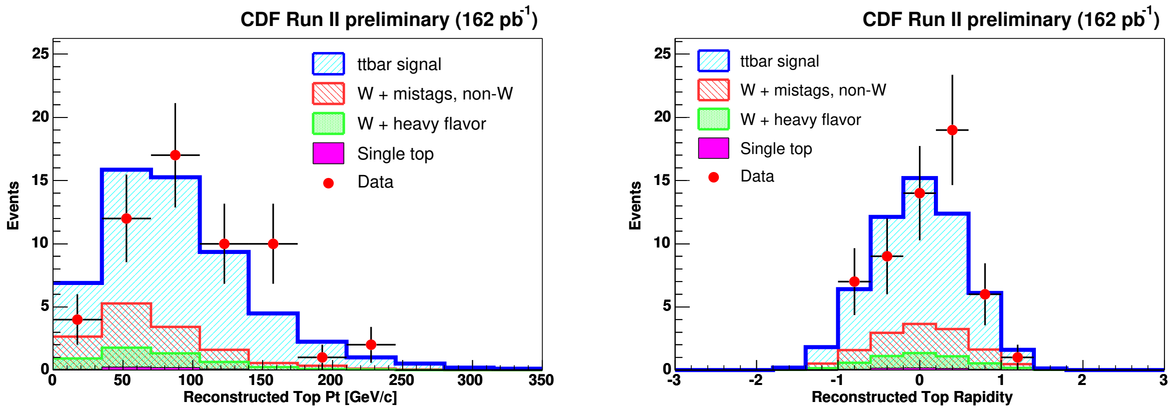

Figure 32: p_T (left) and η (right) distributions of the top for $W+\geq 3.5$ jet events.

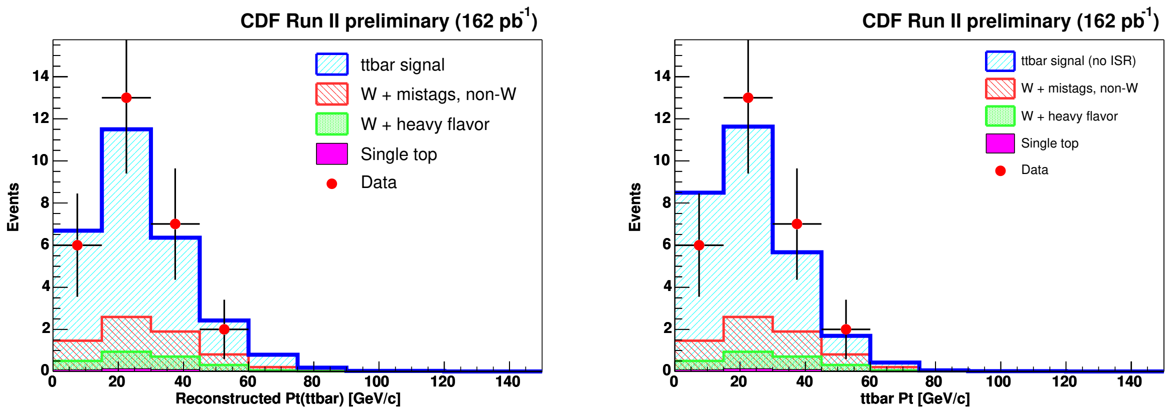

Figure 33: The p_T distribution of the $t\bar{t}$ system using the default 175 GeV/c^2 $t\bar{t}$ Herwig Monte Carlo sample (left plot). The right plot uses the $t\bar{t}$ Pythia Monte Carlo sample without ISR.

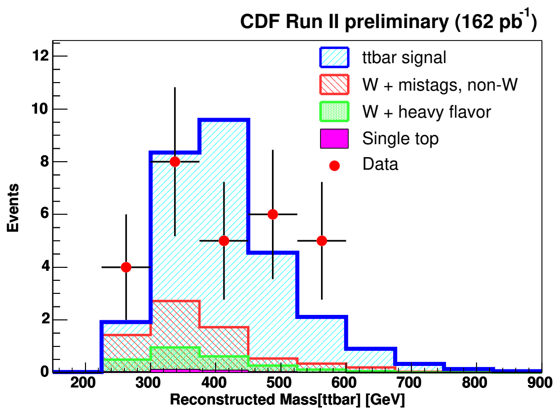

Figure 34: The mass of the $t\bar{t}$ system.

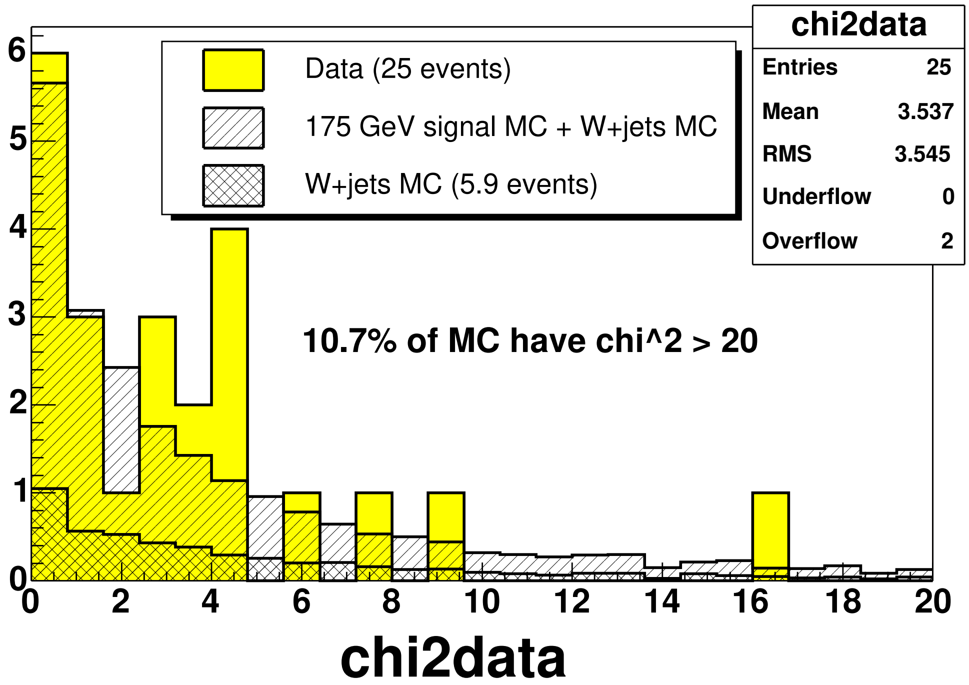

Figure 35: The χ^2_{min} distributions of combined Monte Carlo sample of top and background (hatched histograms) and the data (yellow histogram).

8 Conclusions

The top quark mass is measured using Run II data taken between March 2002 and September 2003. With the requirement of $W+\geq 3.5$ jets, we fit 28 $t\bar{t}$ candidates to a mass of

$$\mathrm{M}_{\mathrm{top}} = 174.9\ ^{+7.1}_{-7.7}\ (\text{stat.}) \pm 6.5\ (\text{syst.})\ \mathrm{GeV}/c^2.$$

There is a dominant systematic of 6.3 GeV/c^2, due to uncertainties in the jet energy scale. This systematic will become the largest source of uncertainty in the top mass measurement with only modest additional statistics.

Acknowledgements

We thank George Velev and Guram Chlachidze for providing the original MINUIT fitter and for many useful discussions. We also thank Un-Ki Yang and the Toronto group for producing MC samples necessary for this analysis. Finally, we thank the top mass group and the top group for many interesting and insightful comments and questions.

A Pseudoexperiments

We would often like to characterize the expected performance of the analysis in a statistically meaningful way, for example to get the expected statistical error, or to understand the shift in the top mass caused by a given systematic effect. We use large ensembles of sets of 28 Monte Carlo events which pass our cuts; each set of events is a pseudoexperiment. The full analysis machinery is used on each pseudoexperiment, and the top mass, with associated uncertainties, is extracted. So, for example, we use the median measured top mass for an ensemble of pseudoexperiments to understand the systematic effect on the top mass due to changing the jet energy scale by 4%.

A problem arises. We would like to use thousands of pseudoexperiments to understand well the results of the analysis, but we would need $28 \times 1000'$s of events to make such an ensemble. A typical sample (see Figure 7) contains only ~ 7000 events that pass all of our selection cuts. We use a form of random sampling with replacement to extend the power of our limited Monte Carlo samples [22]. By taking the same events in different combinations (different sets of 32) we can get thousands of pseudoexperiments that are somewhat statistically independent, though not as much so as thousands of completely disjoint sets of events. Since Monte Carlo generation, simulation, processing, and storage are prohibitively expensive, resampling allows us to maximize the power of reasonably sized MC datasets.

In practice, each event is fully characterized in this analysis by its reconstructed mass. Instead of keeping a *vector* of reconstructed masses and selecting a random entry from the vector 32 times, we keep a *histogram* of reconstructed masses and 32 times select a random mass according to the distribution in the histogram using the root function `TH1::GetRandom`. This selects the bin of the histogram according to the cumulative distribution, and assumes a flat distribution of masses within each bin.[29]

Each pseudoexperiment consists of a number of masses from signal events, and a number of masses from background events, whose sum is a fixed N. (In the current iteration of this analysis, $N = 28$.) The number of background events is chosen at random using the same constraint that will be applied in the likelihood fit, a Gaussian fluctuation followed by a Poisson fluctuation. The background masses are taken as described above from a background template, and the signal masses are taken as described above from a signal template. When a systematic is being estimated, both the signal and background templates should be varied in the same way.

When we use an ensemble of pseudoexperiments to measure the shift in top mass due to a particular systematic source, we would like to understand the uncertainty on our determination. (1.0 ± 1.0 GeV/c^2 is a very different result from 1.0 ± 0.1 GeV/c^2 when no systematic shift is expected.) We define the shift in top mass as the difference between the median measured top mass for pseudoexperiments drawn from the systematically shifted reconstructed mass histogram, and the median measured top mass for pseudoexperiments drawn from the default reconstructed mass histogram. There are two general cases: when the systematically shifted reconstructed mass histogram comes from the same MC sample as the base reconstructed mass histogram, and when they come from different MC samples. An example of the first case is jet systematics, where the systematically shifted masses use the same events as the default masses, but with shifted jet corrections. An example of the second case is PDF systematics, where there is no choice but to generate and simulate an entirely

[29] This is being investigated as a possible source of bias in the pseudoexperiment results. The bins in our reconstructed mass histograms have 5 GeV/c^2 width by default, and the assumption of a flat distribution within such a large bin can have a significant effect, especially in bins where the true distribution is changing rapidly.

new sample with different PDFs. In both cases, there is a simple statistical uncertainty on the median of each ensemble of measured top masses from pseudoexperiments. But this uncertainty can be made arbitrarily small by performing arbitrarily many pseudoexperiments. We clearly have another source of uncertainty due to the limited statistics of the underlying sample, from which the reconstructed mass histograms were derived. In the first case described above, that uncertainty is highly correlated between the sytematically shifted and the default samples, so the uncertainty on the difference between the two medians is taken to be negligible. On the other hand, when the two reconstructed mass distributions are derived from completely independent sets of events, that uncertainty is uncorrelated between the two and must be accounted for. As an estimate of the uncertainty on the median of an ensemble of pseudoexperiments due to the limited statistics of the sample of reconstructed masses from which they were derived, we use the uncertainty on the mean of the reconstructed mass histogram, namely $RMS/\sqrt{N}$, where N is the number of entries (events) in the histogram.

B Pull Distributions and 68% coverage

During the blessing process, a concern arose about the pull widths and fractional coverage of the statistical uncertainties from pseudoexperiments using Monte Carlo samples. This led to various studies in which we confirmed that the fundamental result of our fit, the likelihood curve, is valid. However, that likelihood curve is in general non-Gaussian, and large ensembles of pseudoexperiments yield pull widths greater than one. Similarly, the $\pm 1\sigma$ uncertainties we were using did not provide 68% coverage of the true mass. But many physicists expect this property of Gaussian errors to obtain even in the case of non-Gaussian errors. Therefore we have changed our reporting of the statistical uncertainty to provide 68% coverage as described below. A more careful explication of the choice is laid out in a writeup on the web [23].

A pull distribution with unit width can be obtained whenever the measured parameter has well estimated Gaussian errors. But the likelihood curve obtained using our method is in general non-Gaussian (i.e. the $-\ln L$ is in general non-parabolic). The non-Gaussian likelihood can be due to several factors.

Background The presence of background can lead to likelihoods that are shallow on the low-mass side, since events at low mass (generated as background events) could be due instead to low-mass signal.

Low statistics The limited statistics of each pseudoexperiment lead to various complicated reconstructed mass shapes, such as double peaks, plateaus, holes in the distribution, etc. The likelihood curve for each pseudoexperiment will reflect to some degree the mass distribution.

Templates The non-Gaussian shape of the signal templates (and their parameterization) means that the likelihood curve for even a single event will be non-Gaussian.

But when a likelihood curve is non-Gaussian, it cannot be described with a single number (the Gaussian uncertainty). We had been using the MINOS errors (defined as the masses M_+ and M_- at which the log-likelihood has changed by 1/2 unit from its minimum), which provide one definition of the statistical uncertainty for a general likelihood curve. However, this definition does not necessarily provide pull distributions with width 1, or 68% coverage of the correct value. In particular, if the $-\ln L$ tends to be shallower than a parabola (L is wider than a Gaussian), the pulls will be too wide since events several "sigma" away from the minimum are more likely than they would be in a Gaussian distribution. Even in the absence of background, and with a Gaussian parent distribution (template), typically wider-than-Gaussian likelihoods have been reproduced in a toy Monte Carlo model when the number of events per experiment is small [24].

We verified that the tails and non-gaussian shape of the pull distributions disappear when considering large statistics. Pull distributions for pseudoexperiments with 210 signal events (M_{top} = 175 GeV/c^2) and no background are shown in Figure 36. The pull widths are consistent with one. Figure 37 shows the same with 70 background events added per experiments. The pull widths remain consistent with one. Thus the non-Gaussian shape of a single-event likelihood becomes increasingly gaussian as the statistics increases, as predicted by the central limit theorem, and we conclude the current shape of the pull width is due to low statistics. Note that a bias appears in the pull mean with higher statistics (i.e., smaller errors). There is no apparent bias with the current event sample size (as shown in Figure 14), but from these plots we can expect the bias to become more noticeable as the sample size increases. We have noticed that the bias disappears when selecting the pseudo-data from the template fit functions instead of the template histograms (see Figure 38). This suggests there is a remaining discrepancy between the template shape and their fit functions to which we are not sensitive yet, and we will need to investigate this effect more thoroughly in the future (however, see also footnote 29).

Having satisfied ourselves that the behavior we see in pseudoexperiments is reasonable, we scaled the errors obtained from MINOS so that 68% coverage of the true value is expected. In particular, we investigate pseudoexperiments for which the generated mass is 175 GeV/c^2, very close to the measured central value of 174.9 GeV/c^2.[30] Some information from the 10,000 such pseudoexperiments is shown in Figure 39. In particular, the bottom left curve shows the fraction of pseudoexperiments for which the true mass (175 GeV/c^2) lies within the $\pm 1\sigma$ errors, as a function of a multiplicative factor applied to the errors obtained from MINOS. A fractional coverage of 68.3% is found when the MINOS errors are scaled by 1.065. Therefore the quoted statistical uncertainty on our primary measurement is obtained by scaling the MINOS errors by 1.065.

References

[1] T. Affolder et al. Measurement of the top quark mass with the Collider Detector at Fermilab. *Phys. Rev. D*, 63(032003), 2001.

[30] Unfortunately, there is no obvious (to us) prescription for achieving 68% coverage from the quoted errors. There doesn't seem to be a way to extract such errors directly from a given likelihood curve, so some ensemble of pseudoexperiments must be used. But which ensemble and how to generate or scale the errors is somewhat ambiguous.

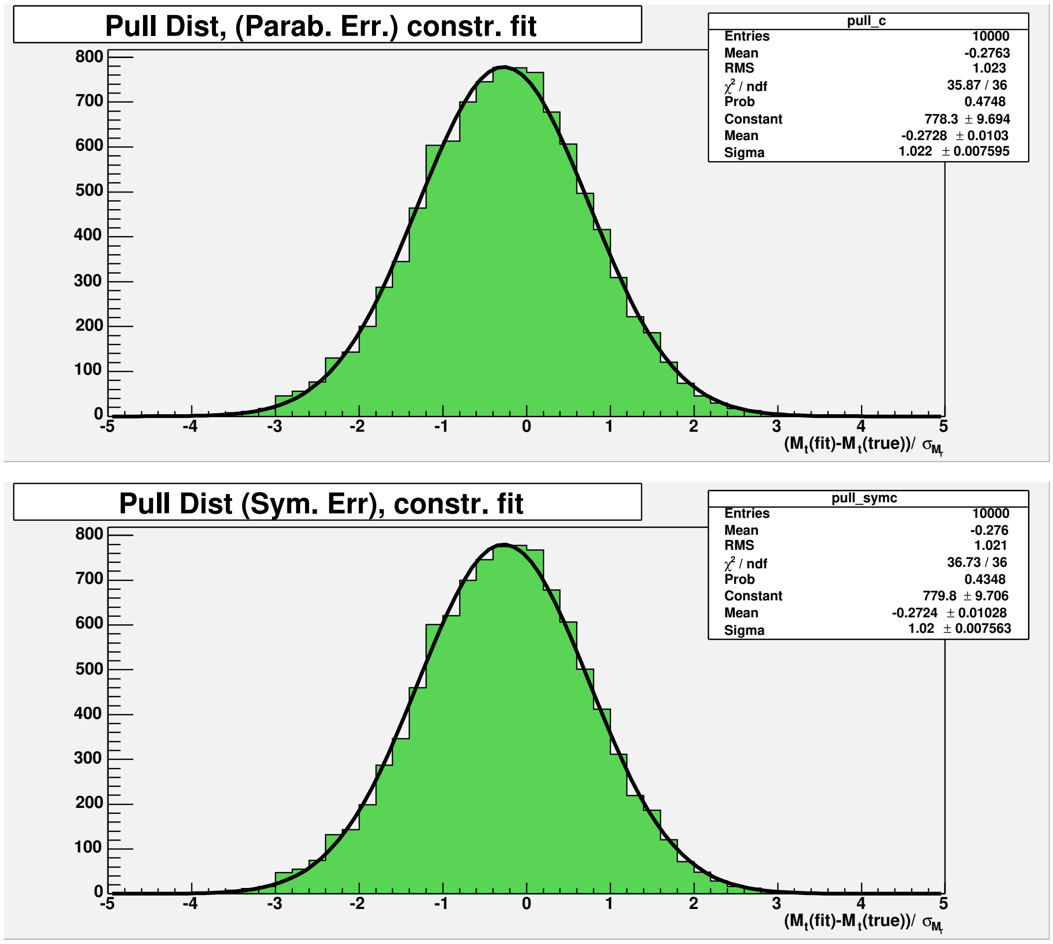

Figure 36: Pull distributions for parabolic errors (upper plot) and symmetrized errors (lower plot) of pseudo-experiments each containing 10 times the signal events statistics (210 events) and no background events.

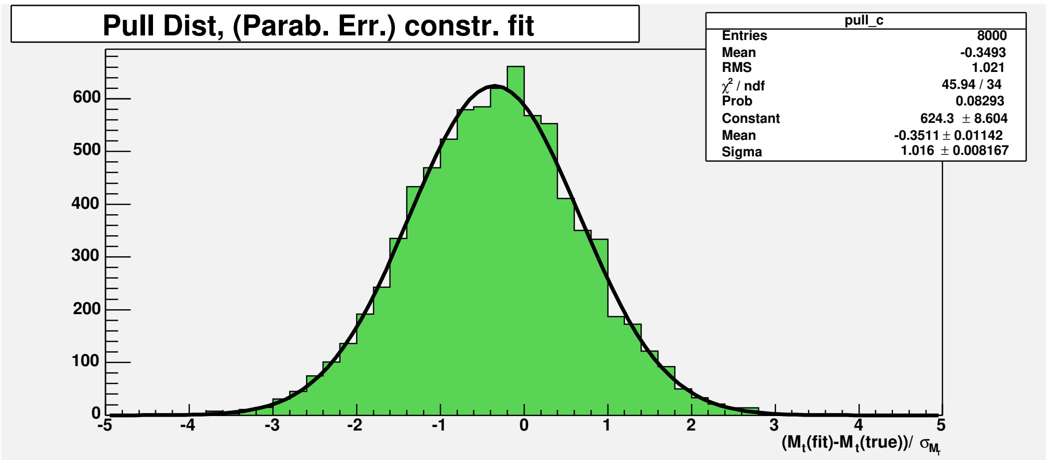

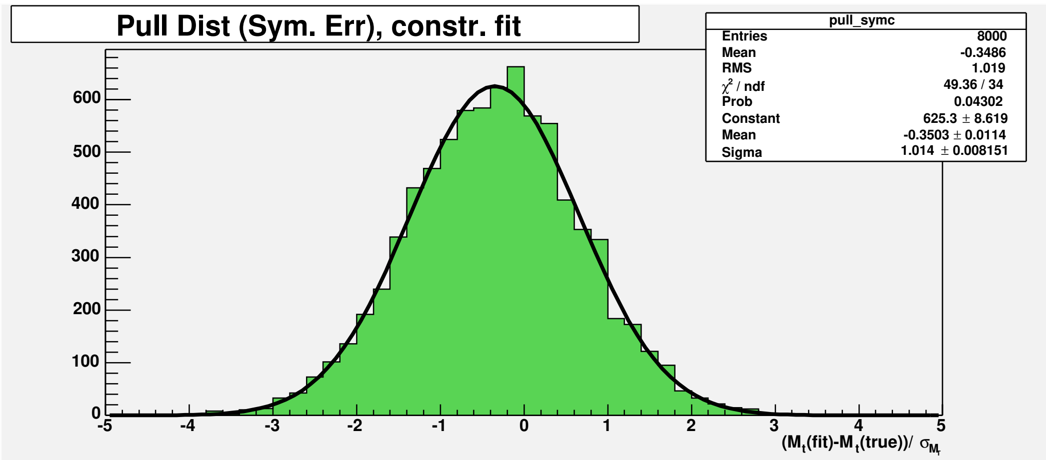

Figure 37: Pull distributions for parabolic errors (upper plot) and symmetrized errors (lower plot) of pseudo-experiments each containing 210 signal events and 70 background events.

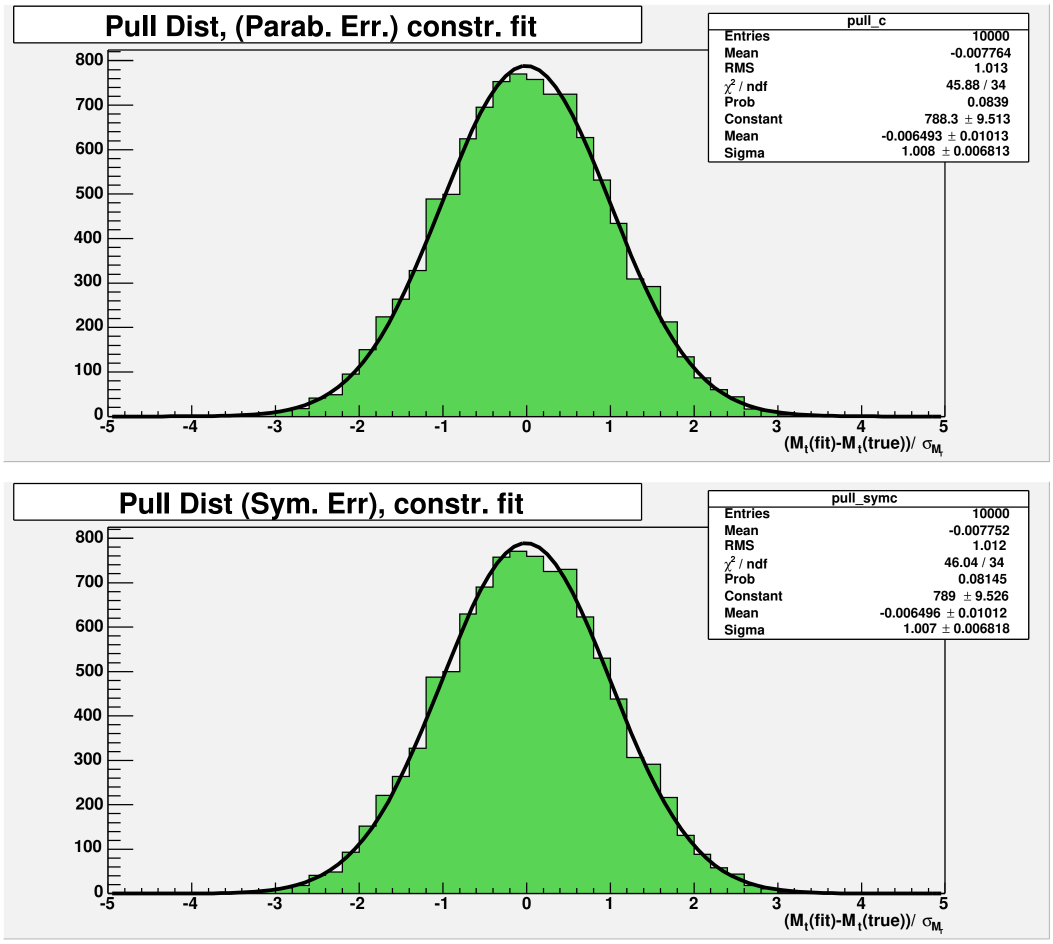

Figure 38: Pull distributions for parabolic errors (upper plot) and symmetrized errors (lower plot) of pseudo-experiments each containing 210 signal events and no background events when pseudo-data is taken from the template fit functions instead of the template histograms. The bias seen in previous figures disappears.

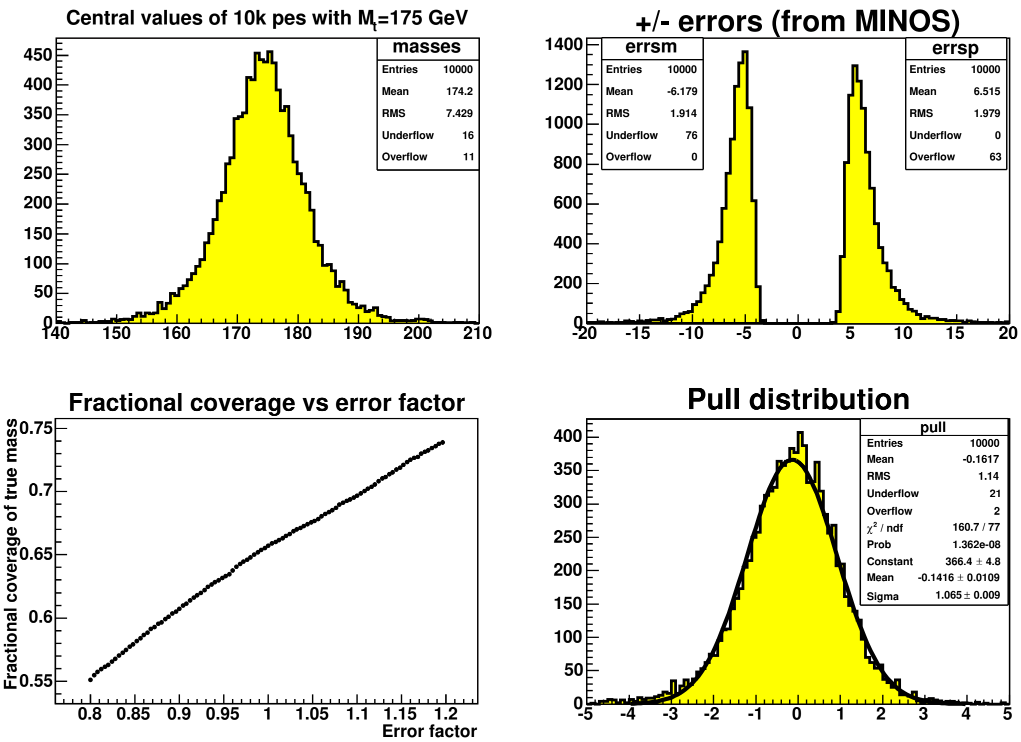

Figure 39: Ten thousand pseudoexperiments were performed with a generated mass of 175 GeV/c^2. The top left plot shows the central values of the likelihood fits. At top right the positive and negative errors from MINOS are plotted. In the bottom right frame is the pull distribution using the MINOS errors. The bottom left shows the fraction of the pseudoexperiments for which the true mass lies within the one sigma errors, as a function of the multiplicative factor applied to the MINOS errors.

[2] Erik Brubaker, Adam Gibson, Young-Kee Kim, Jean-Francois Arguin, Pekka Sinervo, and Un-Ki Yang. Measurement of the top quark mass in the lepton+jets channel. CDF Note 6563, Fermilab, August 2003.

[3] Ken Bloom, Koji Ebina, Evelyn Thomson, and Kohei Yorita. ttbar event selection and detection efficiency for summer 2003 lepton+jets analyses. CDF Note 6574, Fermilab, July 2003.

[4] G. Bellettini, J. Budagov, G. Chlachidze, and G. Velev. Summer 2003 findings on top mass reconstruction in pre-tagged lepton+jets events. CDF Note 6644, Fermilab, December 2003.

[5] CDF High Pt B-Tag Group. Offline defaults summer 2003. http://www-cdf.fnal.gov/internal/physics/top/RunIIBtag/Offline_Defaults_Summer2003.html, July 2003.

[6] L. Cerrito and A. Taffard. A soft muon tagger for Run II. CDF Note 6305, Fermilab, July 2003.

[7] L. Cerrito, T. Liss, L. Miller, and A. Taffard. Measurement of t-tbar cross section with SLT. CDF Note 6677, Fermilab, November 2003.

[8] Evelyn J. Thomson. Description of data samples for top group for summer 2003. CDF Note 6548, Fermilab, July 2003.

[9] Regis Lefevre and Mario Martinez. GOOD RUNS Page. http://www-cdf.fnal.gov/internal/dqm/goodrun/good.html, November 2003.

[10] E. Brubaker and Y.-K. Kim. Jet angle measurement resolution and bias in ttbar events. CDF Note 6927, Fermilab, March 2004.

[11] A. Caner, L. Galtieri, J. Lys, W. Yao, and A. Yagil. Jet corrections for top mass fitting. CDF Note 2469, Fermilab, February 1994.

[12] J.-F. Arguin and P. K. Sinervo. Revisiting the top-specific jet energy corrections. CDF Note 6404, Fermilab, December 2003.

[13] Erik Brubaker and Young-Kee Kim. A comparison of GG and JF top-specific corrections for the top mass analysis in the l+jets channel. CDF Note 6794, Fermilab, December 2003.

[14] C. Campagnari and A. Yagil. Constrained fits in a lepton+jets top search. CDF Note 1935, Fermilab, January 1993.

[15] B. Harral. Kinematic fit method for top candidates. CDF Note 2200, Fermilab, August 1993.

[16] D. Amidei and S. Miller. Method 2 secvtx background estimate and measurement of the ttbar cross section. CDF Note 6907, Fermilab, March 2004.

[17] J.-F. Arguin, A. A. Bhatti, C. A. Currat, A. Gibson, A. Galtieri, B. Heinemann, G. Latino, and M. Shochet. Jet corrections for summer 2003 analyses (offline version 4.10.4). CDF Note 6565, Fermilab, July 2003.

[18] K. Yorita and K. Kondo. Top quark mass measurement by dynamical likelihood method. CDF Note 6829, Fermilab, March 2004.

[19] Stephen Miller. How to estimate pdf acceptance uncertainties using weighted mc. http://cdfrh0.grid.umich.edu/~miller/pdf/pdf_acceptance.html, April 2004.

[20] T. Affolder et al. Measurement of the top quark p_T distribution. *Phys. Rev. Lett.*, 87(102001), 2001.

[21] G. Bellettini, M. Bucciantonio, G. Chlachidze, and G. Velev. Top mass reconstruction on pre-tagged lepton+jets run2 events. CDF Note 6313, Fermilab, March 2003.

[22] Roger Barlow. SLUO lectures on statistics and numerical methods in HEP, Lecture 6: Resampling and the bootstrap. http://www.hep.man.ac.uk/u/roger/sluo6.ps, August 2000.

[23] Erik Brubaker. Error definition for top mass measurement using templates. http://www-cdf.fnal.gov/internal/physics/top/run2mass/ljets/template/errorMethod.ps, April 2004.

[24] John Conway. Private Communication, April 2004.